Title
Design and Characterization of Porous Hyaluronic Acid Hydrogels for in vitro and in vivo Non-Viral DNA Delivery

Author
Tokatlian, Talar

Publication Date
2012

Peer reviewed|Thesis/dissertation

UNIVERSITY OF CALIFORNIA

Los Angeles

Design and Characterization of Porous Hyaluronic Acid Hydrogels for *in vitro* and *in vivo* Non-Viral DNA Delivery

A dissertation submitted in partial satisfaction of the
requirements for the degree Doctor of Philosophy
in Chemical Engineering

By

Talar Tokatlian

2013

ABSTRACT OF THE DISSERTATION

Design and Characterization of Porous Hyaluronic Acid Hydrogels for *in vitro* and *in vivo* Non-Viral DNA Delivery

by

Talar Tokatlian
Doctor of Philosophy in Chemical Engineering
University of California, Los Angeles, 2013
Professor Tatiana Segura, Chair

Natural wound healing and angiogenesis are a result of a cascade of bioactive signals being delivered at specified times in response to local biological cues. However, for ischemic wounds which cannot heal naturally, external therapies are required. We are interested in engineering hydrogel scaffolds for cell-demanded release of non-viral DNA nanoparticles to more efficiently guide blood vessel formation in such tissues. Vascularization within tissue-engineered constructs still remains the primary cause of construct failure following implantation. While a myriad of approaches to enhance the vascularization of implants are being investigated none have completely solved the problem. We investigated two hypotheses to enhance scaffold vascularization, both long-term mechanical support and DNA delivery. Our preliminary *in vivo* studies showed that after subcutaneous implantation for three weeks enzymatically degradable hydrogels had cellular infiltration only at the periphery of the hydrogel,

while hydrogels with micron sized interconnected pores (μ-pore) were extensively infiltrated. Significant positive staining for endothelial markers (PECAM) was also found for μ-pore implants and not for nano-pore implants, even in the absence of pro-angiogenic factors. We hypothesized that an open pore structure will increase the rate of vascularization through enhanced cellular infiltration and that the added delivery of DNA encoding for angiogenic growth factors would result in long lasting angiogenic signals.

To test these hypotheses, two approaches to make DNA-loaded enzymatically degradable μ-pore hydrogel scaffolds were developed. In the first approach, polystyrene nanoparticles, similar in size to DNA polyplexes, were immobilized to the hydrogel pore surface through protease sensitive peptide tethers. Enzymatically degradable tethers have been utilized for the immobilization and release of growth factors and small drugs, which are only liberated by cleavage caused by cell secreted proteases, such as matrix metalloproteinases (MMPs) or plasmins, during local tissue remodeling. These proteases are known to be up-regulated during wound healing, microenvironment remodeling, and in diseased states and can, therefore, serve as triggers for bioactive signal delivery. The goal was to use peptide sequences that have been shown to degrade at different rates through the action of MMPs to achieve temporally controlled nanoparticle internalization by cells that overexpress MMPs. Cellular internalization of the peptide-immobilized nanoparticles was shown to be a function of the peptide sensitivity to proteases, the number of tethers between the nanoparticle and the biomaterial and the MMP expression profile of the seeded cells. By immobilizing nanoparticles through protease sensitive peptide tethers, release was tailored specifically for an intended cellular target, which over-expresses such proteases.

Alternatively, in the second approach, μ-pore hyaluronic acid-MMP (HA-MMP) hydrogels were used to encapsulate a high concentration of DNA/poly(ethylene imine) polyplexes using a previously developed caged nanoparticle encapsulation (CnE) technique. Porous hydrogels provide the additional advantages of being able to effectively seed cells in vitro post scaffold fabrication and allow for cell spreading and proliferation without requiring extensive degradation. Thus, release of encapsulated DNA polyplexes was assessed in the presence of mMSCs in hydrogels of various pore sizes (30, 60, and 100 μm). Steady release was observed starting by day four for up to ten days for all investigated pore sizes. Likewise, transgene expression in seeded cells was sustained over this period, although significant differences between different pore sizes were not observed. Cell viability was also shown to remain high over time, even in the presence of high concentrations of DNA polyplexes. Combined these results suggested that DNA nanoparticle internalization and subsequent transgene expression could be controlled by both the protease expression profile of the seeded or infiltrating cells as well as the structural properties of the hydrogel.

Using the knowledge acquired through these in vitro models, 100 and 60 μm porous and nano-pore HA-MMP hydrogels were used to study scaffold-mediated gene delivery for local gene therapy in both a subcutaneous implant and wound healing mouse models. Hydrogels with encapsulated pro-angiogenic (pVEGF) or reporter (pGFPluc) plasmids were tested for their ability to induce an enhanced angiogenic response by transfecting infiltrating cells in vivo. GFP expression in control hydrogels was used to track transfection at one, three, and six weeks in the subcutaneous implant study. While GFP-expressing transfected cells were present inside all hydrogel samples over the course of the study, transfection levels peaked around week three for 100 and 60 μm porous hydrogels. Transfection in nano-pore hydrogels continued to

increase over time corresponding with continued gel degradation. Transfection levels of pVEGF, however, did not seem to be high enough to enhance angiogenesis by increasing vessel number, maturity, or size. Only in 60 μm porous hydrogels did the VEGF expression play a role in preventing vessel regression and helping to sustain the number of vessels present from three to six weeks. Regardless, pore size seemed to be the dominant factor in determining the angiogenic response with 60 μm porous hydrogels having more vessels present per area than 100 μm porous hydrogels at the initial onset of angiogenesis at three weeks. Increased pore rigidity may have been a key factor.

The effect of porosity on wound healing was even more pronounced than what was observed in the subcutaneous implants. 100 and 60 μm porous hydrogels allowed for significantly faster wound closure than nano-pore hydrogels, which did not degrade and essentially provided a mechanical barrier to closure. Interestingly, total porosity and not specific pore size seemed to be the dominant factor in determining the wound closure rates. GFP-expressing transfected cells were present throughout the newly formed granulation tissue surrounding all hydrogel samples at two weeks. Transfection levels of pVEGF, however, did not seem to be high enough to enhance angiogenesis within the granulation tissue by statistically increasing vessel number, maturity, or size. Although the anticipated enhancement in angiogenesis in either model was not shown, the presence of transfected cells shows promise for the use of polyplex loaded porous hydrogels to produce a response in vivo.

With further optimization we believe the proposed hydrogel system(s) has applications for controlled release of various DNA particles and other gene delivery vectors for in vivo tissue engineering and blood vessel formation.

The dissertation of Talar Tokatlian is approved.

James Liao

Harold Monbouquette

Andrea Kasko

Tatiana Segura, Committee Chair

University of California, Los Angeles

2013

Dedication

I dedicate this dissertation to my family.

Mom and Bob

Tam

Diko and Arman

Gasia and Koko

Without all your love and support this dissertation would not have been possible.

TABLE OF CONTENTS

LIST OF FIGURES AND TABLES

Figures

Tables

ACKNOWLEDGEMENTS

This dissertation would not have been possible without the support and guidance of so many individuals. First I would like to thank my family. Without their continuous and truly unconditional love and support I would not have been able to accomplish this. Mom and Bob, you two are the best parents in the world. Even when you could not help me with my work, you would find the time to call or show up to give me the moral support that I needed. You guys did everything that was possible to make my life easy and less stressful and I love you both so, so much. Tamar, words cannot explain how you have supported me. Writing about you makes me very emotional so I will just leave your part short and sweet. I love you like crazy and I hope I can be a shoulder to you one day as you have been to me. Diko, Arman, Gasia, and Koko, thank you guys for making my life so wonderful and sweet. I love you guys so much and cannot imagine what my life would have been like without even one of you. Thank you Diko for supporting me so much even though you have so many other people you support and take care of. You always made time for me. Also, to my aunt Acku, thank you for always supporting and caring about me. I love you very much.

I want to also thank Tatiana. You have been an amazing mentor and I am so lucky to have worked with you these last five years. You were always so supportive and gave me so many opportunities to grow and be a successful researcher. I appreciate your professionalism, your optimism, and your ability to handle so many different things at once while always maintaining your composure. Thank you for showing me that I do not need to be stressed to be successful and that it is possible to have a great career and a great family all at the same time. I still really don't know how you do it, but hopefully I will learn soon!

Another person who has been so special and important to me is Jerry. Like my family, you have supported me so, so much. We have been so far apart these last years, but you have still managed to be a huge part of my life and supported me emotionally and believed in me. I love you and thank you so much for all you have done.

I also cannot forget my friends and colleagues throughout these years. Quinn, Leo, and Sean. You were my first mentors and I learned so much from each of you. I learned how to be a researcher, how to think critically, how to work respectfully and collaboratively, and to have pride and enthusiasm for my work and my lab. I hope you three all know what you mean to me, because I cannot explain it in words. I really hope we will all have the chance to work together again in the future. I trust and respect you guys so much. Thanks to Anandika for going through this long, crazy journey with me! Thank you to Shiva and Jon. I don't know what lab would have been like without you guys. You supported me so many times more than you will know. Thanks to Jianjun, Lina, Don, and Allyson. I hope I can be as influential of a postdoc in my new lab as you all have been in our lab. You have been great role models for me and each of you has taught me very different things. Thank you to Cynthia, Suwei, Giovanny, Shayne and Sandy. You guys have been great labmates and have all taught me how to be a better researcher and mentor. Cynthia, I especially want to thank you because without your help in the last few months I would not have been able to be nearly as productive. I didn't get enough time with Norman and Nikki, but I know you guys will be great. I also cannot forget all the undergrads and high school students who have worked with me, especially Warren, Rob, Chad, and Shayne. You guys learned as I learned. I am so thankful that I was able to work with each of you. You guys definitely do not know how much you helped me grow. I learned to better manage my time, to explain my

thoughts and ideas, to trust others with my work, and to be a better mentor. No one will replace you guys.

I also want to thank the other mentors I have had along the way. Dr. Kasko, Dr. Monbouquette, Dr. Liao, and Dr. Iruela-Arispe. Your questions and comments have driven me to think more broadly and critically about my work. Thank you to Dr. Iruela-Arispe for allowing me to work in your lab for those three months. I also want to especially thank Dr. Toni Torres-Collado. Toni, you were a great mentor and I very much appreciated the time you spent working with me. You have continued to be a great colleague and I hope we will be able to work together again in the future. I also want to acknowledge my amazing mentors at Novartis, Dr. Jeremy Baryza and Dr. Elizabeth Wiellette. I respect you both very much. Thank you for giving me the freedom to explore my ideas and the opportunities to share my work with others at Novartis. My internship was one of my favorite parts of graduate school!

I would also like to thank some individuals for their invaluable technical support over these last 5 years. Thank you to Dr. Armando Durazo at the UCLA Molecular Instrumentation Center for running all elemental analysis samples and Dr. Jianjun Zhang, Dr. Zheng Chen and Dr. James Dorman for their help with SEM imaging. I especially thank Dr. Joanne Zahorsky-Reeves and Dr. Joanne Sohn for their continuous help with the animal models, as well as Dr. Lloyd Miller for technical support.

I would also like to acknowledge the funding sources that made the research in this dissertation possible – NIH (1R21EB007730-01), NSF (CAREER 0747539), CRCC, and NIH Biotech Training Grant (T32GM067555).

VITA

Education

B.S., Chemical Engineering, emphasis in Biotechnology, University of California, Berkeley, 2007

Honors and Awards

2011-2012 Dissertation Year Fellowship, University of California, Los Angeles
2009-2011 NIH Biotechnology Training Grant, University of California, Los Angeles
2007-2008 Mangasar Mangasarian Scholarship, University of California, Los Angeles

Research Experience

2008-2012 Graduate student researcher; Principal Investigator Tatiana Segura
Chemical & Biomolecular Engineering Department, UC Los Angeles
Research area: Controlled nanoparticle delivery, engineering porous hydrogels
Experience with mouse subcutaneous implant and wound healing models

Summer 2011 Graduate student intern; Managers Jeremy Baryza and Elizabeth Wiellette
Global Discovery Chemistry and Developmental and Molecular Pathways, Novartis Institutes for Biomedical Research
Research area: Engineering defined hydrogel systems for small intestinal organoid culture, nano- and macro-gels for antibody/siRNA delivery

Summer 2010 Graduate student researcher; Principal Investigator Luisa Iruela-Arispe
Molecular and Cell Developmental Biology Department, UC Los Angeles
Research area: Syndecan-4 involvement in tumor metastasis and angiogenesis
Experience with mouse lung metastasis and subcutaneous tumor growth models

2005-2007 Undergraduate research assistant; Principal Investigator Douglas Clark
Chemical Engineering Department, UC Berkeley
Research area: Thermophilic proteins, protein stability and characterization

Peer-Reviewed Publications

1. **Tokatlian, T**, Cam, C, Siegman, SN, Lei, Y, and Segura, T "Design and Characterization of μ-Porous Hyaluronic Acid Hydrogels for in vitro Gene Transfer to mMSCs" Acta Biomaterialia (2012) 8(11):3921-31
2. Zhang, J, **Tokatlian, T**, Zhong, J, Ng, QKT, Patterson, M, Lowry, B, Carmichael, ST, and Segura, T "Physically Associated Synthetic Hydrogels with Long-Term Covalent Stabilization for Cell Culture and Stem Cell Transplantation" Advanced Materials (2011) 23(43):5098-5103
3. Gojgini, S, **Tokatlian, T**, and Segura, T "Utilizing Cell-Matrix Interactions to Modulate Gene Transfer to Stem Cells Inside Hyaluronic Acid Hydrogels" Molecular Pharmaceutics (2011) 8(5):1582-91
4. **Tokatlian, T**, Shrum, CT, Kadoya, WM, and Segura T "Protease Degradable Tethers for Controlled and Cell-Mediated Release of Nanoparticles in 2- and 3-Dimensions" Biomaterials (2010) 31(31):8072-80
5. **Tokatlian, T**, and Segura, T "siRNA Applications in Nanomedicine" WIRES Nanomedicine and Nanobiotechnology (2010) 2(3):305-15
6. Bergeron, LM, **Tokatlian, T**, Gomez, L, and Clark, DS "Redirecting the Inactivation Pathway of Penicillin Amidase and Increasing Amoxicillin Production via a Thermophilic Molecular Chaperone" Biotechnology and Bioengineering (2009) 102(2):417-23
7. Bergeron, LM, Lee, C, **Tokatlian, T**, Höllrigl, V, and Clark, DS "Chaperone Function in Organic Co-Solvents: Experimental Characterization and Modeling of a Hyperthermophilic

Chaperone Subunit from Methanocaldococcus Jannaschii" Biochimica et Biophysica Acta (2008) 1784(2):368-78

Podium Presentations (* represents presenting author)

1. **Tokatlian, T***, Cam, C, Siegman, SN, Lei, Y, and Segura, T "Design and Characterization of μ-Porous HA Hydrogels for Non-Viral DNA Delivery" AIChE National Conference Oct 2012 Lawrence Convention Center, Pittsburgh PA
2. **Tokatlian, T***, Cam, C, Siegman, SN, Lei, Y, and Segura, T "μ-Porous HA Hydrogels for Non-Viral DNA Delivery" 7th Nagoya University – UCLA International Symposium Sep 2012 Hotel Leopalace, Sapporo, Japan *(winner of Best Technical Presentation)*
3. **Tokatlian, T*** and Segura, T "Engineering Cell-Triggered Release to Achieve Temporal Control" UCLA-NIH Biotechnology Symposium June 2011 UCLA Faculty Center, Los Angeles CA
4. **Tokatlian, T***, Shrum, CT, Kadoya, WM, Cam, C, Siegman, S, and Segura, T "Engineering Cell-Triggered Release to Achieve Temporal Control" Society for Biomaterials National Conference April 2011 Disney World Convention Center, Orlando FL
5. **Tokatlian, T***, Shrum, CT, Kadoya, WM, and Segura, T "Immobilization of Nanoparticles Through Protease Degradable Tethers for Controlled and Cell Specific Release" AIChE National Conference Nov 2009 Gaylord Opryland Hotel, Nashville TN
6. **Tokatlian, T*** and Segura, T "Assessment of Biotin-Streptavidin Surface Stability In the Presence of Various Proteases for Controlled Release of DNA Polyplexes" AIChE National Conference Nov 2008 Downtown Convention Center, Philadelphia PA

Poster Presentations (* represents presenting author)

1. **Tokatlian, T***, Cam, C, Siegman, SN, and Segura, T "Design and Characterization of μ-Porous HA Hydrogels for Non-Viral DNA Delivery" BioInspired Materials Gordon Research Conference June 2012 Davidson College, Davidson NC
2. **Tokatlian, T*** and Segura, T "Design of μ-Porous Hydrogels for Stem Cell Culture and Tissue Regeneration" National Graduate Student Research Conference Oct 2011 National Institutes of Health, Bethesda MD
3. **Tokatlian, T***, Siegman, SN, Cam, C, and Segura, T "in vitro and in vivo Gene Transfer from μ-Porous Hydrogels for Tissue Engineering and Angiogenesis" UCLA Engineering Technology Forum March 2011 Covel Commons UCLA, Los Angeles CA
4. **Tokatlian, T***, Shrum, CT, Kadoya, WM, and Segura, T "Engineering Cell-Mediated Release to Control the Release Rate of Nanoparticles" 16th International Vascular Biology Meeting June 2010 UCLA, Los Angeles CA
5. **Tokatlian, T***, Shrum, CT, Kadoya, WM, and Segura, T "Protease Degradable Tethers for Controlled and Cell-Mediated Release of Nanoparticles in 2- and 3-Dimensions" UCLA Engineering Technology Forum Feb 2010 CNSI UCLA, Los Angeles CA
6. **Tokatlian, T***, Kadoya, WM, Zhang, J, and Segura, T "Immobilization of Nanoparticles Through Protease Degradable Tethers for Controlled and Cell-Demanded Release" Gordon Research Conference July 2009 Holderness School, Holderness NH
7. **Tokatlian, T*** and Segura, T "Design of Materials for Sequential Cell-Mediated Gene Transfer" UCLA-NIH Biotechnology Symposium June 2009 UCLA Faculty Center, Los Angeles CA
8. **Tokatlian, T*** and Segura, T "Design of Materials for Sequential Cell-Mediated Gene Transfer" UCLA Engineering Technology Forum Apr 2009 CNSI UCLA, Los Angeles CA

Teaching and Mentoring Experience (F=fall, W=winter, S=spring, Su=summer quarter)

F08	CBE 115/215 "Biochemical Reaction Engineering"
S08, S09	CBE 125/225 "Bioseparations and Bioprocess Engineering"
Su10-S12	Graduate student mentor, Undergraduate Research Center, UCLA
Su08-S12	Graduate research mentor, Segura Laboratory, UCLA

CHAPTER 1

OVERVIEW OF DISSERTATION AND SPECIFIC AIMS

1.1 Motivation and Objectives

Over the last 20 years the field of tissue engineering has emerged in order to compensate for the growing need of organs for transplantation and disease treatment. In certain cases, whole organs may need to be regenerated or replaced due to organ failure (heart, kidney, etc.). Advances have been made by using extracellular matrices to grow new tissues in vitro for implantation or by using synthetic materials, as is the case for some of the first FDA approved engineered skin grafts, Apligraf®, Dermagraft®, Orcel™, and Integra® Dermal Regeneration Template [1]. Alternatively, when it is not feasible to replace the organ completely it may be necessary to regenerate or repair the organ or tissue back to a functional state. For example in skin wounds, heart attack (ischemic tissue), or stroke (ischemic tissue), biologically suitable materials can be used in these instances to facilitate tissue regeneration by providing physical and chemical cues to the surrounding injured tissue or also to be a means to implant stem cells for additional repair.

Current tissue engineering scaffolds for tissue regeneration consist of scaffolds loaded with (1) bioactive signals, such as drugs, proteins, DNA, or siRNA, or (2) stem cells or (3) a combination of the two which are then implanted into the body in the area of disease or injury **(Figure 1.1)**. Although there is promise in delivering adult stem cells to aid in tissue regeneration, the source of viable stem cells, immunogenicity, and

ethical issues have thus far prevented this approach from becoming a realistic option for tissue repair. In the alternative approach of delivering bioactive signals it is assumed that the surrounding tissue is functional enough (i.e. contains enough healthy progenitor cells) to be able to recover and regenerate new tissue based on supportive cues provided by the incorporated signals.

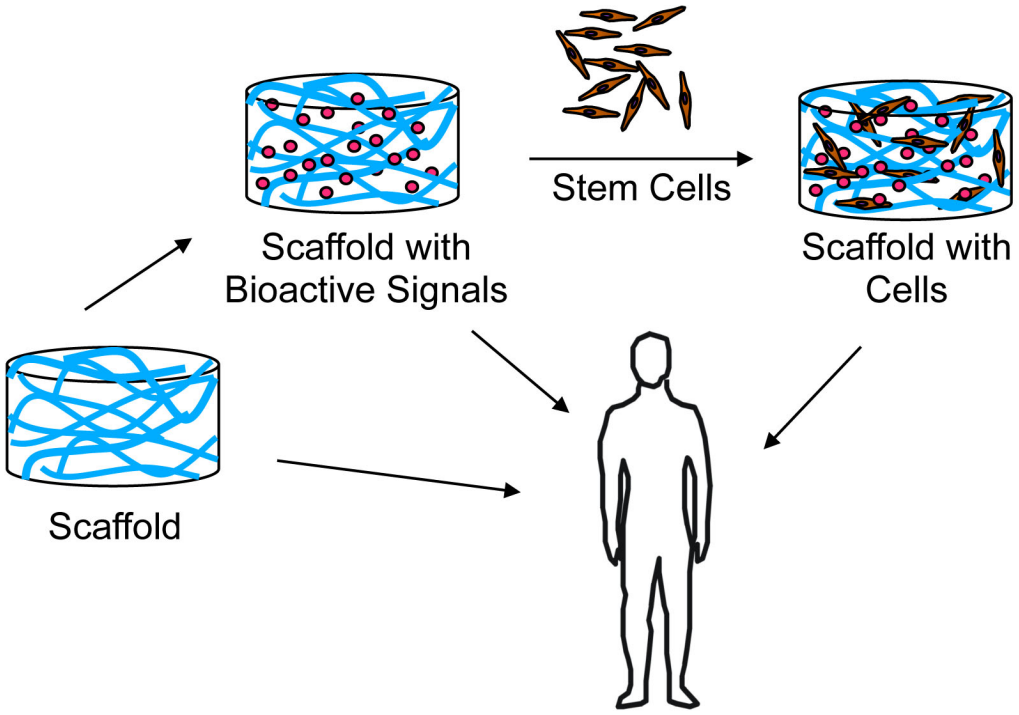

Figure 1.1: General overview of tissue engineering scaffolds. Scaffolds may or may not be loaded with bioactive signals and/or stem cells prior to implantation.

However, many of the recent technologies are still being met with limited success because they are unable to promote rapid vascular in-growth, limiting the size and effectiveness of the implanted scaffold [2, 3]. Without vessels present to allow for diffusion and transport of nutrients and removal of waste products implanted or infiltrating cells will not be able to survive far from the edge of the scaffold. For this reason, so far the main biomaterial products that have succeeded into the clinic are

aimed at regenerating or repairing primarily avascular tissues, such as cartilage or partial-thickness skin which naturally do not rely on a large blood supply [1]. Alternatively, this has been the main challenge in the development of biomaterials for highly vascular tissues, such as full-thickness skin, muscle, liver, heart, and brain. While several strategies have been developed to enhance scaffold vascularization, each strategy alone has been insufficient in providing long-term success. In most cases, angiogenesis, which is the formation of blood vessels from pre-existing vessels, is stimulated as a result of an incorporated bioactive signal, but as soon as the signal fades there is regression of vessels from the implant site [4].

Thus, the overall focus of my research has been to develop scaffolds which will help promote angiogenesis and rapid vascular in-growth into the implanted scaffold.

1.2 Specific Aims

The objective of this research was to develop a porous hyaluronic acid hydrogel for controlled non-viral gene delivery to promote angiogenesis in soft tissue, specifically in skin. Hydrogels are a specific type of scaffold that are formed through covalent or physical interactions between polymers and are composed of 90-98 % water. They resemble soft tissue with respect to their mechanical properties and their swollen networks are similar in structure to collagen or elastin networks found in the extracellular matrix (ECM) surrounding cells in vivo. And although several strategies have been reported (see Chapters 2 – 3) to promote angiogenesis within implanted scaffolds, these strategies have not come together to form a rationally designed hydrogel that promotes angiogenesis over the therapeutic timeframe required for new tissue formation. The research conducted in this dissertation attempts to engineer a hydrogel that meets these criteria. The following section describes the proposed

specific aims, which guided the experimental research described in Chapters 4 – 8. Following each aim, the specific hypothesis will be described.

1.2.1 Specific Aim 1 (Chapter 4)

This aim investigated porous HA hydrogels for enhancement of scaffold vascularization in vivo. Specifically a mouse subcutaneous implant model was utilized for this assessment. The subcutaneous implant model was also optimized in this aim for the Segura laboratory.

Hypothesis 1: The presence of interconnected, micron-sized pores will allow for rapid vascular infiltration in comparison to more traditional nano-pore HA hydrogels which require sufficient degradation for cells to infiltrate.

1.2.2 Specific Aim 2 (Chapter 5)

This aim developed a strategy to deliver tethered nanoparticles in vitro to mouse mesenchymal stem cells from both two-dimensional surfaces and three-dimensional porous PEG hydrogels. The tethers utilized in this aim are matrix metalloproteinase (MMP) degradable peptide tethers, which will only be cleaved in the presence of cell-secreted MMPs.

Hypothesis 2: The sequence (and specificity to MMP-2) of the peptide tethers will determine the release and internalization of the nanoparticles by MMP-2 expressing cells. Alternatively, if cells do not express the appropriate protease they will not be able to cleave the peptide tethers and internalize the nanoparticles.

Hypothesis 3: Increasing tethering to the biomaterial surface by increasing the number of tethers on the nanoparticle surface will slow down the release and internalization of the nanoparticles.

1.2.3 Specific Aim 3 (Chapter 6)

This aim tested the strategy to deliver encapsulated non-viral DNA nanoparticles in vitro to mouse mesenchymal stem cells from porous HA hydrogels. A previously described technique to load high concentrations of DNA/poly(ethylene amine) nanoparticles was utilized in this aim. Gene transfer efficiency was also tested with respect to different pore size hydrogels.

Hypothesis 4: Cells will be transfected with non-viral DNA as the DNA nanoparticles are released from the hydrogel upon hydrogel degradation by cell-secreted MMPs.

1.2.4 Specific Aim 4 (Chapter 7)

This aim used the encapsulated non-viral DNA nanoparticle strategy to enhance angiogenesis in vivo in a mouse subcutaneous implant model over a 6-week period. Techniques for the assessment of transfection and angiogenesis were also developed and optimized in this aim for the Segura laboratory.

Hypothesis 5: Host cells infiltrating the hydrogels will be transfected with non-viral DNA as the DNA nanoparticles are released from the hydrogel upon hydrogel degradation by cell-secreted MMPs.

Hypothesis 6: The incorporation of therapeutic (i.e. pro-angiogenic) VEGF plasmid containing DNA nanoparticles will additionally enhance angiogenesis within porous hydrogels. As infiltrating cells are transfected and VEGF is expressed within the pores of the hydrogels, blood vessels and, specifically, endothelial cells will be directed to migrate into the hydrogel pores.

Hypothesis 7: Pore size will play a role in cellular infiltration and subsequent transfection and angiogenesis in vivo.

1.2.5 Specific Aim 5 (Chapter 8)

This aim used the encapsulated non-viral DNA nanoparticle strategy to enhance angiogenesis and wound closure in a splinted mouse wound healing model over a 14-day period. The splinted wound healing model was also developed in this aim from previously reported techniques and optimized for hydrogel characterization in the Segura laboratory.

Hypothesis 8: The HA hydrogel will aid in wound healing by providing mechanical support to the surrounding tissue, a bridge for re-epithelialization, and, combined with the splint, a barrier for tissue contraction.

Hypothesis 9: Host cells infiltrating the hydrogels will be transfected with non-viral DNA as the DNA nanoparticles are released from the hydrogel upon hydrogel degradation by cell-secreted MMPs.

Hypothesis 10: The incorporation of therapeutic (i.e. pro-angiogenic) VEGF plasmid containing DNA nanoparticles will additionally enhance angiogenesis within porous hydrogels. This will result in faster wound closure and more mature tissue regeneration.

Hypothesis 11: Pore size will play a role in cellular infiltration, re-epithelialization, and wound closure in vivo. Subsequently, transfection and angiogenesis will be affected.

1.3 Dissertation Outline

After this introduction, Chapters 2 – 3 will provide relevant background to the dissertation topic. In Chapter 2 hydrogel design parameters will be discussed as well as recent approaches to promote angiogenesis using biomaterials. Next, in Chapter 3 non-viral gene delivery will be introduced. Justification will be provided for the use of non-viral DNA nanoparticles in comparison to the direct use of growth factors and also to more efficient transfection agents, viral DNA vectors. Following these background chapters, the rest of the dissertation will go into the specifics of the research conducted to design a hydrogel which will help promote angiogenesis and rapid vascular in-growth by smart structural and material design coupled with controlled non-viral DNA delivery. **Figure 1.2** illustrates the flow of the dissertation.

Specifically, in Chapter 4 the preliminary in vivo studies comparing nano-porous to micro-porous hyaluronic acid hydrogels are described. The results clearly demonstrate that while the pre-formed pores are essential for cellular infiltration and angiogenesis, additional bioactive signals may be required for enhanced vessel formation (i.e. increased vessel number and/or maturity). As a result, two approaches for controlled signal delivery are proposed. Chapter 5 discusses the first approach of using tethered nanoparticles, in which the tether is a protease degradable peptide that will be cleaved to release the nanoparticle only in the presence of a specific cell-secreted protease. Here instead of non-viral DNA nanoparticles, fluorescent polystyrene nanoparticles are used for their easy of use (non-aggregating) and

detection/tracking. The tethers are peptide sequences that have previously been reported to have varying sensitivities to MMP-1/2. Both the peptide sequence and the degree of particle tethering are shown to have an effect on particle release and internalization for 2-dimensional surfaces as well as 3-dimension porous hydrogels. Then in Chapter 6 the second approach of using encapsulated nanoparticles is discussed. Here non-viral DNA nanoparticles formed using linear poly(ethylene amine) (L-PEI) are encapsulated within the porous hydrogel material and released as a result of hydrogel degradation. Various pore sizes are also tested, although no significant differences in in vitro transfection efficiency are observed.

After having described these two approaches, Chapters 7 and 8 move on to use the second approach for nanoparticle delivery in two different animal models. In Chapter 7 in vivo transfection of a GFP-luciferase reporter plasmid is assessed in a mouse subcutaneous implant model. To test the effects of transfection on angiogenesis, a therapeutic plasmid encoding for vascular endothelial growth factor (VEGF) is also introduced. The effect of pore size on angiogenesis and transfection are also analyzed. Continuing onto Chapter 8, the same hydrogel conditions are tested in a splinted wound healing model in diabetic (db/db) mice. Here the main goal was to assess the effects of non-viral DNA delivery from porous hyaluronic in a relevant disease model. Similar, although somewhat enhanced, angiogenic responses were observed in porous hydrogels in comparison to what was observed in the less severe subcutaneous implant model. However, as will be described in detail in both Chapters 7 and 8, the delivery of pVEGF/L-PEI was not found to significantly improve angiogenesis inside the hydrogels at the tested concentrations. Finally, in Chapter 9, conclusions, suggestions for experimental changes, and possible future directions are provided.

This dissertation represents over five years of graduate work and ends at a point where several new research projects may begin. Although the goal was to design an optimal porous hydrogel for non-viral DNA delivery, only the surface has been scratched from what will be the hydrogel system that eventually moves on to the clinic. The work described in this dissertation outlines the basic criteria that need to be met for this research to move forward and become a success.

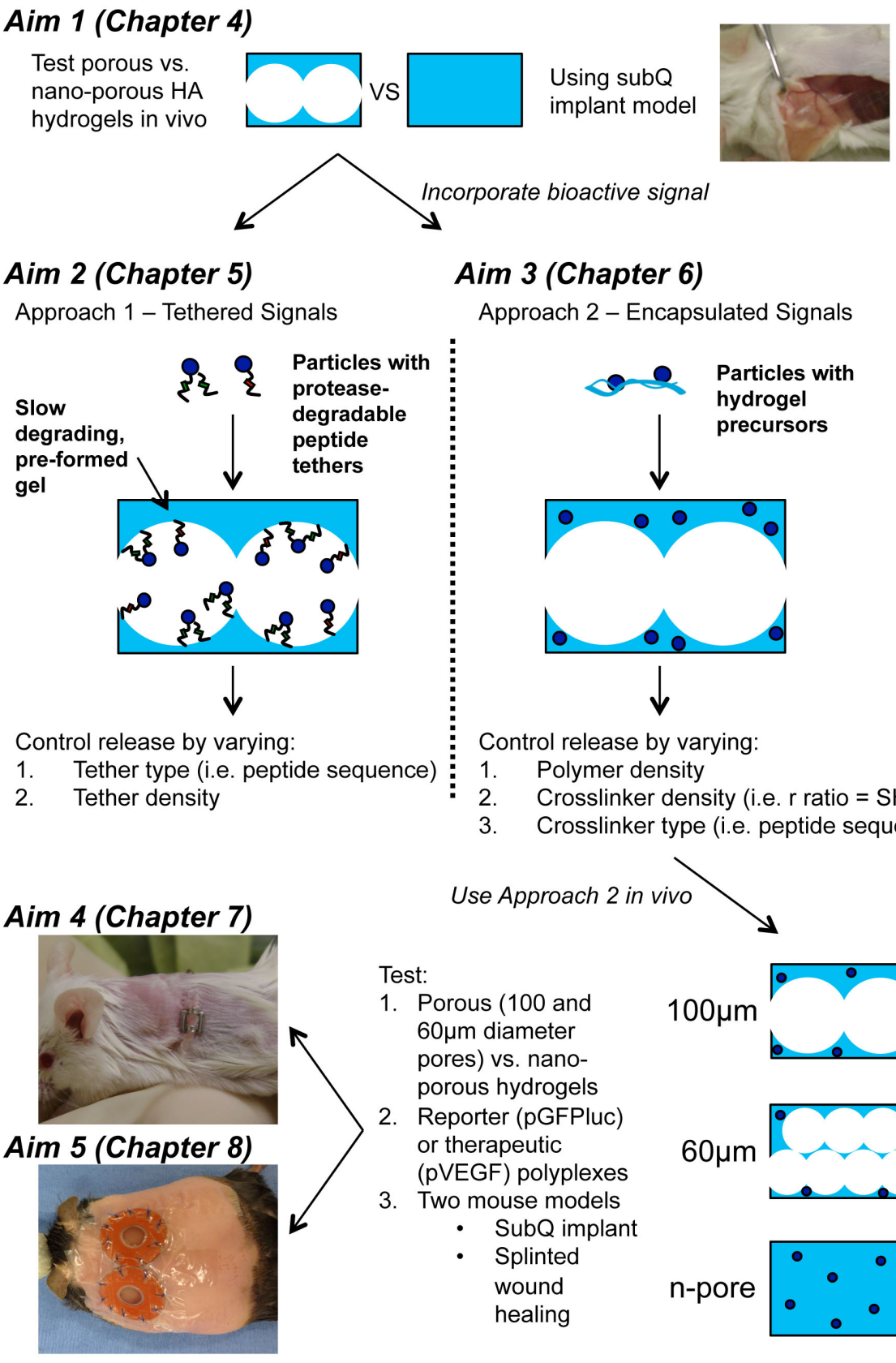

Figure 1.2: General dissertation overview.

CHAPTER 2

SCAFFOLDS FOR VASCULARIZATION

2.1 Vascularization key challenge for tissue engineering

Vascularization of tissue engineering constructs remains the primary reason for construct failure in vivo [2, 3]. Without the rapid infiltration of blood vessels, diffusion alone is insufficient to sustain migrating endogenous or exogenously implanted cells more than 150 – 200 μm from the construct surface **(Figure 2.1)**. For acellular scaffolds, vessels need to grow into the scaffold at a minimum of a few days to a week after endogenous cells begin to infiltrate greater than 200 μm into the scaffold to prevent cells from dying or migrating back out into the native tissue. Alternatively, for scaffolds loaded with cells, without vascular infiltration within the first few days after implantation, cells far from the scaffold surface will begin to die upon oxygen and glucose depletion. Diffusion limitations then dictate the overall size and function of the implant, limiting their applicability in vivo to small injuries and defects [2, 5]. This is especially true for cells types which are more sensitive to hypoxia, such as neurons or cardiomyocytes. Thus, the promotion of angiogenesis (i.e. the formation of new vessels from pre-existing vessels) is essential for tissue engineering construct success. While angiogenic stimulation is the general strategy for vascularizing scaffolds upon implantation, an alternative approach is to pre-vascularize scaffolds in vitro or in vivo prior to implantation in the area of need [5]. Justification for scaffold pre-vascularization stems from the slow physiological growth rate of microvessels (~5

μm/h) in vivo [6, 7], which would prevent cell survival in the center of large constructs soon after implantation even with successful angiogenic stimulation. This idea was first proposed by Mikos, et. al. for porous poly(L-lactic acid) scaffolds which were pre-vascularized in rats prior to use [8]. Scaffolds were initially implanted into the highly vascular mesentery of adult rats where tissue and vascular in-growth occurred for 35 days after which scaffolds were removed and seeded with cells in vitro. Although these scaffolds were not re-implanted, they demonstrated the potential for in vivo pre-vascularization. The main draw-back for this technique is that it involves two highly invasive surgeries to implant and remove the scaffold prior to use. Alternatively, in vitro pre-vascularization entails scaffold seeding with endothelial cells or a co-culture of cells (i.e. endothelial cells with smooth muscle cells or fibroblasts) which are allowed to form into tube like structures prior to implantation. This technique has been especially successful in fibrin gels [9]. Since then more progress has been made to pre-vascularize scaffolds, however, these constructs have only shown success in immune-compromised animals and the source of cells that would be used for in vitro pre-vascularization for future clinical applications is still not clear. For these reasons, we have focused on angiogenic stimulation into acellular constructs.

Efforts have already been made to promote angiogenesis within implanted hydrogels through smart hydrogel design, hydrogel materials, and incorporation of pro-angiogenic growth factors and genes. Evaluation of current techniques in hydrogel design and materials will be discussed here. Localized signal delivery from hydrogels will be expanded on in Chapter 3.

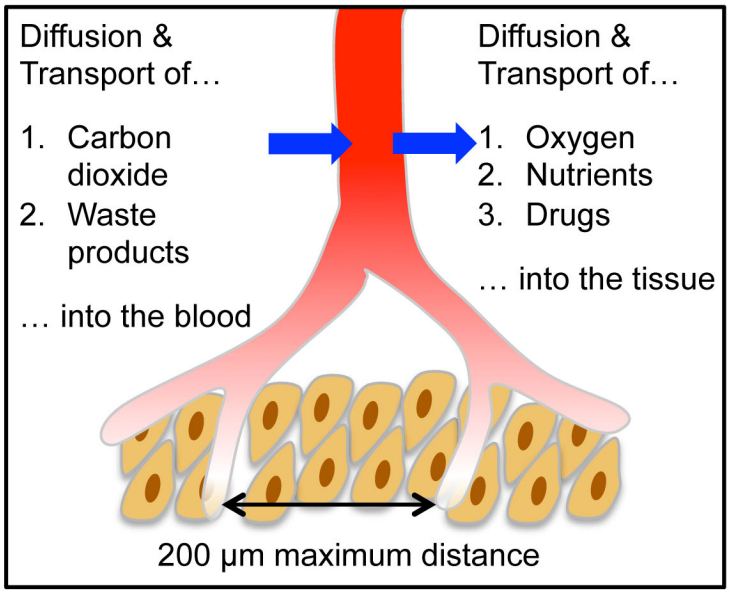

Figure 2.1: Schematic to illustrate requirement for vascularization. Diffusion of oxygen and nutrients is insufficient past 200µm from a vessel.

2.2 Designing porous architecture for angiogenesis

During the course of this thesis, a major emphasis by researchers on macroscopic biomaterial design to help promote biomaterial vascularization has been placed. Patterning technologies, such as micro-contact printing, micro-molding, photolithography, micromachining, and laser-guided writing, have been used to form functional vascular structures inside biomaterials [10]. Although these patterning technologies allow for precise control over structure, issues with mass production has so far limited their clinical use. Alternatively, micro-scale interconnected pores produced through salt-leaching [11-13], gas foaming [14-16], lyophilization [17-20], and sphere templating [21-24] have shown to be effective in allowing for cellular migration in vitro [19, 25, 26] and tissue integration and, subsequent, enhanced scaffold vascularization in vivo [12, 22]. Chiu, et. al. demonstrated that increasing pore size from 25 to 150 µm in synthetic PEG hydrogels increased overall cellular infiltration

and collagen deposition, as well as vascular infiltration from the surrounding tissue into the pores of the PEG hydrogel [12]. Similarly Madden, et. al. incorporated both spherical pores as well as channels into poly(2-hydroxyethyl methacrylate-co-methacrylic acid) hydrogels which were shown to significantly enhance neovascularization four weeks after myocardial implantation [22]. However, they demonstrated that scaffold architecture influenced macrophage polarity and that an intermediate pore size of 30-40 μm lead to increased neovascularization as a result of a shift in macrophages in the M1 pro-inflammatory phase to macrophages in the M2 pro-healing (anti-inflammatory) stage.

In all of these reports, pore size was found to play a crucial role in the rate of angiogenesis and the size and maturity of the formed vessels. Healionics Corp., a company based on the early research conducted in the Ratner lab at University of Washington, has been developed to commercialize porous PLGA, silicon, and hyaluronic acid scaffolds for catheter coatings, implants, and wound healing applications. However, it is important to note that porous hydrogels constitute only ~10 % of tissue engineering scaffolds in the literature to date.

2.3 Hydrogel materials

The type of natural (i.e. collagen, alginate, chitosan, hyaluronic acid) or synthetic (i.e. poly(ethylene glycol), poly(ethylene oxide), poly(vinyl alcohol), poly(acrylic acid), polypeptides) polymer used for hydrogel preparation is an important factor in determining cell-material interactions, mechanical properties, fluid permeability and, subsequently, promotion of angiogenesis [3, 17, 27, 28]. While a synthetic polymer, such as PEG, can be biochemically inert, natural polymers possess intrinsic qualities which can play a role in signaling to surrounding cells. Inflammation has been directly

associated with the host angiogenic response with evidence which indicates a slight pro-inflammatory response may be necessary for the stimulation of angiogenesis in the implant site [5]. Thus, glycosaminoglycans, which elicit relatively mild immune responses, are suitable materials for pro-angiogenic scaffolds, unlike natural collagen gels that have the potential to induce severe inflammation [29, 30]. For the studies described in Chapters 4 – 8, HA is exclusively used.

2.3.1 Hyaluronic acid (HA)

HA, an anionic, non-sulfated glycosaminoglycan and major component of the ECM, is widely distributed in connective, epithelial and neural tissue [31, 32]. HA has gained popularity as a biomaterial for tissue engineering and regeneration due to its high biocompatibility and low immunogenicity [33-36]. Moreover, degraded fragments of HA or HA oligomers are known to promote angiogenesis and up-regulate MMP expression [37-39]. HA specifically interacts with cell surface receptors, such as CD44, RHAMM (receptor for HA mediated motility) and ICAM-1 (intercellular adhesion molecule 1), and contributes to tissue hydrodynamics, cell proliferation and migration [40, 41]. Unlike other natural hydrogels (i.e. fibrin, collagen, matrigel), HA cannot form a hydrogel on its own. However, using mild chemistries the HA backbone can be modified to contain functional groups, such as thiols, acrylates or amines, which can be further used as crosslinking sites to form hydrogels [35, 42-44]. As a result, several studies have demonstrated that HA-based hydrogels are good candidates for culturing stem cells [45-48]. Semi-synthetic hyaluronic acid (HA) hydrogels which are degradable by hyaluronidases as well as matrix metalloproteinases (MMPs) via MMP-degradable peptide crosslinkers have previously been developed for culturing mouse mesenchymal stem cells in three-dimensions [49, 50]. HA and HA-MMP degradable

hydrogels for bench-top use are now commericially available through Glycosan BioSystems, Inc. MMPs are normally expressed during tissue remodeling and are up-regulated during wound healing, microenvironment remodeling, and in diseased states and can, therefore, serve as triggers for bioactive signal delivery. Chapters 5 and 6 will describe two different approaches that will use MMP sensitive peptides to control the release of DNA nanoparticles through cell-secreted MMPs.

CHAPTER 3

NON-VIRAL GENE DELIVERY FROM SCAFFOLDS

3.1 Bioactive signal delivery

In addition to the structural characteristics of the scaffold, the effective local delivery of angiogenic growth factors is necessary to promote blood vessel formation [3, 4, 27]. However, direct delivery of angiogenic factors has been limited due to physical denaturation and rapid degradation by proteases in long-term cell culture and in vivo applications. For example, the biological half-life of PDGF, bFGF and VEGF is less than 2 [51], 3 [52], and 30 minutes [53], respectively, when injected intravenously. To compensate for this, extremely high doses are required. Hydrogel encapsulation helps to prolong growth factor stability and limits access to proteases by acting as a physical barrier [54, 55]. Vascular endothelial growth factor (VEGF) [56-58], platelet derived growth factor (PDGF) [59], basic fibroblast growth factor (bFGF) [60], keratinocyte growth factor (KGF) [61], and others have been widely utilized for this purpose and have demonstrated in vivo success. Richardson, et. al. first demonstrated that the sequential delivery of VEGF and PDGF led to significantly enhanced blood vessel formation when compared to delivery of either growth factor on its own. While growth factor delivery remains the primary method to promote angiogenesis in vivo, growth factors each have different size and charge characteristics so a universal technique to encapsulate or tether sensitive growth factors has not yet been developed.

For tissue regeneration and repair, an alternative approach to growth factor delivery is localized gene delivery. The gene encoding for the growth factor(s) of interest is delivered to encapsulated or infiltrating host cells to promote the expression of these desired factors to guide tissue processes. Relative to protein delivery, gene delivery allows for longer local expression, increased stability and resistance to environmental factors, and the potential to be delivered from an optimized universal delivery system. Gene delivery can be further subdivided into two categories: viral and non-viral. Viral gene delivery utilizes modified viral capsids to deliver genes with high efficiency [62]. However, viral vectors are limited in their clinical use due to safety concerns, immunogenicity, potential for insertional mutations, and their inability to carry large loads of DNA [63]. Alternatively, non-viral gene delivery is safer, less immunogenic, and less oncogenic, while having much lower in vitro and in vivo transfection efficiency relative to viral gene delivery [63-66]. Yet due to the potential for development into a safe and effective therapy, local non-viral gene delivery via hydrogel scaffolds has been studied for over a decade [67].

3.2 Non-viral gene delivery

Early non-viral gene delivery approaches aimed to deliver naked plasmid DNA from hydrogels [15, 68-72]. Although naked DNA can achieve gene expression and guided regeneration in vivo [15, 68, 73], its negative charge limits cellular entry and gene transfer efficiency and rapidly diffuses out of hydrogel scaffolds. These factors motivated the use of DNA nanoparticles instead of naked DNA. Non-viral vectors, such as cationic peptides, lipids, or polymers, can be used to condense large amounts of negatively charged plasmid DNA to form positively charged particles to promote internalization and transfection, while also protecting the DNA from nuclease

degradation prior to cellular entry [67, 74-76]. Poly(ethylene imine) (PEI) is the most widely utilized cationic polymer for non-viral gene delivery; it is able to condense DNA through electrostatic interactions between the positively charged amines on the PEI and the negatively charged phosphates on the DNA **(Figure 3.1)**, forming nanoparticles (polyplexes) in the range of 50 to 200 nm [77-79]. PEI has been successfully used in vivo to deliver DNA or siRNA to the brain [80, 81], lungs [82-86], abdomen [87], liver [88], and tumors [89-91].

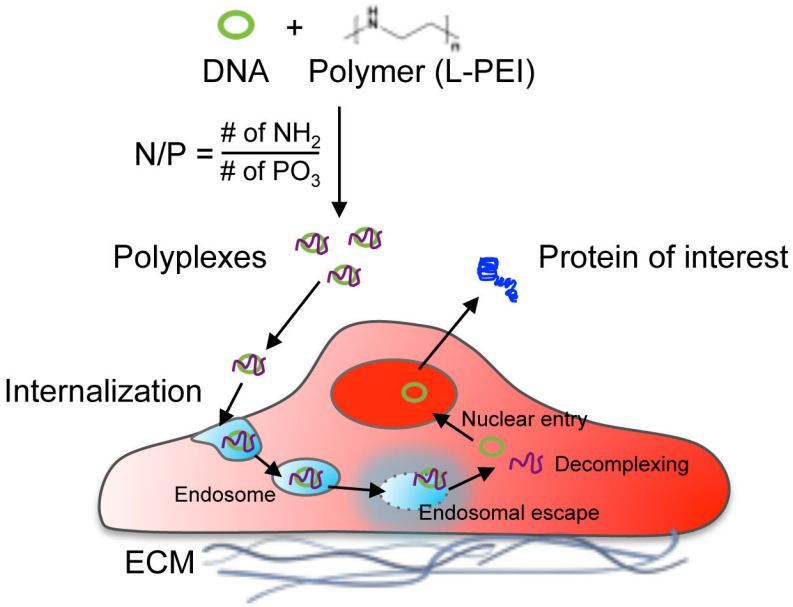

Figure 3.1: Non-viral gene delivery. Negatively charged plasmid DNA is complexed at a specific N/P ratio with positively charged linear PEI. Overall positively charged polyplexes are then endocytosed, after which a fraction achieves endosomal escape (aided by PEI) and entry into the nucleus for final production of the protein of interest.

3.3 Non-viral DNA/PEI polyplex delivery from scaffolds

DNA/PEI polyplex have been incorporated into fibrin [23, 92], alginate [71], gelatin [93], and other natural polymer based hydrogels [65]. Recently researchers have also utilized enzymatically degradable synthetic polymer scaffolds, which release their

payload upon cellular infiltration [94-96]. Lei and Segura proposed a matrix metalloproteinase (MMP) degradable PEG hydrogel system within which DNA/PEI polyplexes were encapsulated [95]. As cells degraded the matrix through secreted proteases, they were transfected with the polyplexes they encountered during their migration. Since then MMP-degradable hyaluronic acid hydrogels have also been used to encapsulate DNA/poly(PEI) polyplexes as a means of non-viral gene delivery to stem cells [97]. However, direct encapsulation of the polyplexes resulted in aggregation when the concentration exceeded 0.2 μg/μL. And for studies that have shown in vivo success, larger doses were required (≥1 μg/μL) [14, 15, 71, 93, 98]. Aggregation of polyplexes can result in increased toxicity and inconsistent transfection of encapsulated or infiltrating cells. To overcome this concentration limitation Lei, et. al. previously developed a caged nanoparticle encapsulation process (CnE) to incorporate DNA polyplexes inside of PEG (synthetic polymer, uncharged), HA (natural polymer, charged), and fibrin (protein, charged) hydrogel scaffolds without particle aggregation [99, 100]. This approach utilizes neutral saccharides (sucrose) and polysaccharides (agarose) to protect the polyplexes from inactivation and aggregation during lyophilization and hydrogel formation, respectively. This technique will be utilized in the studies described in Chapters 6 – 8.

3.4 Encapsulated vs. tethered presentation for controlled release

When polyplexes (and, likewise, other DNA nanoparticles or growth factors) are encapsulated into hydrogel scaffolds, their release is dictated by diffusion out of the gel and gel degradation kinetics. For large polyplexes and DNA nanoparticles (>40 nm) hydrogel mesh size (i.e. pore size) generally limits diffusion and requires that the gel degrade in order for release of encapsulated nanoparticles to occur. Although such

encapsulation may be favorable in some cases, in certain cases in may be important to release the signals while also maintaining the hydrogel structure for long-term mechanical and structural support to the tissue. In these instances it may be ideal to immobilize such signals to the biomaterial surface through electrostatic interactions or through covalent tethers that degrade through hydrolysis or by proteases. Electrostatic adsorption of polyplexes from 2D [101-103] and porous hydrogel [23] surfaces resulted in rapid and non-specific release of polyplexes to surrounding cells. Non-degradable tethers similarly result in non-specific release from the surface, yet have been implicated in both non-viral [104] and viral [105, 106] in situ gene delivery. In a cell-triggered release approach, peptides that are degraded by matrix metalloproteinases (MMP) at different rates are used to immobilize signals directly to the biomaterial surface. Release would then be initiated through the action of cell-released proteases and controlled by the sensitivity of the peptide to cleavage by such proteases. Enzymatically degradable tethers have been utilized for the immobilization and release of naked DNA [107], growth factors [108-110] and small drugs [111, 112], which are only liberated by cleavage caused by cell secreted proteases, such as MMPs or plasmins, during local tissue remodeling. These proteases are known to be up-regulated during wound healing, microenvironment remodeling, and in diseased states and can, therefore, serve as triggers for bioactive signal delivery [113, 114].

Some delivery systems have utilized a combination of presentation approaches or encapsulation within different phases of the scaffold for the sequential delivery of multiple growth factors and DNA polyplexes. One of the earliest examples of sequential delivery was achieved by Richardson, et. al. in 2001. PLGA scaffolds were formed with platelet-derived growth factor (PDGF) embedded into PLGA microspheres to achieve slow release and vascular endothelial growth factor (VEGF) encapsulated

into the surrounding polymer to achieve fast release [59]. Recent studies have expanded on the idea of hydrolytically degradable scaffolds for controlled release of multiple factors by varying polymer type [115], microparticle encapsulation [116], and microparticle type [117]. Sequential release of surface-coated and encapsulated DNA and DNA polyplexes has likewise been demonstrated in fibrin hydrogels [23].

3.5 Design of matrix to promote gene transfer

Since the emergence of non-viral gene delivery from hydrogel scaffolds, emphasis has been placed on matrix design to promote gene transfer. Micron-sized pores is one key factor which has shown to increase both viral [118] and non-viral [14, 15, 23] gene transfer by increasing the available surface area for cells to degrade the biomaterial and release encapsulated non-viral. Additionally, extracellular matrix (ECM) components have been investigated for their ability to up-regulate gene transfer in two-dimensions [119, 120]. Fibronectin has consistently been shown to up-regulate gene transfer in vitro through enhanced clathrin-mediated endocytosis, which resulted in more efficient gene transfer then caveolae-mediated endocytosis and macropinocytosis. Cells plated on collagen I coated surfaces had significantly reduced transfection levels compared to uncoated surfaces. Matrix stiffness, which has been found to play a direct role on stem cell differentiation, has likewise been shown to affect gene transfer in two [121] and three-dimensions [97]. Gojgini, et. al. demonstrated that softer HA hydrogels that were more easily degradable allowed for more efficient gene transfer to encapsulated mMSCs than stiff gels [97]. Within the same study, the presentation and concentration of a peptide-based cell adhesion sequence, RGD, were found to be crucial factors in determining gene transfer rates, similar to what was previously shown in 2D [122]. Finally, gradients of cells that

promote migration and subsequent transfection of cells encountering polyplexes along their path can be used as a means to increase gene transfer rates [95]. The same mMSCs loaded into PEG hydrogels as clots with cells which migrated outward away from the clot or homogeneously showed transfection of migrating cells continued to increase over 21 days while transfection of homogenously distributed cells plateaued after 7 days.

3.6 Summary

Several factors and techniques have been identified as ways to help promote scaffold vascularization for long-term vessel persistence and survival of encapsulated or infiltrating cells far from the scaffold edge. In Chapter 4 some of the basic techniques will be combined to develop a porous HA hydrogel and tested in vivo in a mouse subcutaneous implant model. The hydrogel design will then progress by incorporating DNA nanoparticles in two separate approaches in Chapters 5 and 6. Finally, the latter approach will be used to incorporate pro-angiogenic DNA polyplexes into porous HA hydrogels and assessed for angiogenic enhancement in both a subcutaneous implant and wound healing models in Chapters 7 and 8, respectively. Finally, Chapter 9 will re-visit major conclusions from each chapter (i.e. aim) and potential experiments for future students who wish to continue with this research.

CHAPTER 4

POROUS HYALURONIC ACID HYDROGELS FOR VASCULARIZATION

4.1 Introduction

As mentioned in Chapters 2 – 3, several approaches have been utilized to promote angiogenesis within biomaterial scaffolds for soft tissue repair and regeneration. Due to their relatively similar (and tunable) mechanical properties to natural tissue, hydrogels are suitable biomaterials for long-term treatment and signal delivery vehicles [123]. Here we describe an approach to incorporate a porous microstructure with a suitable natural hydrogel material, hyaluronic acid, to promote angiogenesis in vivo. At the time these experiments were being conducted (i.e. mid-2010), micron-sized pores had been shown to allow for effective cell seeding and migration in vitro [19], while very little was known about the effect of pores in vivo. A simple mouse subcutaneous implant model was used to demonstrate the effects of micro-pores on cellular infiltration and angiogenesis over a three-week period. Initially 4 % nano-pore and 100 μm porous HA hydrogels were used in order to ensure the hydrogels would not be degraded too rapidly and still be present after three weeks since protease expression levels were not exactly known, but anticipated to be much higher than in vitro levels. In vitro 3 % nano-pore HA hydrogels were used at that time to embed mMSCs [49]. These hydrogels would only last for in vitro cell culture for one to two weeks. We hypothesized that the long-term presence of interconnected, micron-

sized pores will allow for rapid vascular infiltration in comparison to more traditional nano-pore HA hydrogels which require sufficient degradation for cells to infiltrate. (Note: At this point in my research I had just started making porous hydrogels and, although I assumed the pores would make a difference in cellular infiltration, was still very surprised by the in vivo results. The data obtained from this experiment changed the direction of my research from focusing on sequential delivery to delivery from porous hydrogels!)

4.2 Materials and Methods

4.2.1 Materials

Peptides Ac-GCRDGPQGIWGQDRCG-NH2 (HS-MMP-SH) and Ac-GCGYGRGDSPG-NH2 (RGD) were purchased from Genscript (Piscataway, NJ). Sodium hyaluronan (HA) was a gift from Genzyme Corporation (60 kDa, Cambridge, MA). All other chemicals were purchased from Fisher Scientific (Pittsburgh, PA) unless otherwise noted.

4.2.2 Hyaluronic acid modification

Sodium hyaluronan was modified to contain acrylate functionalities. Briefly, hyaluronic acid (2.00 g, 5.28 mmol carboxylic acids, 60 kDa) was reacted with 18.38 g (105.50 mmol) adipic acid dihydrazide (ADH) at pH 4.75 in the presence of 4.00 g (20.84 mmol) 1-ethyl-3-[3-dimethylaminopropyl] carbodiimide hydrochloride (EDC) overnight and purified through dialysis (8000 MWCO) in DI water for 2 days. The purified intermediate (HA-ADH) was lyophilized and stored at –20 °C until used. Approximately 56 % of the carboxyl groups were modified with ADH, which was determined using 1H-NMR (D_2O) by taking the ratio of peaks at δ = 1.6 and 2.3 corresponding to the 8 hydrogens of the methylene groups on the ADH to the singlet

peak of the acetyl methyl protons in HA (δ = 1.88). HA-ADH (1.9 g) was reacted with N-Acryloxysuccinimide (NHS-Ac) (1.33 g, 7.89 mmol) in HEPES buffer (10 mM HEPES, 150 mM NaCl, 10 mM EDTA, pH 7.2) overnight and purified through dialysis in DI water for 2 days before lyophilization. The degree of acrylation was determined to be ~10 % using ^{1}H NMR (D_2O) by taking the ratio of the multiplet peak at δ = 6.2 corresponding to the cis and trans acrylate hydrogens to the singlet peak of the acetyl methyl protons in HA (δ = 1.88).

4.2.3 Design template using PMMA microspheres

PMMA microspheres (90-125 μm, Bangs Laboratories) were bought dry. Approximately 25-30 mg of beads were then added into glass-bottom silicon wells (Electron Microscopy Sciences) and covered with a glass slide. Unlike previously published techniques (e.g. rotating slide at 250 rpm for 4 h [24], the beads were then packed by slight tapping for 1-2 min and examined for even packing through phase microscopy. Once satisfactory packing was observed the glass slide was placed into an oven and the beads were sintered for 26 h at 150 °C. The glass slide was then removed from the oven and cooled to room temperature.

4.2.4 Agarose/sucrose lyophilization

For "empty" hydrogels not containing DNA polyplexes, 35 mg (0.10 mmol) of sucrose (Ultra pure, MP Biomedicals, Santa Ana, CA) and 1.0 mg of low-melting point agarose (UltraPureTM Agarose, Tm = 34.5-37.5 °C, Invitrogen, Grand Islands, NY) were dissolved in 5.0 mL water and lyophilized. Each aliquot was intended for a 100 μL hydrogel. For smaller hydrogel volumes, both sucrose and agarose were scaled down proportionally.

4.2.5 Porous (and nano-porous) HA hydrogel formation

Hydrogels were formed by Michael-type addition of acrylate-functionalized HA (HA-Ac) with bis-cysteine containing MMP peptide crosslinkers at pH 7.8-8.0. Prior to reaction, a hydrogel precursor solution was made by mixing a fraction of the total HA-Ac with a lyophilized aliquot of cell adhesion peptide, RGD, for 30 min at 37 ^{o}C. After incubation, HA-RGD was mixed with the remaining HA-Ac, lyophilized agarose/sucrose, and .3 M TEOA pH 8.0 for a final gel concentration of 4.0 w/v% HA and 100 μM RGD. Finally lyophilized aliquots of the crosslinker were diluted in .3 M TEOA immediately before addition to the hydrogel precursor solution. For porous hydrogels, 20 μL of gel solution was then added directly on top of a PMMA microsphere template, covered with a glass slide, and perfused into the template by centrifugation at 1500 rpm for 6 min at 4 ^{o}C. The slide was then incubated at 37 ^{o}C for 30-45 min to induce polymerization. Once complete, the gels were removed from the silicon wells and placed directly into 100 % acetone for 48 h to dissolve the PMMA microsphere template. The acetone solution was replaced 2-3x during this incubation. The gels were then serially hydrated into sterile PBS and left in PBS until ready for use. For nano-porous hydrogels, the gel solution was sandwiched between two Sigmacoted slides using 1 mm thick plastic spacers and incubated at 37 ^{o}C for 30-45 min to induce polymerization. Once complete, the gels were placed directly into sterile PBS and left in PBS until ready for use. Prior to surgery all gels were placed in sterile PBS with 1 % P/S overnight.

4.2.6 Gel preparation for SEM imaging

A Nova 230 Nano SEM in low vacuum mode was used. Hydrogels were slightly dried and imaged directly without further dehydration or metal coating.

4.2.7 Subcutaneous implant model

All in vivo studies were conducted in compliance with the NIH Guide for Care and Use of Laboratory Animals and UCLA ARC standards. 6 to 8-week old male Balb/c mice each 20-30 grams were used to study cellular infiltration and blood vessel formation in HA hydrogels since this strain and size has been previously used for wound healing and angiogenesis assays [124, 125]. (Note: This will later be changed to female mice in Chapters 7 and 8 due to aggression issues with male mice!) Nanoporous or single-phase porous hydrogels were made exactly as described above with sucrose and agarose (but without DNA polyplexes) and cut to 6 mm in diameter using a biopsy punch, for final overall dimensions of 6 mm x 1 mm, D x H. All porous hydrogels were made using 100 μm beads. In fabricating the hydrogels, the starting reagents were sterilized through filtering with a 0.22 μm filter. After scaffold fabrication, the hydrogels were washed with sterile PBS and kept in PBS with 1 % P/S. Immediately prior to surgery, mice were anesthetized with 4-5 % isoflurane through a nose cone inhaler. After anesthesia induction, the isoflurane concentration was lowered to 1.5-2.5 % for the remainder of the surgery. The back of the mouse was subsequently shaved and washed with Betadine and 70 % ethanol. Two incisions appropriate to the size of the implant were made in the skin aside the midline of the animal using scissors. Two subcutaneous pockets were subsequently created by blunt dissection using hemostats. Within the created pockets, the implants were inserted. After insertion of the hydrogels, each incision was subsequently closed with a single wound clip. All animals were observed daily for signs of inflammation and pain and also administered

Carprofen injections for the first 48 h post survival surgery. After 1, 2, and 3 weeks, mice were sacrificed with CO_2 overdose (note: this was later changed to isoflurane overdose in Chapters 7 – 8). Two 1 cm^2 pieces of tissue were collected from each mouse containing the implant and the surrounding tissue and skin, fixed in 4 % PFA overnight at 4 °C (note: this was later changed to 2 % PFA for experiments conducted in Chapters 7 – 8), dehydrated in 70 % EtOH, and finally paraffin embedded. A total of 12 mice were used in this study, with 6 mice per hydrogel condition. Two animals were sacrificed per condition at each time point.

4.2.8 Immunofluorescence and immunohistochemistry

Paraffin embedded sections (5 µm) were deparaffinized by incubation in multiple xylene washes followed by serial hydration from 100 % ethanol into 100 % water. Antigen-retrieval was conducted with a 15 min incubation at 37 °C in .1 mg/mL proteinase K solution. Sections were then washed with PBS and incubated in blocking buffer (1 % goat serum (Jackson Immuno Research Labs, West Grove, PA) + .05 % Tween-20 in PBS) for 1 h at RT before being incubated in primary antibody solution (1:100 dilution in blocking buffer of rat anti-mouse CD31 (BD Pharmingen, San Diego, CA)) overnight at 4 °C. Sections were again washed with PBS and incubated in blocking buffer for 10 min at RT before being incubated for 2 h at RT in secondary antibody solution (1:200 dilution in blocking buffer of goat anti-rat Alexa 568 (Invitrogen, Grand Islands, NY) which also contained α-smooth muscle actin-FITC (1:500 dilution, Sigma-Aldrich, St. Louis, MO) and DAPI nuclear stain (1:500 dilution, Invitrogen). Sections were then washed twice in PBS, mounted and imaged using an inverted Zeiss fluorescence microscope. All hematoxylin and eosin staining of sections was conducted by the Translational Pathology Core Laboratory (TPCL) at UCLA.

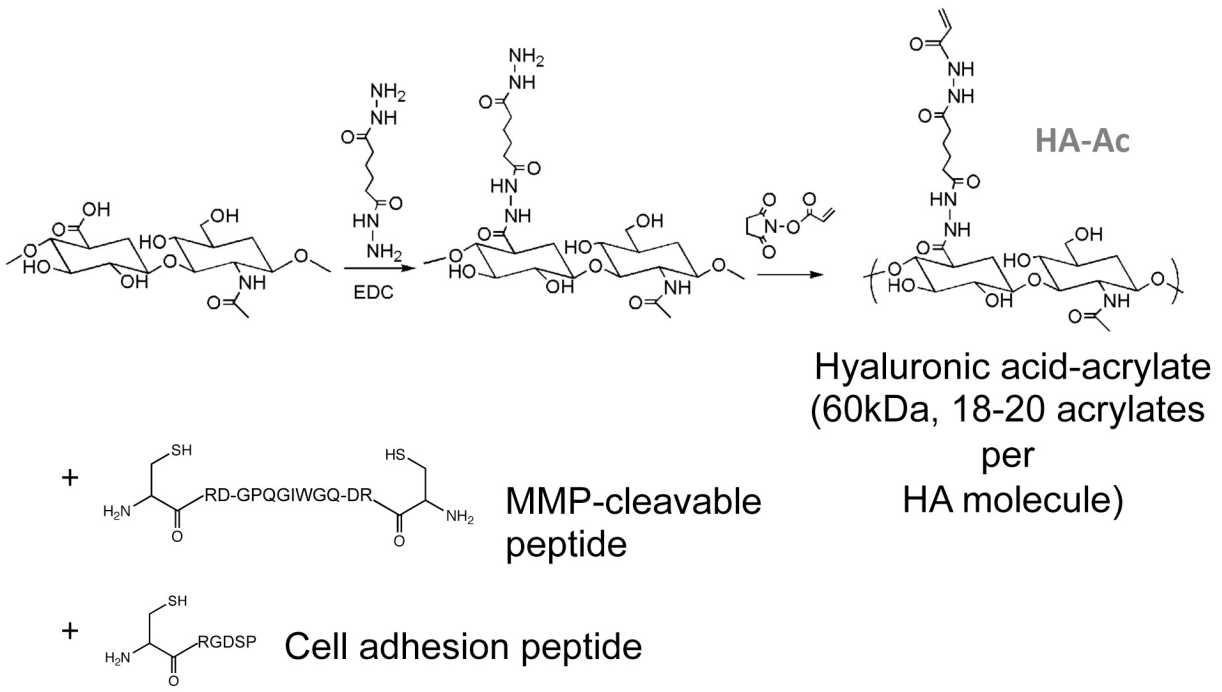

Figure 4.1: HA is modified using a two-step chemistry to contain acrylates and then crosslinked using an MMP degradable peptide sequence terminated on both ends with cysteines to allow for Michael-type addition chemistry above a pH of 7.4. A cell adhesion peptide, specifically RGD, is also included through a single cysteine to allow for cell adhesion and spreading. When these components are mixed together in .3M TEOA buffer pH 8.0 a hydrogel is formed via Michael-addition.

4.3 Results and Discussion

4.3.1 Hyaluronic acid modification for Michael-addition chemistry

In our lab specifically, we have established a general protocol for making semi-synthetic HA-MMP degradable hydrogels. First, acrylates were conjugated onto the HA backbone through a two-step process. Briefly, HA was first modified with adipic acid dihydrazide (ADH) by 1-ethyl-3-(3-dimethylaminopropyl) carbodiimide (EDC) coupling and the resulting hydrazide group was then modified with NHS-acrylate (NHS-AC) to obtain acrylamide functionalities **(Figure 4.1)**. Analysis by NMR showed that ~56 % of the carboxylic acids were modified with ADHs. After reacting the HA-ADH with NHS-

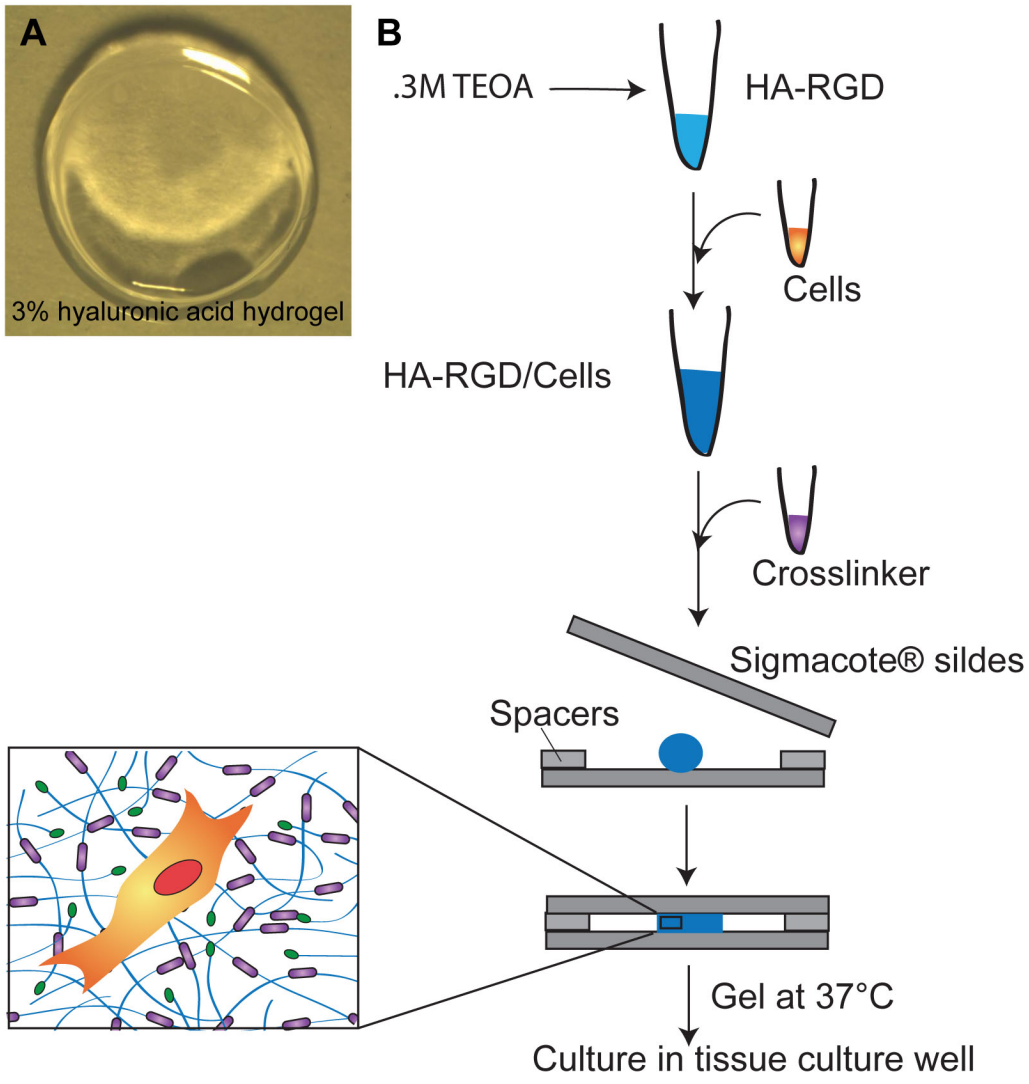

Figure 4.2: (A) Digital image of a 3% hyaluronic acid hydrogel. (B) Schematic of general protocol for nano-porous HA hydrogels formed through Michael-addition.

AC at pH 7.2 overnight, analysis by NMR showed that ~10-12 % of the carboxylic acids were modified with acrylates, resulting in approximately 16 acrylates per HA chain. RGD adhesion peptides were incorporated through Michael-type addition of the cysteine side chain in the peptide to the acrylate groups on the HA backbone, followed by addition of an MMP-degradable peptide crosslinker to form the final hydrogels. In general the components are all mixed together in the absence or presence of cells, and formed at 37 °C for 30 min between two Sigmacoated slides producing nano-porous

HA gels **(Figure 4.2)**. The crosslinker (and also HA) concentration can be varied to produce different stiffness hydrogels. For those gels with agarose and sucrose, the storage modulus of 3 % HA hydrogels with 0.4 – 0.6 r-ratios (SH/Ac) can range from 700 – 1300 Pa. This range corresponds to 110 – 60 kg/mol between crosslinks and approximately 22 – 16 nm mesh size, respectively, as determined by the Flory–Rehner and Rubber Elasticity theories [126]. These hydrogels are termed nano-pore.

4.3.2 Porous hydrogel formation

For porous hydrogels, the complete gel solution was placed on top of a poly(methyl methacrylate) (PMMA) microsphere template, centrifuged into the void space between the spheres, and then gelled **(Figure 4.3)**. The hydrogel/template was then placed into acetone for 48 h to dissolve the PMMA microspheres, leaving behind a porous hydrogel structure. Scanning electron microscopy was used to examine the structural differences between gels made with and without the bead template **(Figure 4.4A-D)**. Hydrogels made with lyophilized agarose and sucrose with the bead template had large, interconnected pores that were uniformly distributed (porous, μ-pore), while those made directly without the template had no visible micron-sized pores (nano-pore, n-pore).

4.3.3 Preliminary in vivo study using mouse subcutaneous implant model

As a preliminary study to determine the potential for porous hydrogels to enhance cellular infiltration in vivo, both porous and nano-pore hydrogels were implanted subcutaneously into the back of Balb/c mice **(Figure 4.5)**. Briefly in this model we used female Balb/c mice in the young adult range since they have previously been used to study wound healing and are in a rapid growing phase. Two hydrogels

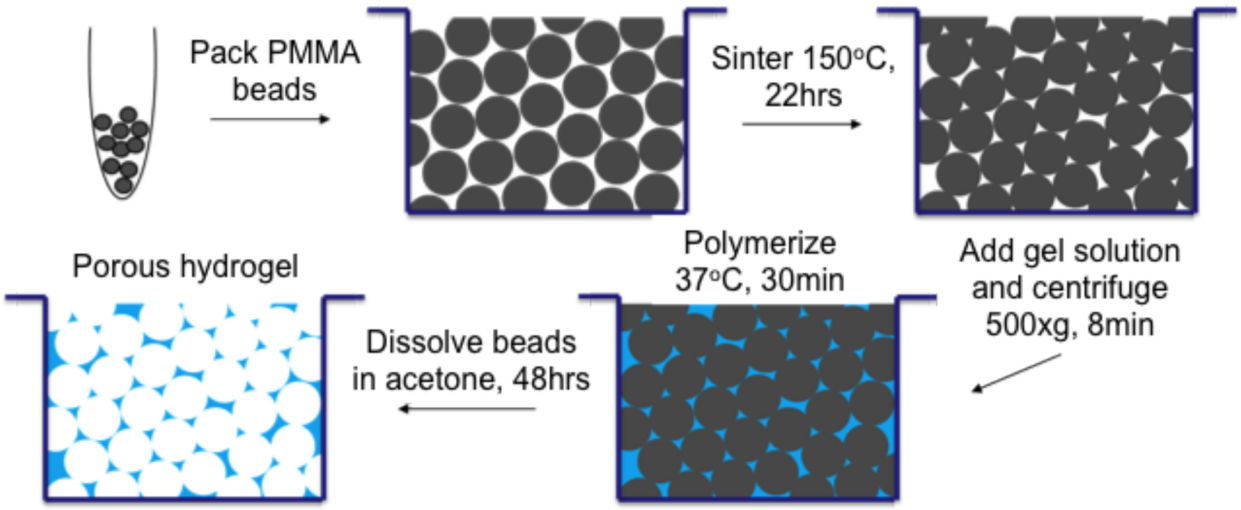

Figure 4.3: Schematic for porous hydrogel formation using a modified PMMA bead template. PMMA beads were packed and sintered overnight at 150°C to allow for µ-sized interconnected pores. After addition and centrifugation of the hydrogel precursor solution into the void space, the gel was polymerized at 37°C for 30min. Lastly, the PMMA beads were dissolved in acetone over 48hrs. The entire process takes ~3 days to complete.

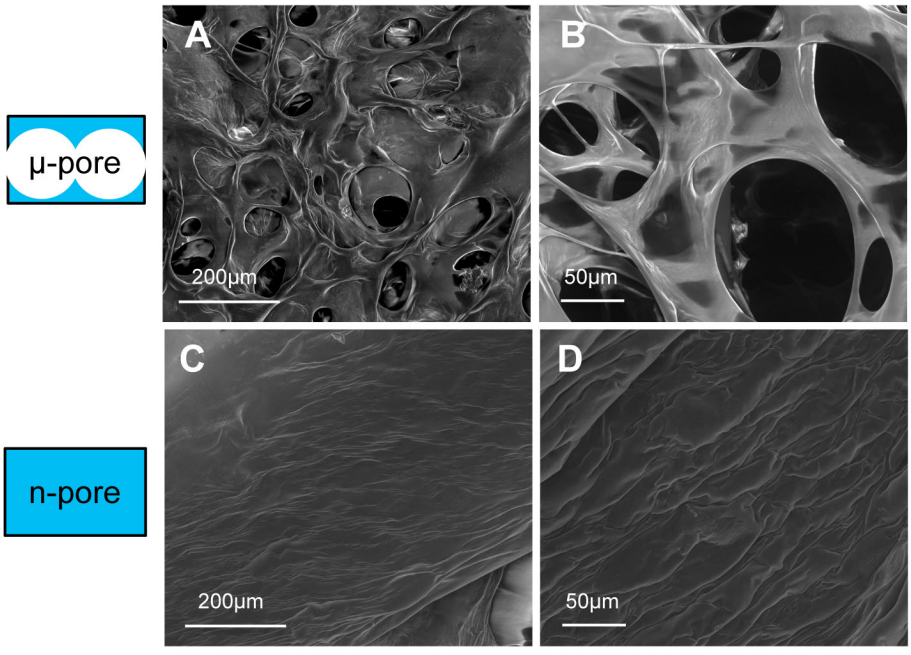

Figure 4.4: SEM was used to characterize gel structure of µ-pore hydrogels (A, B) made using the bead template and n-pore hydrogels (C, D) made directly without the template. A, C = 200x, B, D = 750x magnification images.

were implanted per mouse. Implants were excised each week for three weeks, paraffin-embedded and sectioned along the height of the gel to include the attached muscle and skin. Hematoxylin and eosin (H&E) stained sections showed micro-scale interconnected pores allowed for enhanced cellular infiltration from the host into the biomaterial increasingly with time **(Figure 4.6A, B, E, F)**. By one week, cells were able to infiltrate into almost all visible 100 μm diameter pores without noticeable gel degradation. Conversely, nano-pore hydrogels had minimal cellular infiltration along the periphery of the hydrogel even after three weeks **(Figure 4.6C, D, G, H)**. At sites where cells were present the hydrogel appeared to be degrading and large pores became visible. Staining for PECAM positive endothelial cells showed thin vessel-like structures within porous hydrogels at three weeks **(Figure 4.6I, J)**, while no endothelial cells could be observed in any of the nano-pore implants at the same time point **(Figure 4.6K, L)**. Thus, in the absence of any pro-angiogenic factors, the presence of emerging vasculature could be attributed to the pre-existing interconnected porous structure. In many of the vessels we also observed red blood cells indicating perfusion of these newly formed vessels.

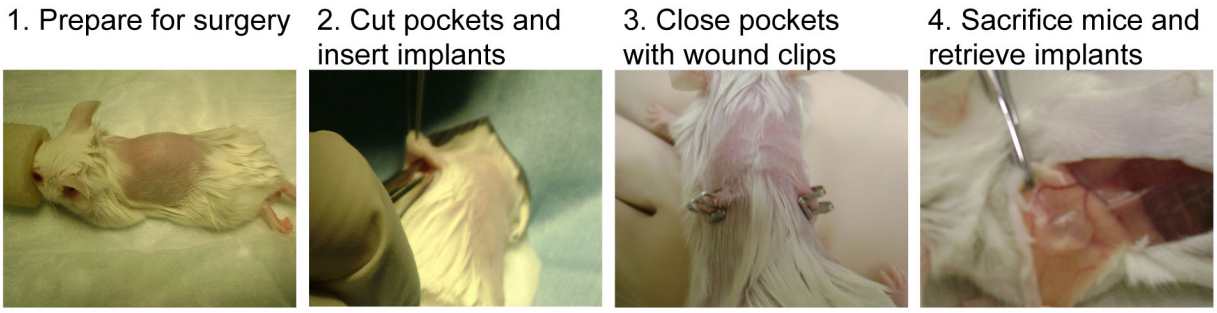

Figure 4.5: Mouse subcutaneous implant model. The back of the mouse is prepared in a sterile fashion before the surgeon creates two side-by-side incisions slightly wider than the pre-formed hydrogels. Hemostats are then used to create pockets under the skin through the incisions, the hydrogel is placed into the pocket, and the pocket is closed using a single wound clip. After a given period of time, the mice are euthanized and the hydrogels are retrieved with the surrounding tissue and attached skin.

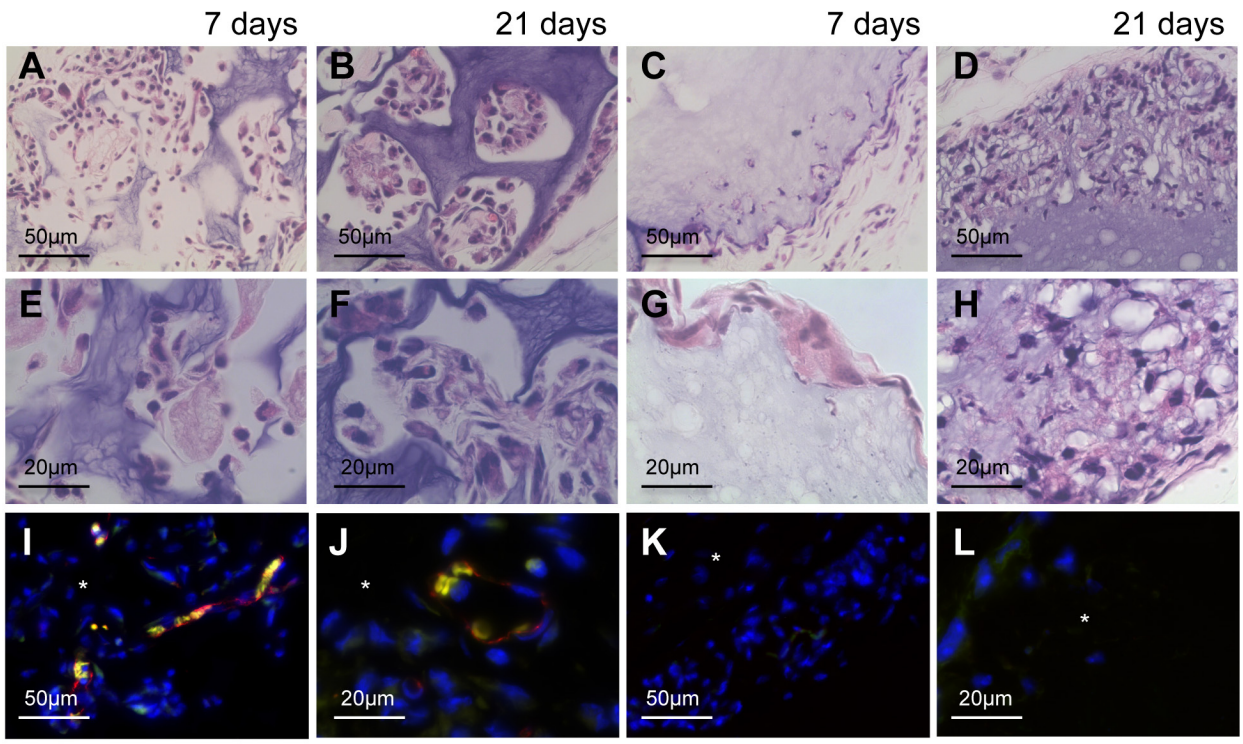

Figure 4.6: Sections from a mouse subcutaneous implant model show large micro-sized pores (A, B, E, F) allow for enhanced cellular infiltration from the host into the HA hydrogels when compared to n-pore counterparts (C, D, G, H). Staining for endothelial markers indicated significant positive staining for μ-pore hydrogel implants (I, J) and not for the n-pore implants (K, L). Red = PECAM positive staining = endothelial cells, yellow appear to be erythrocytes, blue = cell nuclei. A-D, I, K = 40x, E-H, J, L = 100x magnification images. The * indicates gel area.

4.4 Conclusions

Although the processing time to create porous hydrogels compared to the more commonly used nano-pore HA hydrogels is significantly longer (3.5 days compared to ~1 h), these results highlighted the potential for the use of porous hydrogels in vivo. Future results by the Ratner and Brey groups further validated these findings [12, 22]. We anticipated that with the addition of pro-angiogenic growth factors through the delivery of non-viral vectors encoding for the factors, blood vessel formation within porous hydrogels could further enhance vessel number, maturity, and rate of formation. Chapters 5 and 6 will describe two different approaches for delivering non-viral DNA nanoparticles in a controlled fashion from porous HA hydrogels.

CHAPTER 5

TETHERED NANOPARTICLES FOR CONTROLLED PARTICLE DELIVERY

5.1 Introduction

In this chapter we describe a strategy to achieve temporal control over nanoparticle release from biomaterials using cell-secreted proteases. This cell-triggered release approach utilizes peptides that are degraded by matrix metalloproteinases (MMP) at different rates to immobilize nanoparticles directly to the biomaterial surface. Release would then be initiated through the action of cell-released proteases and controlled by the sensitivity of the peptide to cleavage by such proteases. Enzymatically degradable tethers have been utilized for the immobilization and release of growth factors [108-110] and small drugs [111, 112], which are only liberated by cleavage caused by cell secreted proteases, such as MMPs or plasmins, during local tissue remodeling. These proteases are known to be up-regulated during wound healing, microenvironment remodeling, and in diseased states and can, therefore, serve as triggers for bioactive signal delivery [113, 114]. At the time these experiments were conducted cell responsive systems were yet to be developed for the delivery of larger nanoparticles, which show efficacy in cellular environments.

Here we developed a strategy to immobilize nanoparticles through peptide tethers and allow for their release and internalization through a cell-triggered approach. Fluorescent polystyrene nanoparticles, similar in size to pDNA/L-PEI

polyplexes (~60–80 nm), were used as model nanoparticles to (1) initially avoid complications with polyplex aggregation and (2) because they were easy to detect in fluorescence based release and internalization assays. We hypothesized that internalization would depend on both the sequence of the peptide tether and the number of tethers between the nanoparticle and the biomaterial. Further, the internalization rate would be a function of the protease expression profile, with cells that express less proteases resulting in significantly less internalization than cells which over-express proteases.

5.2 Materials and Methods

All supplies and reagents were purchased from Thermo Fisher Scientific unless otherwise noted.

5.2.1 Peptide modification with NHS-PEG-biotin or NHS-LC-biotin (NHS-PEG-acrylate or NHS-LC-acrylate)

Peptides were purchased from Anaspec (MMP_{high} Ac-KRGPQGIWGQDRCGR-NH_2, MMP_{med} Ac-KRGPQGIAGQDRCGR-NH_2, MMP_{low} Ac-KRGDQGIAGFDRCGR-NH_2). Peptides were reacted with NHS-PEG-biotin or NHS-LC-biotin (Laysan Bio Inc.) at a 1:2 molar ratio. Sample pH was adjusted to 7.4 and allowed to react at RT for 2 h. The sample was then dialyzed overnight against DI water to remove any unreacted substrates, lyophilized and stored at -20 °C until ready for use. Methods and quantities to produce acrylate modified particles are identical to those just described, with the exception of NHS-PEG-acrylate or NHS-LC-acrylate being used instead of NHS-PEG-biotin or NHS-LC-biotin.

5.2.2 Particle modification with peptide-PEG-biotin or peptide-LC-biotin or biotinPDA (peptide-PEG-acrylate or peptide-LC-acrylate) tether

Carboxylate-modified, 40 nm polystyrene beads (Invitrogen) were modified to possess peptide tethers. A 2 % bead solution (50 µL) was incubated with 50 µL of 5.9 mM EMCH solution in MES buffer for 15 min at RT before adding EDC (10 µL of a 2 mM solution) and adjusting the pH to 6.5 ± .1 with 1 N NaOH/HCl and incubating at RT for 2 h. Samples were kept in the dark to prevent fluorescence quenching. Sample pH (and size) was monitored throughout the reaction period. The sample was dialyzed against DI water overnight to remove any unreacted substrates. BiotinPDA (PDA control particles) or peptide samples were reduced using 10 mM TCEP with mixing for 1 h at RT with either 97 mM biotinPDA in DMSO or 9.7 mM of peptide-PEG-biotin/LC-biotin in MES, respectively. Next either 2.5 µL of 9.7 mM biotinPDA in DMSO (10-fold dilution) or peptide-PEG-biotin/LC-biotin in PBS was added to the partially modified bead solution (now ~150 µL after overnight dialysis). Sample pH was adjusted to 7.4 ± .1 and the sample was allowed to react for 2 h at RT while being mixed. The sample was then dialyzed overnight for a second time against H_2O. Final particle concentration was determined using a fluorimeter and comparison against a standard curve. Methods and quantities to produce acrylate-modified particles are identical to those just described, with the exception of the secondary conjugation molecules containing acrylate groups instead of biotins.

5.2.3 Particle modification with NHS-PEG-biotin (NHS-PEG-acrylate or NHS-LC-acrylate) tether

A 2 % bead solution (50 µL) was incubated with 50 µL of 5.9 mM ADH solution in MES buffer for 15 minutes at RT. Next, 10 µL of 2mM EDC was added. The pH was

adjusted to 6.5 ± .1 with 1 N NaOH/HCl and the sample was incubated at RT for 2 h. Samples were kept in the dark to prevent fluorescence quenching. Sample pH (and size) was monitored throughout the reaction period. The sample was dialyzed against DI water overnight to remove any unreacted substrates. Next 2.5 µL of 9.7 mM NHS-PEG-biotin (PEG control particles) in PBS was added to the partially modified bead solution (now ~150 µL after overnight dialysis). Sample pH was adjusted to 7.4 ± .1 and the sample was allowed to react for 2 h at RT while being mixed. The sample was then dialyzed overnight for a second time against H_2O. Final particle concentration was determined using a fluorimeter and comparison against a standard curve. Methods and quantities to produce acrylate-modified particles are identical to those just described, with the exception of the secondary conjugation molecules containing acrylate groups instead of biotins. Controls containing no PEG were formed using NHS-LC-acrylate.

5.2.4 Particle characterization

Sample particle size was measured, when required, using dynamic light scattering with a 10 to 100-fold dilution of the stock bead solution. Particles were also analyzed for degree of modification using elemental analysis for detection of sulfur. Samples (200 µL) were diluted to 10^{12} particles/mL in DI H_2O and analyzed at the UCLA Molecular Instrumentation Center.

5.2.5 Binding of biotinylated PS nanoparticles to 2D surface

Covalently bound streptavidin to 96-well plates were bought from Nunc Company. Particles were blocked with 1 % BSA/1xPBS solution at 4 °C overnight (minimum) in the dark. Wells were washed 3x with 1xPBS-Tween and then either incubated with 100 µL 1xPBS or 5 mM free biotin in PBS for samples which tested for

specific binding for 1 h. After 1 h the samples in the wells were removed and 100 µL blocked particles were added to each well ($3.2x10^{11}$ particles/mL). All samples were run in triplicate. The plate was incubated at RT for 3 hours after which the wells were again washed 3x with 1xPBS-Tween buffer, the first wash of which sat for ~1 h. Imaging of the plate was conducted using a Typhoon scanner using either a 488 nm blue laser (excitation/emission 505/515) with 520 nm BP 40 nm emission filter at 450 V for yellow-green particles or a 532 nm green laser (excitation/emission 580/605) with 610 nm PB 30 nm emission at 600 V for red particles.

5.2.6 Release of biotinylated particles from surface

After the plate was bound with particles according to the protocol described above, release of the particles was measured over time. Each well was filled with 100 µL 1xPBS and the plate was incubated at 37 °C for 20-24 h. The PBS in the wells was changed 3-4x during this period. Collagenase I (Worthington Biochemical Corp.) or mMSC conditioned media was then added to each well and the plate was incubated at 37 °C for usually 120 h, during which several readings were conducted. A single triplicate was left untouched (100 % control) and would later be used to normalize the release data. At each time point the solution was removed and the plate was imaged dry using the Typhoon scanner. Release data was all normalized to the 100 % control within each individual bead type and then evaluated with respect to the release of particles incubated in PBS (i.e. background release).

5.2.7 Cell culture and zymography

HEK293T-MMP-2 cells were a kind gift from Jeffrey Smith from the Burnham Institute for Medical Research. mMSC, HEK293T, and HEK293T-MMP-2 cells were

cultured in DMEM medium supplemented with 10 % bovine growth serum and 1 % penicillin/streptomycin at 37 °C and 5 % CO_2. The cells were passaged using trypsin following standard cell culture protocols every 2-3 days. To determine the extent to which these cells express matrix metalloproteinases, a gelatin zymogram was used. Cells were plated in 12-well TC treated plates at a density of 100,000 cells/mL and conditioned cell media was collected after exactly 24 h and assayed for total protein concentration using a Bradford assay. Each lane was loaded with 50 µg of total protein and the gel was run in Tris–Glycine SDS running buffer at 110 V. The gel was then placed in renaturing buffer (2.5 % Triton-100) for 30 min at room temperature and then incubated in the developing buffer (0.5–1 % tris(hydroxymethyl)aminomethane, 1–2 % sodium chloride) for 30 min at room temperature with further development in fresh buffer at 37 °C overnight. The gel was stained with coomassie blue for 60 min (0.5 % w/v) and de-stained in a methanol, acetic acid, and water solution (40:10:50) until clear bands appeared where active protease was present. Active human matrix metalloproteinase 2 and 9 (5 ng/well, Calbiochem), Collagenase I (20 ng/well), and cDMEM (50 µg/well - background) were run in the gel for comparison.

5.2.8 Particle internalization assay

Particles were bound and stabilized in PBS as described above. Cells were then plated at a density of 7,000 cells/well and allowed to attach and spread at 37 °C. At either 24 or 48 h (separate wells were used for each time point) media was removed and replaced with sterile 1xPBS. Cells were fixed using 4 % PFA for 15 min at RT, after which their nuclei were stained for 30 min using HOESCHT dye (Invitrogen) in the dark. Finally, samples were analyzed in PBS using an inverted Zeiss Observer Z1 fluorescence microscope. Flow cytometry analysis was also conducted at these time points to

quantify the degree of particle internalization. Cells were washed with PBS and detached using 0.25 % Trypsin for 2 min. They were then re-suspended into a solution of 1 % BGS/1xPBS with 10 % Trypan blue and remained on ice until they could be analyzed. Trypan blue was used to quench any external fluorescence on the cells so any fluorescence detected by the flow cytometer was due to *internalized* particles and not by particles nonspecifically bound to the external surface of the cells [127].

5.2.9 Design template using PMMA microspheres

PMMA microspheres (90-125 μm, Bangs Laboratories) were bought dry. Approximately 25-30 mg of beads were then added into glass-bottom silicon wells (Electron Microscopy Sciences) and covered with a glass slide. Unlike previously published techniques (e.g. rotating slide at 250 rpm for 4 h [24], the beads were then packed by slight tapping for 1-2 min and examined for even packing through phase microscopy. Once satisfactory packing was observed the glass slide was placed into an oven and the beads were sintered for 26 h at 150 °C. The glass slide was then removed from the oven and cooled to room temperature.

5.2.10 RGD peptide modification

RGD peptide (Ac-GCGYGRGDSPG-NH_2), purchased from GenScript Corp., was reacted at a 2:1 mole ratio with 4-arm PEG-vinyl sulfone (PEG-VS, MW 20,000) for 2 h with mixing at pH 8.5. The final solution was stored at -20 °C until ready for use.

5.2.11 Porous PEG-acrylate hydrogel formation

A hydrogel precursor solution was made using PEG dimethacrylate (PEG-DA, MW 575), PBS (pH 7.4), and Irgacure 2959 photoinitiator (Ciba) for a final concentration of

10 % (w/v) PEG and 0.05 % Irgacure in 35 % EtOH. For cell-adhesive gels to be used for in vitro experiments, modified RGD-PEG-VS was also added to the gel mixture for a final concentration of 1000 μM RGD. Approximately 45 μL of gel solution was then added directly on top of a PMMA microsphere template, coved with a second slide, and perfused into the template by centrifugation at 1500 rpm for 3 min. The slide was then exposed to low intensity UV light for 90 sec to induce polymerization. Once complete, the top slide was removed and the gels were removed from the silicon wells and placed into fresh 100 % acetone for 48 h to dissolve the PMMA microsphere template. The gels were then serially re-hydrated into DI H_2O and left in fresh water until ready for use.

5.2.12 Characterization of mechanical properties

Plate-to-plate rheometry was used to determine the mechanical properties of the porous hydrogels. The hydrogels were cut to 6 mm in diameter, which was slightly smaller than the size of the rheometer plate (8 mm) to ensure the gel did not exceed the size limits when under compression, as compression was necessary to avoid slipping. An Anton Parr rheometer under a constant strain of 0.5 and frequency from 0.1 to 10 Hz was used to measure both the storage and loss moduli.

5.2.13 Gel preparation for SEM imaging

Each porous hydrogel was serially dehydrated in 20, 40, 60, 80, and 100 % EtOH for 10 min at a time. Hydrogels were left in 100 % EtOH overnight after which they were placed in a dry holder, air dried and, finally, placed under vacuum until time for imaging. The gels were then attached to an SEM holder using carbon tape and coated with a thin layer of gold using a gold sputterer. Images were taken using a JEOL JSM-

6700F FE-SEM in the UCLA MCTP core facility. Hydrogels used solely for characterization by SEM did not contain any RGD adhesion peptide.

5.2.14 Binding acrylate-modified particles to porous hydrogels

Acrylate-modified PS nanoparticles (40 µL of $1x10^{13}$ particles/mL) with .05 % Irgacure 2959 photoinitiator were added directly on top of porous hydrogels in dry glass-bottom silicon well. The hydrogels were incubated for 10 min at RT. Low intensity UV light was shined for 1 min to induce binding of the particles to the hydrogel through surface acrylate groups left unpolymerized by the initial gelling process. The gels were washed using PBS-Tween buffer in the dark and then imaged on glass coverslips with fluorescence microscopy. To test for non-specific binding, unmodified particles were used.

5.2.15 Cell seeding onto porous hydrogels

Porous hydrogels were rinsed with 3 consecutive 10 min washes in sterile PBS. Gels were then placed into dry low-binding plates. Cells, which may have been previously stained using a fluorescent live cell stain (CFDA cell tracker, Invitrogen) using the manufacturer's suggested protocol, were then seeded in 2 steps. First 15,000 cells at a density of 15,000 cells/10 µL were added directly on top of each gel, centrifuged down for 3 min at 700 rpm, after which an additional 15,000 cells were added without further centrifugation. The gels were then incubated at 37 ^{o}C for 15 min, after which 180 µL of fresh media was added for a final volume of 200 µL/well. The gels were incubated at 37 ^{o}C for 24-48 h. Prior to imaging, the media was removed from each well and replaced with sterile PBS. Cell spreading was observed using both phase and fluorescent microscopy.

5.2.16 Cell spreading and viability assessment

Cell spreading and viability in the porous hydrogel was studied with the LIVE/DEAD viability/cytotoxicity kit (Invitrogen). At various time points each hydrogel was stained with 150 µL of the staining solution for 30 min at room temperature in the dark (as per manufacturer's protocol) and imaged in PBS using fluorescence microscopy.

5.2.17 Internalization assay of acrylate-modified particles from porous hydrogels

Once PS nanoparticles were bound to the porous hydrogels, 30,000 unstained cells were seeded onto each gel as described above. The gels were then incubated at 37 ^{o}C. After 48 h, hydrogels were transferred individually to microcentrifuge tubes and cells were detached from the gels with 2 min incubation in 0.25 % trypsin followed by an addition of cDMEM and centrifugation for 5 min at 350x*g*. The cell solution was then pipetted into a glass coverslip-bottom flexiperm well and incubated at 37 ^{o}C for 24 h. Cells were fixed using 4 % PFA and cell nuclei were stained using HOESCHT dye as previously described. Samples were imaged in PBS using fluorescence microscopy.

5.3 Results and Discussion

5.3.1 Experimental design and rationale

Strategies to control the release rate of bioactive signals from tissue engineering scaffolds are essential for tissue regeneration and tissue engineering applications. Here we report on a strategy to achieve temporal control over nanoparticle release from biomaterials using cell-secreted proteases. This cell-triggered release approach utilizes peptides that are degraded by MMPs at different rates [128, 129] to immobilize

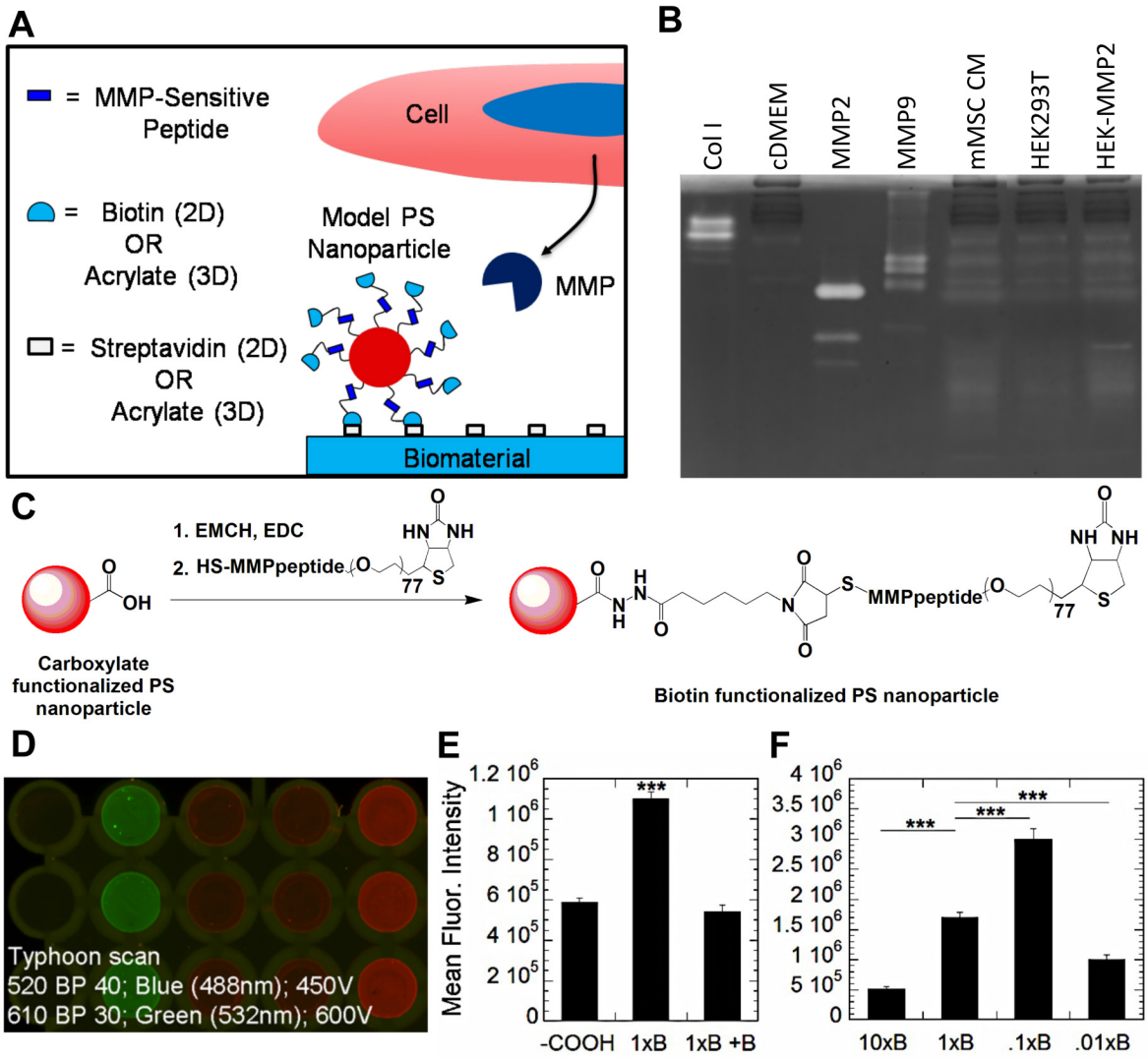

Figure 5.1: Protease sensitive peptides are used to immobilize model nanoparticles to biomaterials and released as a result of peptide cleavage by cell-released proteases (A); Gelatin zymography was used to determine MMP2 and MMP9 expression of multiple cell types (B). HEK293T cells were shown to express significantly lower levels of MMP2 and 9 compared to mMSCs and HEK293T-MMP2 cells, which specifically and stably produce MMP2; Biotinylated peptide-containing particles were prepared by reacting carboxylate-functionalized polystyrene (PS) nanoparticles with a heterobifunctional cross-linker, namely EMCH, followed by reaction with SH-MMP_x-PEG_{3400}-biotin (C); To determine if sufficient biotinylation had been achieved, fluorescent particles were incubated on a streptavidin surface and analyzed for binding using a Typhoon scanner (D); Fluorescence was quantified and showed that in a competitive binding assay of biotinylated particles (1xB) in the presence of excess free biotin (1xB +B) the degree of binding was significantly reduced to the level of unmodified (-COOH) particles (E); Particles prepared with 10-fold dilutions of SH-MMP_{med}-PEG_{3400}-biotin (xB) revealed that a specific particle surface density of both PEG and biotin resulted in the highest degree of binding (F). The ** and *** symbols indicate statistical significance at levels of $p<.01$ and $p<.001$, respectively, calculated using a multiple comparisons Tukey test. Statistics for Figure F were determined with respect to 1xB particles.

nanoparticles directly to the biomaterial surface. Thus, the peptide-immobilized nanoparticles are expected to be released with temporal control through the action of cell-released MMPs.

Fluorescent polystyrene (PS) nanoparticles were immobilized to a cell binding surface through either protease sensitive peptide tethers or poly(ethylene glycol) (PEG) polymer chains. Terminal biotins on each tether allowed for the immobilization of the modified PS nanoparticles onto a streptavidin surface through robust ($K_{binding}=10^{15}$) biotin-streptavidin interactions **(Figure 5.1A)**. Various peptides, previously reported to have varying degrees of sensitivity towards MMP-2 [130] and MMP-1 [128], were then used to allow for control over release rates. Particles with varying degrees of tethering were also made to determine whether this could result in an effect on the release kinetics. Cells which express high or low levels of MMPs were then used to study nanoparticle internalization **(Figure 5.1B)**.

5.3.2 Particle modification

Biotinylated peptide-containing particles were prepared by reacting carboxylate-functionalized PS nanoparticles with a heterobifunctional cross-linker, namely 3,3‘-[N-e-Maleimidocaproic acid] hydrazide (EMCH), followed by reaction with HS-MMP_x-PEG_{3400}-biotin or HS-MMP_x-biotin for tethers with no PEG polymer chain **(Figure 5.1C)**. PEG control particles, containing no cleavable peptide, were similarly produced using adipic acid dihydrazide (ADH) for amine functionalization, followed by reaction with NHS-PEG_{3400}-biotin. For controls containing no PEG polymer chain (PDA control particles) the particles were modified with EMCH followed by reaction with reduced biotinPDA. The degree of modification was characterized using elemental analysis for sulfur content **(Table 5.1)**. Each biotin and each peptide contain a single sulfur atom. Only non-

peptide tethered control particles made using NHS-PEG-biotin contained a single sulfur atom per tether. 200 nm commercially available biotinylated particles were also analyzed and showed that the degree of biotinylation of our 40 nm manually modified particles was similar to those commercially manufactured.

Particle Type	Biotin Density (biotin/particle)	Inverse Biotin Density (nm^2/biotin)
10xMMP_{med}-PEG-b	2607	1.93
1xMMP_{med}-PEG-b	1508	3.33
.1xMMP_{med}-PEG-b	1361	3.69
.01xMMP_{med}-PEG-b	1022	4.92
1xMMP_{high}-b	1389	3.62
1xMMP_{med}-b	1685	2.98
1xMMP_{low}-b	1864	2.70
1xbPDA (control)	2302	2.18
1xPEG-b (control)	1739	2.89
200nm biotin (control)	118364	1.06

Table 5.1: The degree of modification per particle was determined using elemental analysis for sulfur.

5.3.3 Two-dimensional acellular release studies

Particle immobilization and release was determined using a typhoon scanner, which can measure the fluorescence intensity of the surface **(Figure 5.1D)**. Particles were subjected to a competitive binding assay either in the presence or absence of excess free biotin to ensure particle binding was specific to the interaction of biotinylated particles with surface streptavidin **(Figure 5.1E)**. We were also able to determine an ideal PEG-biotin surface density, which resulted in the highest amount of particles binding to the surface **(Figure 5.1F)**. Particles averaging less than 1000 tethers (5 biotin/nm^2) or greater than ~2500-2600 tethers (~2 biotin/nm^2) were unable to

adequately bind to the streptavidin surface. We believe this trend resulted from a subtle balance between biotin and PEG for binding and binding inhibition, respectively. Generally highly PEG-ylated particles had difficulty binding due to increased steric hindrance, as has been suggested for biotin-PEG conjugates [131]. High tether density also lead to increased multivalent binding which limited the total number of particles being able to make sufficient interactions for binding on a confined streptavidin surface.

Preliminary acellular release studies were conducted to show potential for controlled release of tethered nanoparticles in protease rich environments **(Figure 5.2)**. Non-peptide tethered control particles showed minimal release (10-12 %) in the presence of Col I (bacterial equivalent to human MMP-1) and mMSC conditioned media **(Figure 5.1B)**, which indicated that any observed release of peptide-tethered particles is a result of the tether sensitivity to proteases and not the instability of the biotin-streptavidin surface. Peptide-modified particles were then shown to release over five days with the rate of release being determined by both the peptide sensitivity to Col I **(Figure 5.2A, E)** and proteases in mMSC conditioned media **(Figure 5.2B, F)**. Although documented sensitivities of the peptides to MMP-1 were designated high, medium, and low [128], this same trend was not observed in the presence of Col I **(Figure 5.2A, E)** and mMSC conditioned media **(Figure 5.2B, F)**, where MMP_{med} tethered particles resulted in statistically faster release. This difference may be explained as the documented sensitivities were only shown with respect to pure MMP-1, which is inherently different from crude bacterial collagenase, and will differ with respect to a mixture of proteases as is expected to be present in mMSC media. The complex and rich nature of the mMSC media may also explain the accelerated release rates of peptide-tethered particles when compared to their release in Col I. This notion was

confirmed when release was tested in varying concentrations of Col I which confirmed that release was dependent on protease concentration **(Figure 5.2C, G)**. A higher concentration of proteases would cleave more peptide tethers in a given period of time,

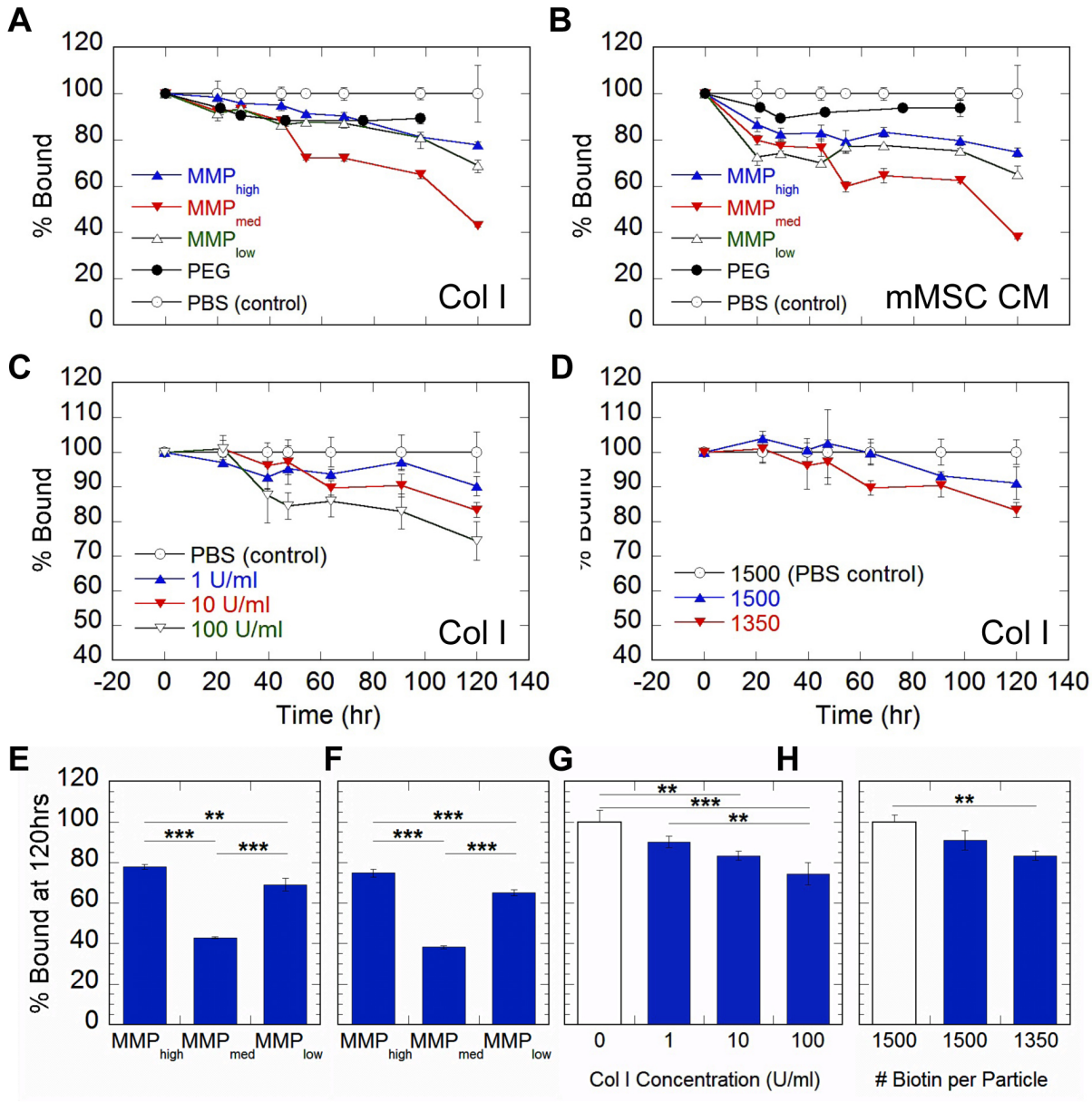

Figure 5.2: Release profiles show nanoparticle release is dictated by peptide sensitivity to Col I (A, E) and those proteases found in complex mMSC conditioned media (B, F). Additionally, release is a function of protease concentration (C, G) and the degree of particle tethering to the surface (D, H). MMP_{med} particles were used to study the effects of protease concentration and tethering. Figures E-H show statistical differences between release at 120hrs. White bars in Figures G, H indicate release media was PBS. The ** and *** symbols indicate statistical significance at levels of $p<.01$ and $p<.001$, respectively, calculated using a multiple comparisons Tukey test.

increasing the overall rate of release. Tether density was also tested as a means of controlling nanoparticle release rate. We hypothesized that if a single nanoparticle had more or less interactions with the biomaterial, it would take more or less time for a protease or multiple proteases to be able to fully cleave all of its tethers and allow for it to release. Similar studies have been previously conducted which indicated the same principles could dictate the non-specific release and gene transfer rates of immobilized DNA/poly(lysine) polyplexes [104]. Particles with fewer tethers and, consequently, fewer interactions with the surface were released more rapidly than those with a greater number of tethers. However, only slight differences in release were observed in the presence of Col I **(Figure 5.2D, H)**.

5.3.4 Two-dimensional release and internalization studies with protease-expressing cells

To determine if the cellular internalization rate of the immobilized nanoparticles followed the observed release kinetics, cells that express either high or low levels of proteases were incubated on top of bound particles and particle internalization was assessed using fluorescence microscopy and flow cytometry. Internalization studies were conducted with high protease-expressing mMSCs. A gelatin zymogram was used to characterize the MMP-2 and MMP-9 expression profile of the cells using conditioned cell media **(Figure 5.1B)**. No extensive internalization of nanoparticles immobilized though non-peptide tethers was observed for protease-expressing cells (e.g. mMSCs), while nanoparticles immobilized through peptide tethers were internalized to a significantly greater extent **(Figure 5.3A-F)**. Although qualitative differences in internalization between different peptide-modified nanoparticles could be observed using inverted fluorescence microscopy, flow cytometry analysis showed

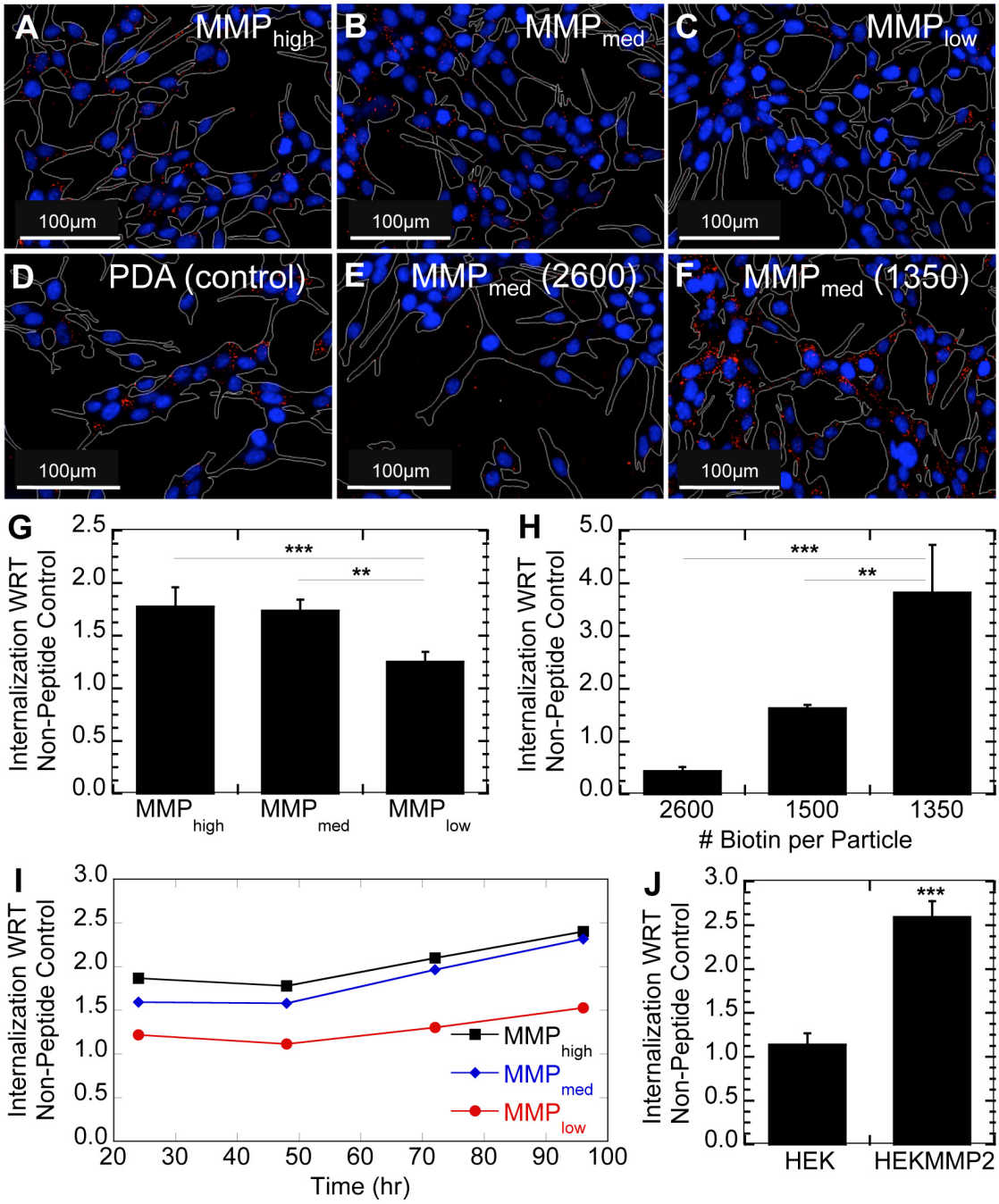

Figure 5.3: Fluorescence microscopy was used to qualitatively analyze particle internalization by protease-expressing mMSCs (red = particle, blue = nucleus, white = cell perimeter) (A-F – 20x magnification). Internalization was found to be a function of peptide sensitivity to cell-released MMPs (A-C) and minimal with respect to non-peptide tethered control particles (D). Particle tethering to the surface was a strong determinant for internalization (E-F); Quantitative characterization of internalization by flow cytometry confirmed peptide sensitivity to proteases (G) and the degree of particle tethering, using MMP_{med} particles (H), dictated release and internalization into protease-expressing mMSCs; Internalization of peptide-modified particle increased with time (I); HEK293T-MMP2 cells internalized MMP_{med} peptide-modified particles 2.6-fold more than control particles, while HEK293T cells internalized only 1.1-fold more (J). The ** and *** symbols indicate statistical significance at levels of $p<.01$ and $p<.001$, respectively, calculated using a multiple comparisons Tukey test. Statistics for Figure J were determined using a single pair comparison Dunnet test.

definitively that protease-expressing cells internalized peptide-modified particles in a manner dependent on peptide sensitivity to cell released proteases, namely MMPs **(Figure 5.3G)**. It is important to note that the trends were unlike what was observed in our acellular release studies, with the trend high > medium > low for peptide cleavage rate holding **(Figure 5.3A-C, G)**. Protease expressing cells have a much higher local protease concentration directly around their surface than is found in the bulk conditioned media [132], thus protease dependent effects can be amplified when the particles are directly in contact with cells. This phenomenon also explains the significant differences in internalization as a result of differences in tether density **(Figure 5.3E-F, H)**, for which the observed trend in our two-dimensional in vitro study was far more significant when compared to that from the acellular release studies using cell conditioned media **(Figure 5.3H)**. These results show the importance of testing cell-triggered delivery strategies directly with cells rather than relying on acellular studies since the same trends are not always observed.

All peptide-tethered nanoparticles were also shown to release steadily for up to four days **(Figure 5.3I)**. Such sustained release is essential for a biomaterial, which will eventually be used in vivo where the tissue regeneration process will be on the time scale of days to weeks.

Since the internalization rate of nanoparticles can vary widely among different cell types, HEK293T, which express low levels of proteases **(Figure 5.1B)**, were genetically engineered to over-express MMP-2 (HEK293T-MMP-2) [133]. By testing the rate of peptide-tethered nanoparticle internalization by HEK293T cells in direct comparison with HEK293T-MMP-2 cells, the effect of a cell's protease expression profile on internalization of immobilized nanoparticles can be studied. HEK293T-MMP-2 cells internalized 2.6-fold more peptide-tethered nanoparticles with respect to non-

peptide tethered particles compared to HEK293T cells, which only internalized 1.1-fold more **(Figure 5.3J)**. The statistically significant difference in overall internalization demonstrated that the protease expression profile of the seeded cells was the main factor in determining the release and internalization kinetics of peptide-tethered nanoparticles.

5.3.5 Three-dimensional translation to porous PEG hydrogels

To determine if cell-triggered delivery of peptide-immobilized nanoparticles, which was previously observed on two-dimensional surfaces, was possible in a three-dimensional microenvironment we translated our approach for cell-triggered internalization to a three-dimensional PEG hydrogel. This allowed for increased surface area and set the stage for potential in vivo applications. Because our strategy for controlling nanoparticle internalization rate requires the immobilization of the nanoparticles to the hydrogel scaffold, we used micro-porous hydrogels rather than nano-porous hydrogels to ensure that no encapsulated nanoparticles were present **(Figure 5.4)**. The micron-sized pores allow for increased diffusion and ability to remove nonspecifically bound particles through washing and allow for the attachment of the PS nanoparticles after gel formation. This ensures the nanoparticles are not encapsulated and bound only to the pore surfaces. And although the ultimate goal is to be able to deliver genes from a porous HA(-MMP degradable) hydrogel, in this proof of principle system a non-degradable, UV-crosslinked PEG based hydrogel was used to be able to easily monitor particle internalization as a function of tether cleavage and not gel degradation. Interconnected pores in a non-degradable porous PEG hydrogel additionally allow for uninhibited cellular spreading and migration. To produce the porous hydrogels we modified a previously described poly(methyl methacrylate)

(PMMA) microsphere template method [24] to produce our porous PEG hydrogels **(Figure 5.4A)**. Gels were characterized using rheometry to test for mechanical properties **(Figure 5.4B)** and phase **(Figure 5.4C, F)** and scanning electron microscopy (SEM) **(Figure 5.4D, G)** to produce micro- and nano-scale structural images, respectively. Next, acrylate-modified PS nanoparticles were covalently bound to the surface of these porous hydrogels through reaction with previously unreacted surface acrylate groups

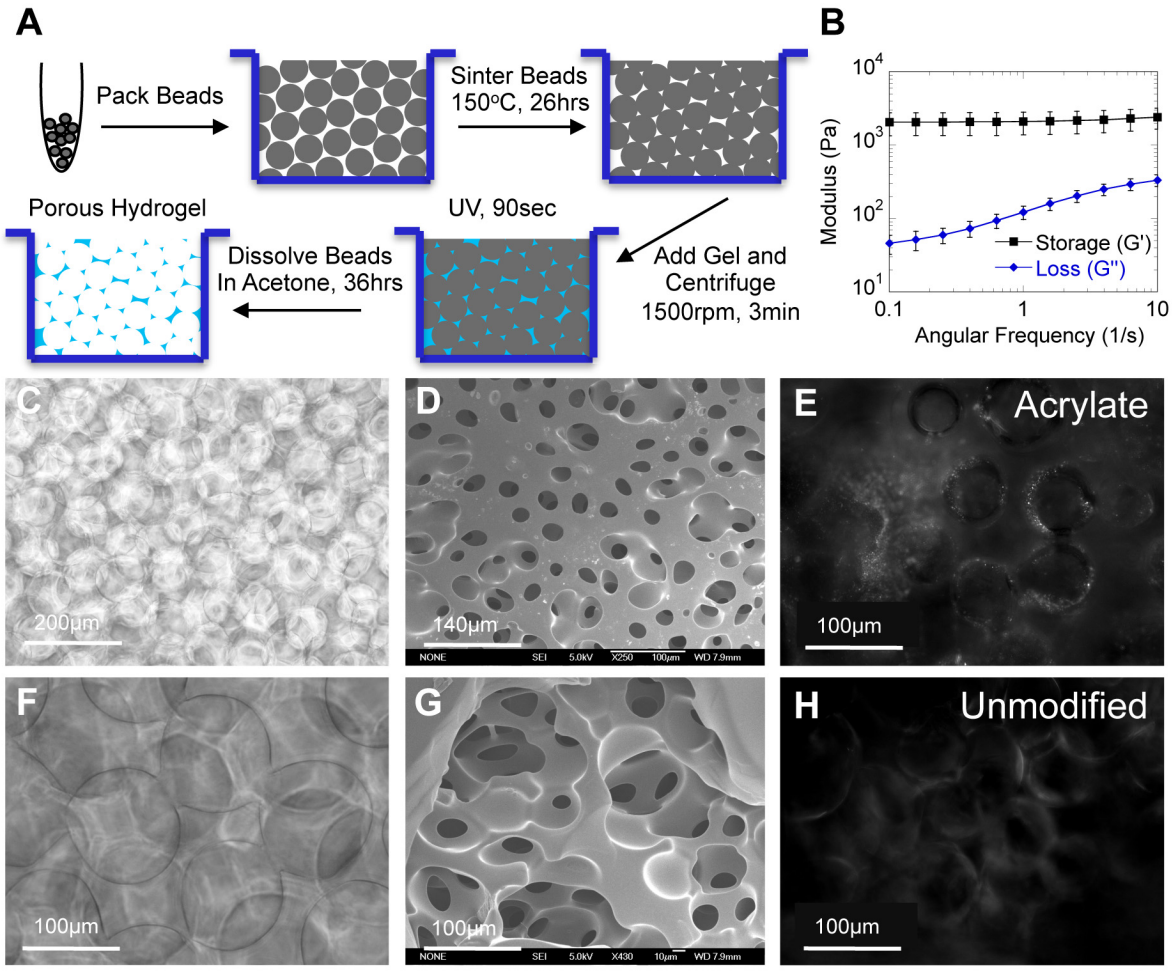

Figure 5.4: Porous PEG hydrogels were made using a modified PMMA bead template (A). PMMA beads were packed and slightly sintered to allow for µ-sized interconnected pores. Once the PEG-DA monomer was added into the void space and polymerized, the PMMA beads were dissolved in acetone; Plate-to-plate rheometry was used to determine the mechanical properties of the porous hydrogels which were found to be very stiff as the storage modulus was almost constant over the frequency range tested (B); Phase images of porous PEG hydrogels made using a PMMA microparticle template (C, F); SEM images show interconnected pores throughout the gel (D, G); Acrylate-modified particles were covalently cross-linked onto the pore surfaces (E), while non-specific binding of unmodified particles was minimal (H).

in the presence of Irgacure 2959 photoinitiator with low intensity UV light **(Figure 5.4E, H)**. (Note: Some particles could have also bound to each other or crosslinked with themselves through this process. Also, the degree of binding was only qualitatively assessed through fluorescence microscopy and not quantified.)

MMP-expressing mMSCs were once again used to study internalization of peptide-tethered nanoparticles in the PEG hydrogels. Cells were seeded on top of the porous gels containing 500 μM RGD and lightly centrifuged to evenly disperse them throughout the gel **(Figure 5.5A-C)**. The cells were then incubated at 37 °C for 24 h, after which they were released from the gels by trypsin treatment and re-plated onto glass coverslips to assess nanoparticle internalization. Without re-plating cells onto a flat surface, internalization was difficult to visualize using fluorescence microscopy. The observed internalization trend was similar to that seen on the 2-dimensional surface. The extent of internalization of peptide-modified particles by protease-expressing mMSCs was controlled by the sequence of the peptide tether with MMP_{high} tethered particles resulting in the most internalization and MMP_{low} tethered particles resulting in the least internalization **(Figure 5.5D-F)**. While further optimization to produce 3-dimensional environments to study immobilized nanoparticle internalization may be done in the future, these results show significant promise for cell-demanded nanoparticle release from porous hydrogel surfaces.

5.4 Conclusions

Here we demonstrated the use of cell-demanded controlled-release systems on nanoparticle delivery. We found that release rates of peptide-immobilized nanoparticles were a function of peptide sensitivity to proteases, the number of tethers between the nanoparticle and the surface, and protease concentration. Cellular

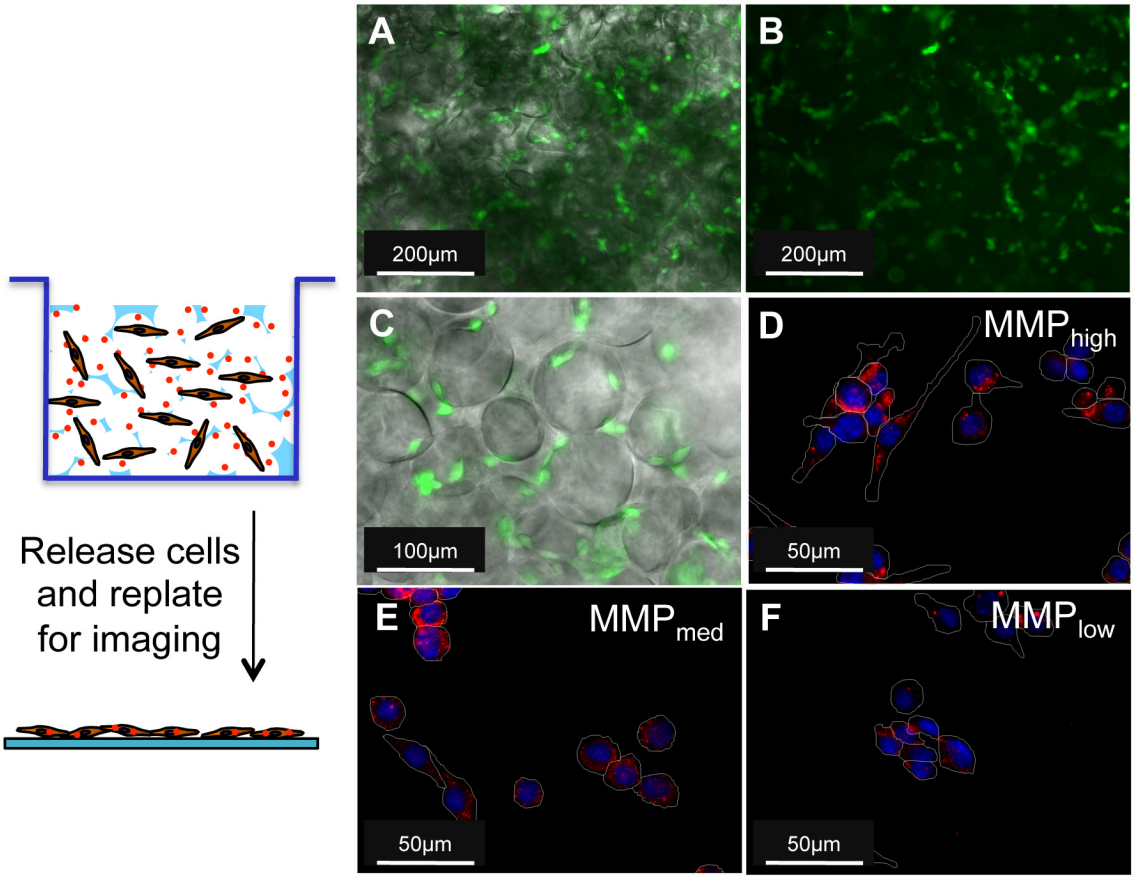

Figure 5.5: Live stained mMSCs were able to spread on porous hydrogels and visualized using fluorescence microscopy (A, B – 10x magnification, C – 20x magnification). Phase image overlaid with fluorescence (B, C); For 3-D in vitro studies, mMSCs were seeded and cultured in the gels for 24hrs, after which they were released and re-plated on glass coverslips to visualize particle internalization via fluorescence microscopy (red = particle, blue = nucleus, white = cell perimeter) (D-F – 40x magnification). Internalization was found to be a function of peptide sensitivity to cell-released MMPs (D-F).

internalization was likewise a function of the peptide sensitivity to proteases and the number of tethers on the nanoparticle. However, release and internalization were shown to vary significantly in the presence or absence of cells, indicating the importance of such cellular release studies, which have generally not been conducted in previous sequential release studies. We observed that the protease (namely MMP) expression profile of the seeded cells was the main factor in determining the release and internalization kinetics of MMP-sensitive peptide-modified particles. By immobilizing nanoparticles through protease sensitive peptide tethers, release could

be tailored specifically for an intended cellular target, which over-expresses such proteases. Similar trends were observed in three-dimensional porous PEG hydrogels indicating protease sensitive tethers are effective in controlling release rate and internalization of nanoparticles, with direct applications to the controlled release of DNA and siRNA polyplexes and other nanoparticles in three-dimensional hydrogels in vivo. The Sullivan group at the University of Delaware later applied MMP-degradable tethers to naked DNA [107].

CHAPTER 6

ENCAPSULATED DNA NANOPARTICLES FOR CONTROLLED DNA DELIVERY

6.1 Introduction

We investigated gene transfer to mouse mesenchymal stem cells (mMSCs) seeded within porous hyaluronic acid hydrogel scaffolds. Porosity in hydrogels has previously been shown to promote cell migration in vitro [19, 25, 26], as well as hydrogel integration and vascularization in vivo [12, 22]. In addition, these porous constructs may serve as non-viral gene carriers by either coating the porous hydrogels or embedding bioactive signals directly within the gel, allowing for cellular uptake [14, 15, 23]. Porous fibrin hydrogels loaded with DNA polyplexes were able to deliver genes to attached fibroblasts [23], however, both encapsulated and surface-coated polyplexes aggregated and elicited cellular toxicity. In the work presented here, the CnE technique was employed to load higher amounts of polyplexes without inducing aggregation. (Note: Although we could have used model polystyrene nanoparticles to avoid dealing with aggregation issues, similar to the approach used in Chapter 5, at this stage in my research it was important to be able to find a way to incorporate polyplexes effectively and to assess gene transfer since the final goal was to use these porous hydrogels for in vivo gene delivery.) For the in vitro studies described below, a Gaussia luciferase reporter plasmid complexed with linear-PEI was incorporated into porous scaffolds using the CnE technique. (Note: Gaussia luciferase is a secreted protein, so unlike

firefly luciferase, cells do not need to be lysed and the surrounding conditioned media can be directly tested for protein expression. This also reduces the number of samples required since the same samples can be tested at multiple time points.)

Since the technique of direct cell seeding onto porous hydrogels described in Chapter 5 was not always reproducible, to optimize cell seeding we proposed a two-phase hydrogel system that contains polyplexes in a stiff (3.5 %) μ-pore HA-MMP gel and mMSCs in a softer (2.5 %) n-pore HA-MMP hydrogel within the μ-sized pores. As the inner gel is degraded quickly in the presence of cell-secreted proteases, it will allow for cell spreading and proliferation, while the polyplexes in the stiff μ-pore backbone will have a more gradual and sustained release upon hydrogel degradation. Studies were focused on how pore size influenced the efficiency of gene transfer and the kinetics of transgene expression. These factors are important for designing successful scaffolds to mediate gene delivery in vivo. The goal is to transfect either: (i) encapsulated stem cells in a DNA- or siRNA-loaded hydrogel scaffold in vitro or (ii) cells infiltrating an acellular scaffold containing DNA or siRNA in vivo.

6.2 Materials and Methods

6.2.1 Materials

Peptides Ac-GCRDGPQGIWGQDRCG-NH2 (HS-MMP-SH) and Ac-GCGYGRGDSPG-NH2 (RGD) were purchased from Genscript (Piscataway, NJ). Sodium hyaluronan (HA) was a gift from Genzyme Corporation (60 kDa, Cambridge, MA). Linear poly(ethylene imine) (PEI, 25 kDa) was purchased from Polysciences (Warrington, PA). Vectors expressing mammalian secreted Gaussia Luciferase (pGluc) were obtained from New England Biolabs (Ipswich, MA) and expanded using a Giga Prep kit from Qiagen

following the manufacturer's protocol. All other chemicals were purchased from Fisher Scientific (Pittsburgh, PA) unless otherwise noted.

6.2.2 Hyaluronic acid modification

Sodium hyaluronan was modified to contain acrylate functionalities. Briefly, hyaluronic acid (2.00 g, 5.28 mmol carboxylic acids, 60 kDa) was reacted with 18.38 g (105.50 mmol) adipic acid dihydrazide (ADH) at pH 4.75 in the presence of 4.00 g (20.84 mmol) 1-ethyl-3-[3-dimethylaminopropyl] carbodiimide hydrochloride (EDC) overnight and purified through dialysis (8000 MWCO) in DI water for 2 days. The purified intermediate (HA-ADH) was lyophilized and stored at –20 °C until used. Approximately 56 % of the carboxyl groups were modified with ADH, which was determined using 1H-NMR (D_2O) by taking the ratio of peaks at δ = 1.6 and 2.3 corresponding to the 8 hydrogens of the methylene groups on the ADH to the singlet peak of the acetyl methyl protons in HA (δ = 1.88). HA-ADH (1.9 g) was reacted with N-Acryloxysuccinimide (NHS-Ac) (1.33 g, 7.89 mmol) in HEPES buffer (10 mM HEPES, 150 mM NaCl, 10 mM EDTA, pH 7.2) overnight and purified through dialysis in DI water for 2 days before lyophilization. The degree of acrylation was determined to be ~10 % using ^{1}H NMR (D_2O) by taking the ratio of the multiplet peak at δ = 6.2 corresponding to the cis and trans acrylate hydrogens to the singlet peak of the acetyl methyl protons in HA (δ = 1.88).

6.2.3 Polyplex lyophilization

For CnE, plasmid DNA (100-250 µg) and L-PEI (91.3-228.3 µg) were mixed in 3.5 mL water in the presence of 35 mg (0.10 mmol) of sucrose (Ultra pure, MP Biomedicals, Santa Ana, CA) and incubated at room temperature for 15 min. Low-melting point

agarose (1.0 mg, UltraPureTM Agarose, Tm = 34.5-37.5 °C, Invitrogen, Grand Islands, NY) in 1.5 mL water was added before lyophilization. Each aliquot was intended for a 100 µL hydrogel. For smaller hydrogel volumes, the sucrose concentration remained unchanged (relative to DNA levels) while the agarose concentration was proportionally decreased.

6.2.4 Design template using PMMA microspheres

Microsphere templates for porous hydrogels were prepared using dry PMMA microspheres (27-33, 53-63, and 90-106 µm, Cospheric, Santa Barbara, CA). Approximately 12-14 mg of microspheres were then added into glass-bottom silicon wells (6 mm x 1 mm, D x H) and covered with a glass slide. The microspheres were then packed by slight tapping for 1-2 min and examined for even packing through phase microscopy. The glass-bottom silicon wells were then placed into an oven and the microspheres were sintered for 22 h at 150 °C.

6.2.5 Porous (and nano-porous) HA hydrogel formation

Hydrogels were formed by Michael-type addition of acrylate-functionalized HA (HA-Ac) with bis-cysteine containing MMP peptide crosslinkers at a final pH of 7.6-7.8. Prior to reaction, a hydrogel precursor solution was made by mixing a fraction of the total HA-Ac with a lyophilized aliquot of cell adhesion peptide, RGD, in PBS pH 9.0 for 30 min at 37 °C. After incubation, HA-RGD was mixed with the remaining HA-Ac and PBS pH 9.0 for a final gel concentration of 3.5 w/v% HA and 500 µM RGD. Finally lyophilized aliquots of the crosslinker (HS-MMP-SH) were diluted in PBS buffer pH 7.4 immediately before addition to a mixture of lyophilized (CnE) or fresh (direct encapsulation) DNA/PEI polyplexes and the hydrogel precursor solution. For direct

encapsulation, DNA and PEI were mixed to form nanoparticles through vortexing for 15 s and incubating for 15 min at RT before being mixed with the HA solution and crosslinkers to form hydrogels. For porous hydrogels, 20 µL of gel solution was then added directly on top of a PMMA microsphere template, covered with a glass slide, and perfused into the template by centrifugation at 1500 rpm for 6 min at 4 °C. The slide was then incubated at 37 °C for 30-45 min to induce polymerization. Once complete, the gels were removed from the silicon wells and placed directly into 100 % acetone for 48 h to dissolve the PMMA microsphere template. The acetone solution was replaced 2-3x during this incubation. The gels were then serially hydrated into sterile PBS and left in PBS until ready for use. For nano-porous hydrogels, the gel solution was sandwiched between two Sigmacoted slides using 1mm thick plastic spacers and incubated at 37 °C for 30-45 min to induce polymerization. Once complete, the gels were placed directly into sterile PBS and left in PBS until ready for use.

6.2.6 Polyplex visualization

To visualize the polyplex distribution, hydrated gels were stained with ethidium bromide (12 µM) for 1 h before imaging with a fluorescent (Observer Z1 Zeiss) microscope. To better visualize the distribution throughout the hydrogel, multiple z-stacks 1.9-2.3 µm thick were taken for each image, deconvoluted to minimize background, and presented as maximum intensity projections.

6.2.7 DNA loading

In order to determine the extent of release of the encapsulated polyplexes, plasmid DNA was radiolabeled with 3H-dCTP (100 µCi, MP Biomedicals, Santa Ana, CA) using a Nick translation kit (Roche, Indianapolis, IN) as per the manufacturer's protocol.

Briefly, an equimolar mixture of dATP, dGTP, dTTP, and 3H-dCTP was prepared and added to the DNA (5 µg) solution. Once the enzyme solution was added to the mixture, the final solution (200 µL) was gently mixed by pipetting and incubated for 2 h at 15 °C. The reaction was stopped by addition of 10 µL 0.2 M EDTA pH 8.0 and heating to 65 °C for 10 min. The DNA was purified using the mini Prep kit from Qiagen (Valencia, CA) following the manufacturer's instructions. The final DNA concentration was 0.2 µg/µL. In order to determine the extent of release of the encapsulated polyplexes, gels were formed using the protocols indicated above with 1 % radiolabeled DNA. To determine the overall loading, all of the acetone and hydrating washes were collected and analyzed for DNA content. Once completely hydrated, the gels were incubated with 0.25 % trypsin/EDTA to completely degrade the gel in order to determine the total amount of DNA still encapsulated. DNA concentrations were measured using a scintillation counter at the UCLA Chemistry core facility. The readout was analyzed using a standard curve.

6.2.8 Gel preparation for SEM imaging

Each porous hydrogel was serially dehydrated in 25 % increments of water/EtOH for 10 min at a time. Hydrogels were left in 100 % EtOH overnight after which they were placed in a dry holder, air dried and, finally, placed under vacuum until time for imaging. The gels were then coated with a thin layer of gold using a gold sputterer and imaged using a JEOL JSM-6700F FE-SEM in the UCLA MCTP core facility.

6.2.9 Preparation and characterization of two-phase gels

Porous hydrogels were prepared exactly as described above, with final overall dimensions of ~8 mm x 1 mm, D x H, after swelling in PBS. After the initial porous gel

was formed it was stained with FITC using a 10x dilution in PBS of a 1 mg/mL stock in DMSO. The gel was incubated at RT for 30 min in the dark, followed by several washes in PBS until the wash solution was no longer changing color. Prior to formation of the second phase, some HA had been modified with Alexa-350 using NHS-Alexa350 (Invitrogen, Grand Islands, NY). NHS-Alexa350 was added at a 1:5 ratio of HA:NHS. The solution was allowed to react for 2 h with mixing in the dark, after which it was dialyzed and lyophilized. To form the second phase, 15 µL per 20 µL porous gel of 2.5 % HA-Alexa350 was mixed with MMP crosslinker and immediately added on top of the 3.5 % HA porous gel. Due to the fluid nature of the 2.5 % HA gel solution prior to gelation, it was able to infiltrate evenly into the pores and form a soft gel after incubation at 37 °C for at least 30 min. The two phases were then visualized using fluorescence microscopy.

6.2.10 Cell culture

Mouse bone marrow derived mesenchymal stem cells (D1, CRL12424) were purchased from ATCC (Manassas, VA) and cultured in DMEM (Invitrogen, Grand Islands, NY) supplemented with 10 % bovine growth serum (BGS, Hyclone, Logan, UT) and 1 % penicillin/streptomycin (Invitrogen) at 37 °C and 5 % CO_2. The cells were passaged using trypsin following standard cell culture protocols every 2-3 days.

6.2.11 Preparation of two-phase gels with mMSCs

Hydrogels were prepared exactly as described above with a final HA concentration of 2.5 w/v%, 500 µM RGD, and 5000 cells/µL (final volume). For those two-phase gels that did not contain cells, PBS pH 7.4 was used in place of the cell solution. Immediately after mixing the precursor solution with crosslinker, 15 µL of

the gel solution was pipetted directly on top of a previously made 20 µL porous hydrogel (~8 mm x 1 mm, D x H, after swelling in PBS) in a low-attachment 96-well plate for a total of 75,000 cells per gel. Due to the fluid nature of the 2.5 % gel solution, it was able to evenly distribute within the pores of porous hydrogel before completely gelling. The gel was allowed to sit at RT for 2-3 min after which it was incubated at 37 °C for 30 min to induce polymerization. 100 µL complete DMEM was then added to each well and replaced daily. All two-phase gels containing cells had µ-pore gels with 1 µg/µL DNA.

6.2.12 Cell viability and spreading

Cell viability was studied with the LIVE/DEAD® viability/cytotoxicity kit (Molecular Probes, Eugene, OR). Briefly, 1 µL of ethidium homodimer-1 and 0.25 µL of calcein AM from the kit were diluted with 500 µL DMEM to make the staining solution. Each gel (2-3 gels per condition per time point) was stained with 150 µL of staining solution for 30 min at 37 °C in the dark before imaging. To better analyze cell spreading, gels (2-3 gels per condition per time point) were fixed for 30 min at RT using 4 % PFA, rinsed with PBS, treated with 0.1 % triton-X for 10 min and stained for 90 min in the dark with DAPI for cell nuclei (500x dilution from 5 mg/mL stock, Invitrogen, Grand Islands, NY) and rhodamin-phalloidin (5 µL per 200 µL final stain solution, Invitrogen) in 1 % bovine serum albumin solution. The samples were then washed with 0.05 % tween-20. For both cell viability and cell spreading, an inverted Observer Z1 Zeiss fluorescence microscope was used to visualize samples. To better visualize the distribution throughout the hydrogel, multiple z-stacks 1.9-2.3 µm thick were taken for each image, deconvoluted to minimize background, and presented as maximum intensity projections.

6.2.13 Cell proliferation

MTT assay (CellTiter 96R AQueous One Solution Cell Proliferation Assay, Promega, Madison, WI) was used to quantify the cell proliferation rate. 20 µL MTT reagent with 100 µL DMEM was added to each gel in a 96-well plate and incubated at 37 °C for 2 h. The cells were lysed after 2 h with addition of 10 % sodium dodecyl sulfate. The solutions were transferred to a new plate and absorbance was measured at 490 nm using a standard plate reader. Three gels for each condition were analyzed at each time point.

6.2.14 DNA release in the presence of mMSCs

In order to determine the extent of release of the encapsulated polyplexes, two-phase gels were formed as indicated above with 1 % radiolabeled DNA. Gels (n=3) were placed in 150 µL of release solution. At the indicated time points, 150 µL of the solution was removed and an additional 150 µL of fresh release medium was added. Following the final release medium collection, the gels were incubated with 0.25 % trypsin/EDTA to result in complete release of the DNA from the gel upon degradation. DNA concentrations were measured using a scintillation counter at the UCLA Chemistry core facility. The readout was analyzed using a standard curve and plotted as percent of total DNA encapsulated.

6.2.15 Gel degradation in the presence of mMSCs

Gel degradation was determined using a slight modification of a previously established carbazole assay to quantify the uronic acid content in solution [134]. The same two-phase samples used for the DNA release studies were also used to determine

degradation. 5 µL of release solution was diluted 20-fold using saturated benzoic acid and added to 600 µL of chilled 25 mM sodium tetraborate in concentrated sulfuric acid. The sample was vortexed, incubated at 100 °C for 10 min, and brought back down to 4 °C. Next, 20 µL of 0.125 % carbazole in absolute ethanol was added to each sample, vortexed, incubated at 100 °C for 15 min, and finally brought back down to 4 °C. Sample absorbance was determined at 530 nm with a pure benzoic acid sample used as a blank. Concentration was then obtained in reference to a D-glucuronolactone standard curve and finally plotted as % uronic acid released based on the total amount of HA in both phases. Alternatively, pore size measurements were made manually from phase images of gels with cells growing within the pores over time. At each time point 3 gels were analyzed per condition, with 9 measurements per gel (3 measurements at 3 different z-planes). AxioVision software was used to make measurements.

6.2.16 Gene transfer from two-phase hydrogels

pGluc/PEI nanoparticle loaded hydrogels with mMSCs were made as described above. Each day the media was collected and frozen immediately at -20 °C and fresh media was added to each gel. To quantify secreted Gaussia luciferase levels in the media, the samples were thawed on ice and assayed using a BioLuxTM Gaussia Luciferase Assay Kit (New England Biolabs, Ipswich, MA) as per the manufacturer's protocol. Briefly, 20 µL sample was mixed with 50 µL 1x substrate solution, pipetted for 2-3 s, and read for luminescence with a 5 s integration. Background was determined with media from gels that did not contain any DNA and values were expressed as relative light units (RLU).

6.2.17 Gaussia luciferase escape from hydrogels

Mouse MSCs were transfected for 24 h in tissue culture (TC) plastic and then detached using trypsin/EDTA and either re-plated onto TC plastic or encapsulated within HA-MMP degradable hydrogels at a density of 5000 cells/μL gel. The total number of cells was kept constant. After 48 h, conditioned media was collected from all samples and Gaussia luciferase expression was determined for both systems. Total Gaussia luciferase expression in HA hydrogels was normalized to that on TC plastic.

6.2.18 Statistical analysis

All statistical analysis was performed using Instat (GraphPad, San Diego, CA). Experiments were statistically analyzed using the Tukey test to compare all pairs of columns using a 95 % confidence interval. Outliers in the gene transfer studies were detected using the Grubbs' outlier test. All errors bars represent the standard error of the mean (SEM).

6.3 Results and Discussion

6.3.1 Experimental design and rationale

To optimize the design of porous hydrogels with encapsulated non-viral vectors, in vitro studies were initially conducted. Lyophilized polyplexes were incorporated into the hydrogel during hydrogel gelation **(Figure 6.1A)** to achieve a final DNA concentration of either 1.0 or 2.5 μg DNA/μL hydrogel (20 or 50 μg DNA total per 20 μL gel, respectively). The distribution of the polyplexes inside the hydrogel scaffold was determined by staining with ethidium bromide post hydrogel formation. Polyplexes made using the CnE technique were observed mostly as nonaggregated particles and uniformly distributed throughout the gel **(Figure 6.1B, C)**. In contrast, those made even at 1 μg/μL without agarose and sucrose were highly aggregated

(Figure 6.1D). These results confirmed that the CnE technique for incorporating high amounts of DNA into HA hydrogels was essential for nonaggregated distribution. Using radiolabeled DNA, we were also able to verify that there was minimal loss of incorporated DNA during gel formation, acetone washes, and initial swelling in PBS **(Figure 6.1E)**.

In addition to the incorporation of non-viral DNA nanoparticles, pore size was also assessed as a potential factor in determining gene transfer kinetics. PMMA beads

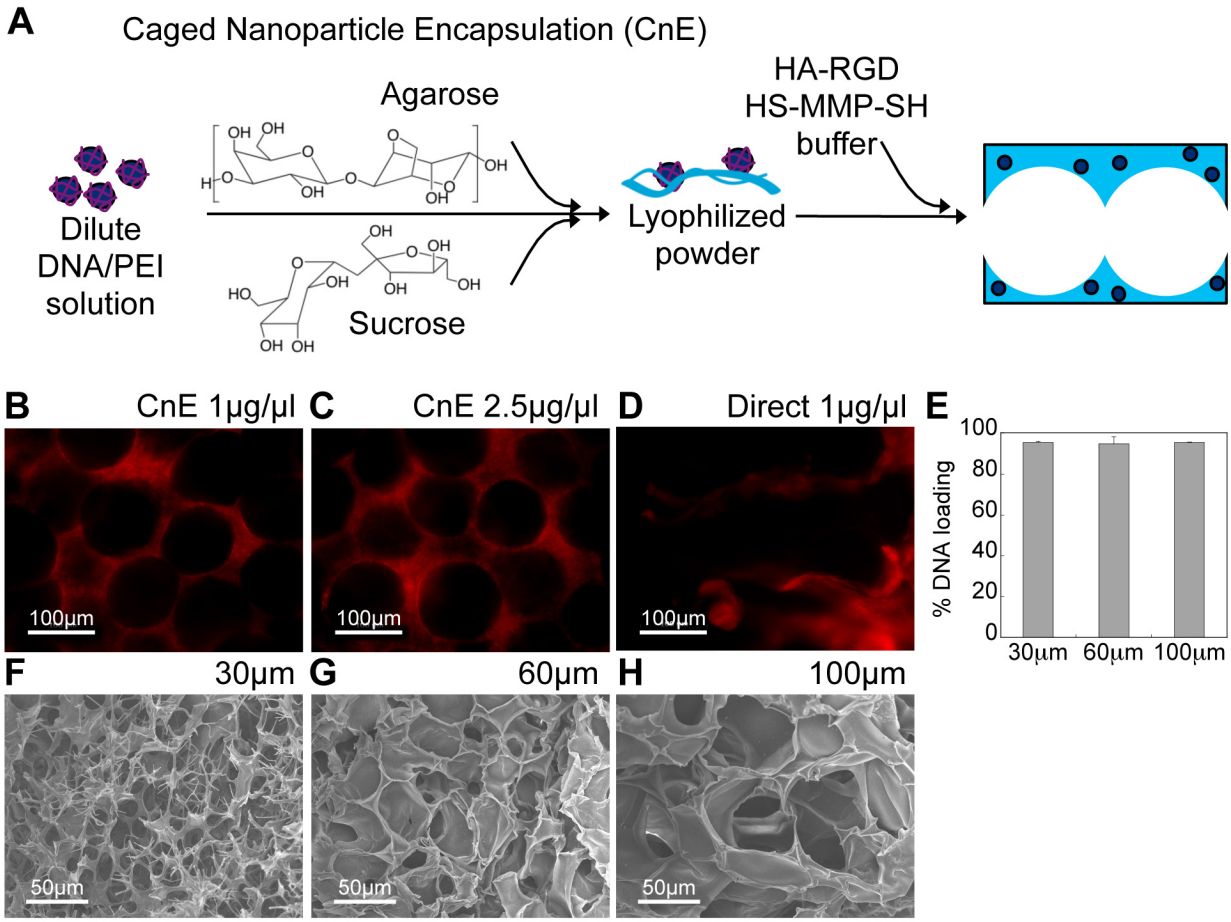

Figure 6.1: (A) Schematic of CnE process to incorporate non-aggregated DNA/PEI polyplexes into porous hydrogels. (B-D) Using the CnE technique 1-2.5 µg/µl DNA could be incorporated without significant aggregation, while direct incorporation of 1 µg/µl resulted in highly aggregated particles; DNA was visualized via ethidium bromide staining. (E) 3H-dCTP labeled DNA was used to verify over 95% of loaded DNA remained in the gel after porous gel processing. Porous hydrogels were synthesized by using different sized PMMA template beads. (F-H) SEM was used to characterize gel structure as a function of bead size. F-H = 500x magnification images.

of various sizes (~30, 60, and 100 μm) were used to form the template. To visualize the porous structure and specifically the differences in porous hydrogels made using the various sized microspheres, hydrogels were dehydrated in ethanol and imaged using scanning electron microscopy **(Figure 6.1F-H)**. Due to the tight range in bead size, the pore size distribution in each hydrogel was qualitatively uniform. However, exact pore size could not be measured from these SEM images since ethanol dehydration resulted in a significant reduction in overall gel size to ~40 % of the original size. Lastly, as a result of sintering the microspheres, interconnectivity was present between almost every neighboring pore.

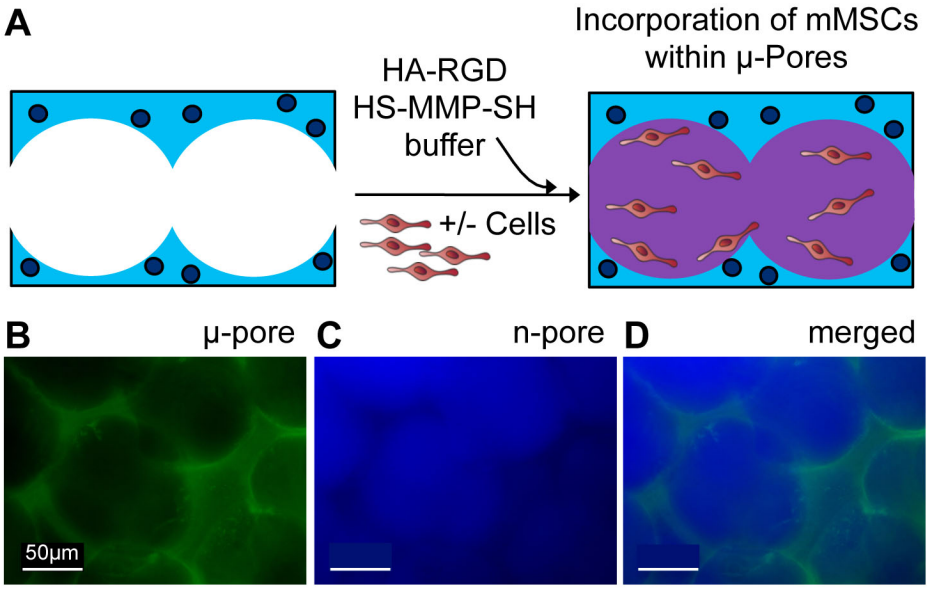

Figure 6.2: (A) To effectively seed cells and allow for rapid cell spreading without significant gel degradation, cells were seeded within the pores of a 3.5% μ-pore HA gel directly with a soft 2.5% HA gel. To visualize each phase separately the μ-pore phase was stained with FITC (B) and the inner, n-pore phase was stained with Alexa-350 (C). (D) Merged fluorescence image of a two-phase hydrogel.

6.3.2 Cell seeding using two-phase gel approach

To easily seed cells within pores in vitro, we utilized a two-phase hydrogel technique. Once μ-pore 3.5 % HA hydrogels were formed, mouse MSCs were mixed into

a thin 2.5 % n-pore HA-MMP hydrogel precursor solution and pipetted directly on top of the µ-pore hydrogel **(Figure 6.2A)**. Due to the fluid nature of the 2.5 % hydrogel precursor solution initially at room temperature, the gel solution was able to flow throughout the pores of the porous hydrogel and distribute the cells within the pores. In this situation, the porous hydrogel was used as a template upon which to seed cells in a softer gel phase. To ensure even distribution of the second phase within the pores of the porous hydrogel, two-phase HA hydrogels were prepared in the absence of cells. After the initial porous gel was formed it was stained with FITC. HA modified with Alexa350 was then used to form the inner phase gel. The two phases were then visualized using fluorescence microscopy. Both phases could clearly be distinguished and were present in most parts of the gel system **(Figure 6.2B-D)**.

6.3.3 Cell viability, spreading, and proliferation

The toxicity of the DNA/PEI polyplexes was assessed using the LIVE/DEAD assay. Since the concentrations used in this study were in general high for in vitro culture systems, some toxicity was expected. However, since most cells were not in direct contact with the polyplexes embedded within the porous phase and were only exposed to the released polyplexes and those near the pore surfaces, toxicity remained low throughout the culture period **(Figure 6.3A-F)**. With respect to the total number of cells, very few dead (i.e. red) cells could be observed in all pore sizes. However, a number of cells could be seen exiting the hydrogel from the bottom surface and binding to the tissue culture well, especially with increasing pore size. Likewise these cells stained green **(Figure 6.4)**, indicating low levels of toxicity from released DNA polyplexes. Cell spreading as a function of pore size was also investigated. Cell spreading was observed for all conditions even by two days as a result of the soft 2.5 % HA second phase the

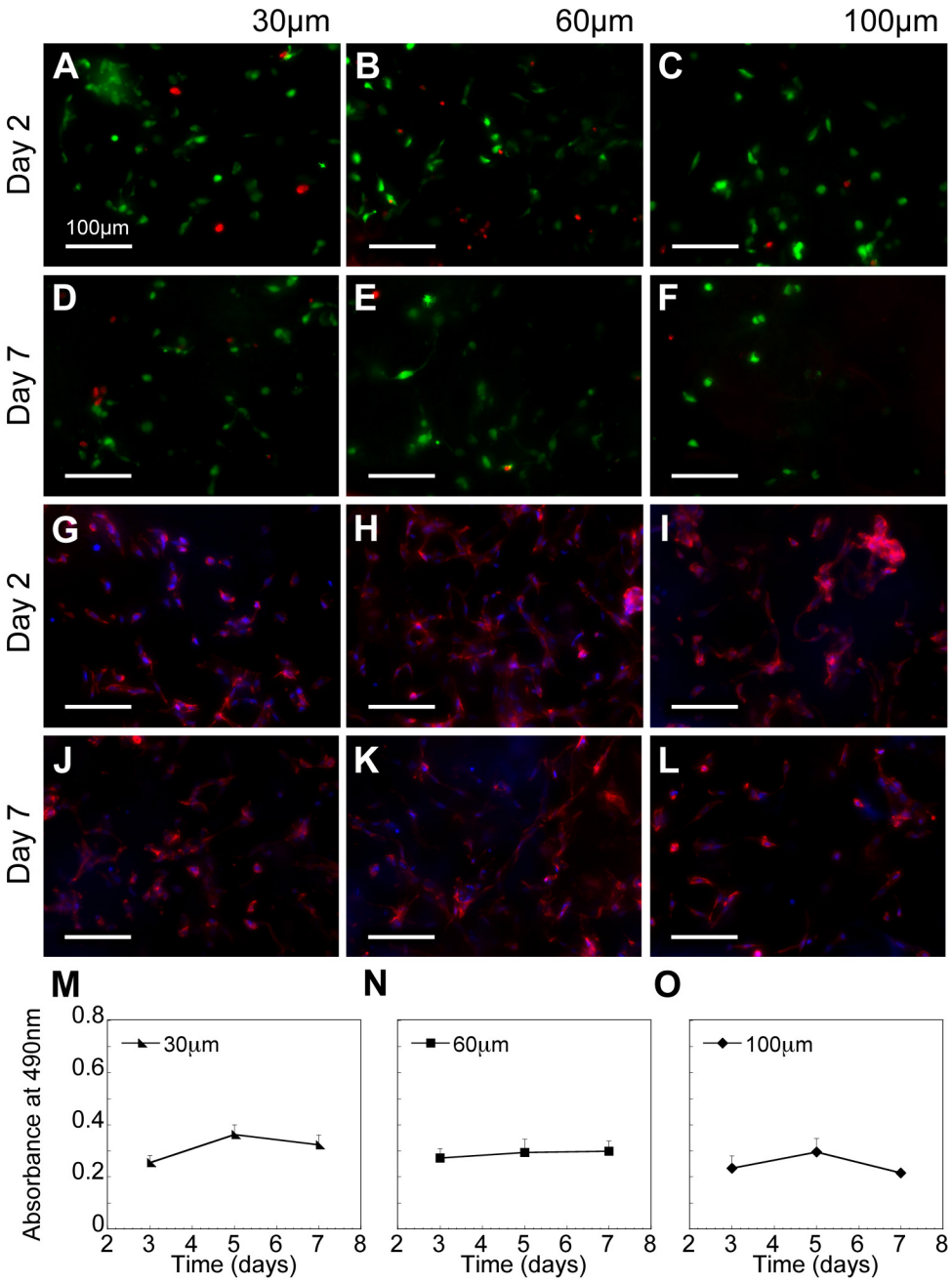

Figure 6.3: (A-F) Live/dead staining showed most cells were alive (live = green, dead = red) in all pore size hydrogels after 2 and extending through 7 days. (G-L) Cells were also fixed with 4% paraformaldehyde and stained with rhodamine-phalloidin (actin) and DAPI (cell nuclei) to better visualize cell spreading. (M-O) MTT assay indicated similar cellular metabolism between various pore sizes (n=3).

cells were seeded within **(Figure 6.3G-L)**. Last, the metabolic activity of the cells inside the DNA-loaded hydrogels was studied using the MTT assay. No significant changes in metabolic activity were observed within the hydrogel **(Figure 6.3M-O)**. To measure the

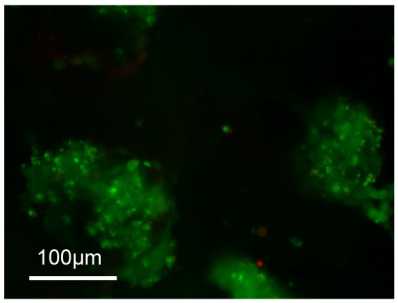

Figure 6.4: Live/dead staining showed most cells that had exited the hydrogel were alive (live = green, dead = red). Cells appear as clumps on non-TC treated plastic below the hydrogel surfaces.

metabolic activity of the cells solely within the hydrogels, we placed each gel into a new well immediately prior to measuring. As a result, we cannot directly correlate these findings to a decrease or halt in cell proliferation, but rather maintain that the number of cells within each gel remained relatively constant over time.

6.3.4 DNA release and hydrogel degradation as a function of pore size

The release of the entrapped polyplexes was assessed using radiolabeled DNA either in the absence (i.e. PBS control) or presence of cells. Release studies indicated a sustained release of polyplexes in the presence of cells over ten days **(Figure 6.5A)**, while less than 2 % of the polyplexes were released in PBS in all pore size hydrogels both due to the absence of enzymes and potentially in part due to the electrostatic interactions of the positively charged polyplexes with the negatively charged HA backbone. By day 10, polyplexes in 30 µm gels had the greatest percentage of release compared to the 60 and 100 µm pore sizes, but because of the increased variability among the 100 µm gels were only significantly greater than the 60 µm gels **(Figure 6.5B, $p<.05$)**. The sustained release of DNA polyplexes was a significant improvement over the burst release of naked DNA from porous PEG gels, with over 50 % of DNA

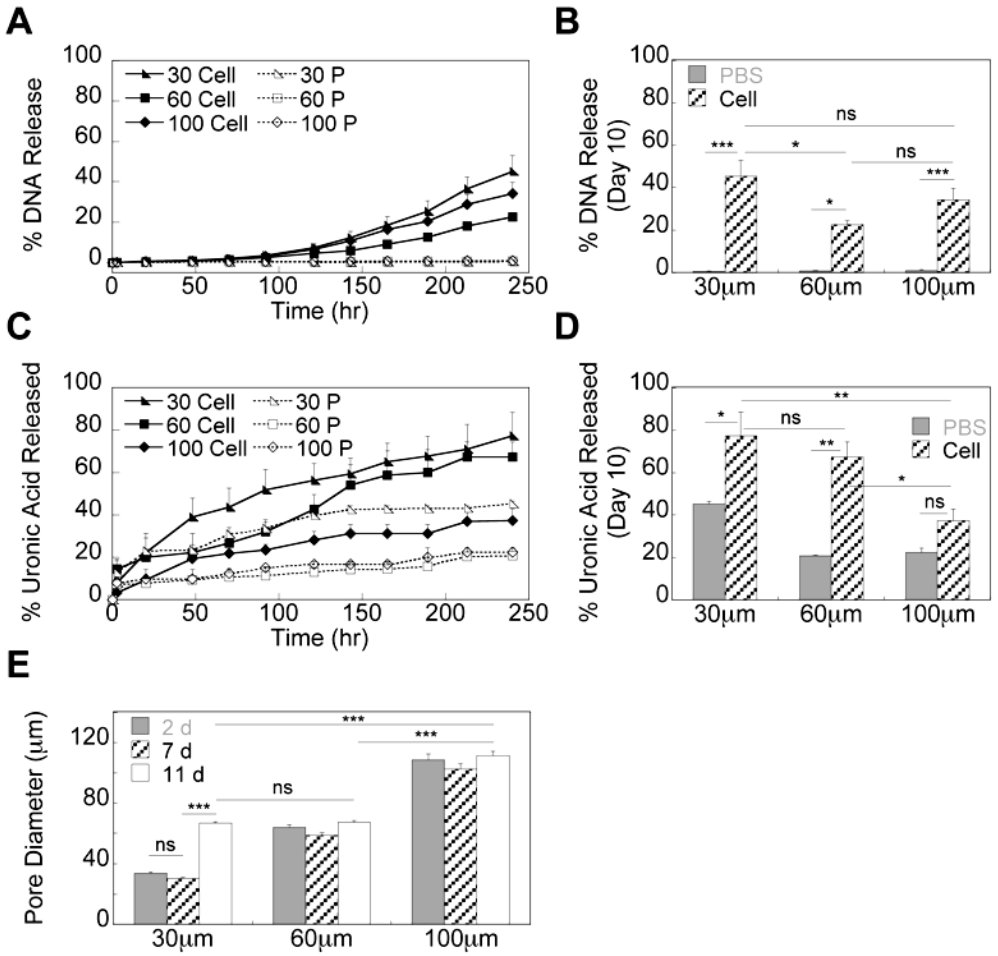

Figure 6.5: (A) 3H-dCTP radiolabeled DNA was incorporated into the hydrogels to study release kinetics in the presence of mMSCs (Cell). PBS (P) was used as an acellular control. (B) Cumulative release data at Day 10 shows 30 μm pore size gels had the largest percentage of released DNA. (C, D) Hydrogel degradation was monitored using a carbazole assay to directly quantify uronic acid in solution. Release of uronic acid after 92 hrs is assumed to be primarily from the μ-pore phase. (E) Two-phase gel degradation was also assessed by measuring pore size over time (n=27) using phase microscopy.

being released by day three [15] in PBS, yet comparable to the release of DNA/PEI polyplexes from porous fibrin hydrogels [23].

The same release samples were also used to measure hydrogel degradation by measuring uronic acid content in the release solution using a modified carbazole assay. For all pore sizes, HA gel degradation was greater in the presence of cells compared to the PBS control, although this difference was not significant for the 100 μm pore size **(Figure 6.5C, D)**. However, for all pore sizes some uronic acid release was observed

even in PBS up until about 96 h after which no further release was observed **(Figure 6.5C)**. This directly corresponded to the time at which polyplexes started to be released in the presence of cells. We believe that the majority of the uronic acid released into solution until this point came from the 2.5 % inner phase gel, especially since the 2.5 % gel is naturally very weak with a storage modulus of only 130.00 ± 4.92 Pa **(Figure 6.6A-B)**. When used as a second-phase gel, it is likely that there was incomplete crosslinking occurring, particularly in the case of smaller pores where you are forcing macromolecular chains into a smaller, more tortuous space and thus the likelihood of the reactive groups encountering one another decreases. After ~96 h, it is expected that a larger contribution is made by degradation of the porous, outer phase

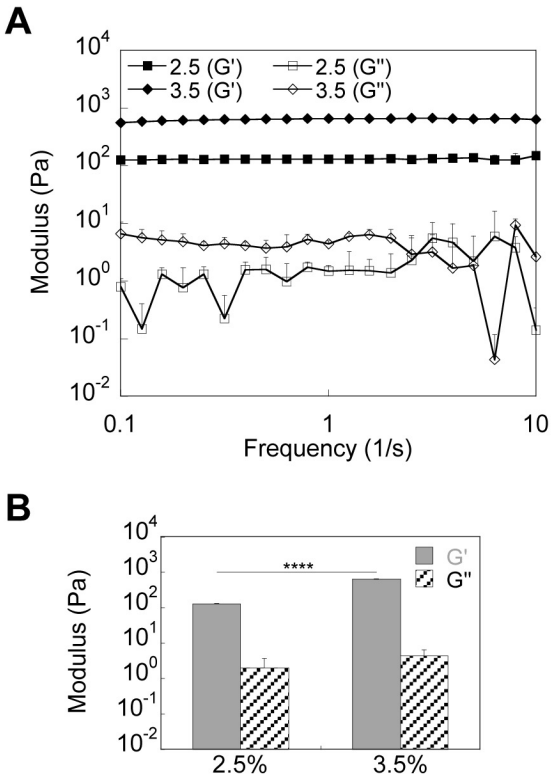

Figure 6.6: (A) A frequency sweep was used to determine the storage (G') and loss (G") moduli of 2.5% HA hydrogels (without agarose and sucrose) which are identical to those used in the second phase of the two-phase hydrogel. The storage and loss moduli of 3.5% gels were plotted for comparison. (B) Average modulus values.

since degradation is required for polyplex release. Again, we observed that the amount of uronic acid released was the greatest in the 30 µm gels with almost 80 % being released. At this point the gels became extremely soft, but were still held together by the remaining crosslinks. We hypothesized that the second-phase was completely gone by this point and those cells still remaining in the gel were then mostly in contact with the porous phase. As a secondary approach to monitoring degradation over time, pore size measurements were made from phase images of two-phase gels with cells at various time points (n=27). The porous, outer structure could still be clearly distinguished even in the presence of the second phase and showed that in only the 30 µm gels did the pore size significantly increase from ~30 to ~60 µm in diameter **(Figure 6.5E, p<.005)**. Based on the degree of uronic acid release we expected to see an increase in pore size as a result of degradation in the 60 µm gels and a smaller change in the 100 µm gels; however, due to a large degree of error in the carbazole assay so there was no clear discrepancy between the findings of the two separate experiments, as well as those trends found between the DNA release and carbazole assays. Importantly, all the results do indicate that with a 30 µm pore size, significantly more degradation occurs (compared to larger pore size gels.) This difference may be a result of greater confinement of encapsulated cells leading to an increased need for degradation to allow growth and subsequently a greater polyplex release rate.

6.3.5 in vitro gene transfer as a function of pore size

Gene transfer was also assessed as a function of pore size and DNA concentration. Gaussia luciferase (Gluc) reporter plasmid was incorporated into the various pore size hydrogels at a concentration of 1 µg/µL hydrogel solution and transgene expression was quantified using a Gaussia luciferase quantification assay.

Histograms show kinetic data of all samples (n=8) over time **(Figure 6.7A-C)**. Cumulative data shows an increase in Gluc expression with time, although by day 10 the differences between various pore size gels were not statistically significant **(Figure 6.7D)**. The lack of any trend in transfection with respect to hydrogel pore size is most likely a result of the high variability between samples even within a single pore size, as demonstrated in the histograms **(Figure 6.7A-C)**. We hypothesize that the variability arises from the local distribution of the cells within the pores with respect to the polyplexes in the first gel phase. Cells that are closer to the pore surfaces or are able to infiltrate into the first gel phase are in direct contact with polyplexes and are transfected at higher levels than those far from the pore surfaces **(Figure 6.7E)**. To alleviate this issue, cells could have been directly seeded onto pore surfaces without

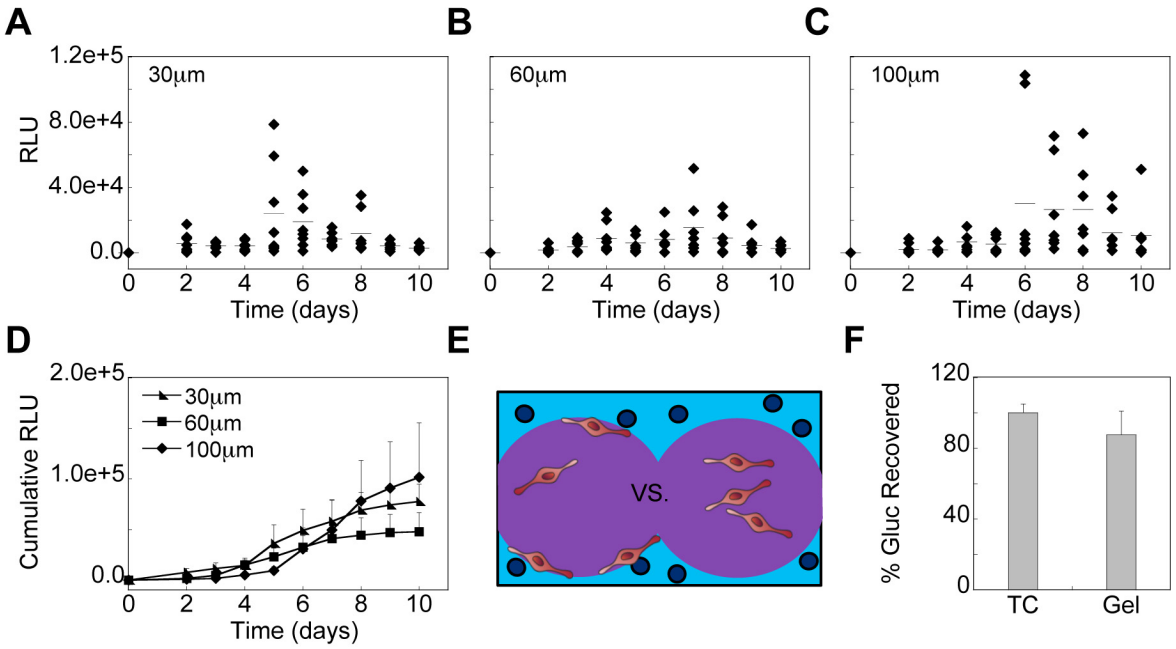

Figure 6.7: Gaussia luciferase reporter plasmid was incorporated into the various pore sized hydrogels at 1 μg/μl hydrogel and transgene expression was quantified using a Gaussia luciferase quantification assay. (A-C) Histograms show kinetic data of all samples (n=8) over time for each pore size hydrogel. (D) Cumulative data shows an increase in Gluc expression with time, although by day 10 the differences between gels types are not statistically significant. (E) To verify all protein expressed was being accounted for, previously transfected cells were placed into HA gels and assessed for Gluc expression after 48 hours and compared to those cells on tissue culture (TC) plastic. The results were not significantly different.

the presence of the second gel phase. However, seeding cells in this manner within HA based gels is very difficult because of the lack of immediate adhesion to the pore surfaces even in the presence of 500 μM RGD. Cells then tended to flow through the pores and fall out of the gel more easily, which is specifically why we utilized the two-phase cell seeding technique. Finally, to ensure all expressed protein was being recovered for analysis and not the cause of the transfection variability, cells were first transfected for 24 h in tissue culture (TC) plastic and then detached using trypsin/EDTA and either re-plated onto TC plastic or encapsulated within HA-MMP degradable hydrogels. After 48 h, Gaussia luciferase expression was determined for both systems and showed similar levels of expression indicating no significant sequestration of Gaussia luciferase within the hydrogel **(Figure 6.7F)**.

6.4 Conclusions

Porous HA-MMP hydrogels were used to encapsulate DNA/PEI polyplexes and transfect seeded stem cells as they slowly degraded the matrix. Porous hydrogels allowed for effective cell seeding in vitro post scaffold fabrication, and when coupled with high loading efficiency of DNA polyplexes, allowed for long-term sustained transfection and transgene expression of incorporated mMSCs in various pore size μ-pore hydrogels. For all investigated pore sizes transgene expression was sustained for up to ten days. Cell viability was also shown to remain high over time, even in the presence of high concentrations of DNA polyplexes. Based on these results we believed that the proposed hydrogel system has applications for controlled release of various DNA particles and other gene delivery vectors for in vivo tissue engineering and blood vessel formation. We anticipated that the presence of an open pore structure would increase the rate of vascularization through enhanced cellular infiltration into the gel

and that the added delivery of DNA encoding for angiogenic growth factors would result in long lasting angiogenic signals. Chapter 7 describes the results when this hydrogel system was used to deliver DNA in vivo in a mouse subcutaneous implant model.

CHAPTER 7

DNA DELIVERY FROM POROUS HYALURONIC ACID HYDROGELS TO MICE

7.1 Introduction

In Chapters 5 and 6 two different approaches for the incorporation of (DNA) nanoparticles into porous hydrogels were described. Although it seemed there was greater control over the release of tethered nanoparticles, technically this system was difficult to translate to the delivery of DNA polyplexes mainly due to issues surrounding polyplex aggregation. Thus, moving forward we utilized the second approach to encapsulate DNA polyplexes into various pore size HA hydrogels. The same mouse subcutaneous implant model described in Chapter 4 was used here to assess the effects of pVEGF gene delivery on cellular infiltration and angiogenesis from porous hydrogels at one, three, and six weeks after implantation. To assess levels of transfection and also serve as a non-therapeutic control plasmid in control hydrogels, a GFP-firefly luciferase fusion protein reporter plasmid (pGFPluc) was used. (Note: In previous experiments, other reporter plasmids were used, including pβgal and pGluc encoding for β-galactosidase and Gaussia luciferase, respectively, but good antibodies were not available for these. Using pGFPluc we had the choice to detect transfection either by staining for GFP or firefly luciferase. Based on my experience, GFP was the best detectable reporter protein.)

Vascular endothelial growth factor (VEGF) is a known initiator of vessel branching and angiogenesis and the controlled delivery of VEGF both in vitro and in vivo has been shown to enhance angiogenic responses when compared to a single bolus delivery [4, 56, 58, 110, 135]. In addition to the sustained dosage, VEGF presentation (i.e. soluble or electrostatically or covalently immobilized, clustered or homogeneous) is likewise an important parameter in directing new vessel phenotype [136, 137]. VEGF alone or in combination with other growth factors, including platelet derived growth factor (PDGF) or angiopoietin-1 (Ang-1), has been incorporated into hydrogels for localized treatment of normal and diabetic wounds [75, 138, 139]. However, as described in Chapter 3, there are several disadvantages to the direct delivery of growth factors. As an alternative, non-viral plasmid DNA can be delivered to transfect implanted or infiltrating cells to produce the protein(s) of interest. The work described here aims to deliver pro-angiogenic pVEGF polyplexes to infiltrating cells from a porous hydrogel in vivo to promote sustained blood vessel infiltration.

7.2 Materials and Methods

7.2.1 Materials

Peptides Ac-GCRDGPQGIWGQDRCG-NH2 (HS-MMP-SH) and Ac-GCGYGRGDSPG-NH2 (RGD) were purchased from Genscript (Piscataway, NJ). Sodium hyaluronan (HA) was a gift from Genzyme Corporation (60 kDa, Cambridge, MA). Linear poly(ethylene imine) (PEI, 25 kDa) was purchased from Polysciences (Warrington, PA). Vectors expressing mammalian GFP-firefly luciferase (pGFPluc) and human VEGF-165 (pVEGF) were obtained from New England Biolabs (Ipswich, MA) and expanded using a Giga Prep kit from Qiagen following the manufacturer's protocol. All other chemicals were purchased from Fisher Scientific (Pittsburgh, PA) unless otherwise noted.

7.2.2 Hyaluronic acid modification *(slightly variable to procedure in Chapters 4 and 6)*

Sodium hyaluronan was modified to contain acrylate functionalities. Briefly, hyaluronic acid (2.00 g, 60kDa, 5.28 mmol carboxylic acids) was reacted with 36.77 g (211.07 mmol) adipic acid dihydrazide (ADH) at pH 4.75 in the presence of 4.00 g (20.84 mmol) 1-ethyl-3-[3-dimethylaminopropyl] carbodiimide hydrochloride (EDC) overnight and purified through dialysis (8000 MWCO) in a 100 mM to 0 mM salt gradient for 1 day followed by dialysis in DI water for 4-5 days. The purified intermediate (HA-ADH) was lyophilized and stored at –20 ^{o}C until used. Approximately 54 % of the carboxyl groups were modified with ADH, which was determined using ^{1}H NMR (D_2O) by taking the ratio of peaks at δ = 1.6 and 2.3 corresponding to the 8 hydrogens of the methylene groups on the ADH to the singlet peak of the acetyl methyl protons in HA (δ = 1.88). All of the modified HA-ADH was reacted with N-Acryloxysuccinimide (NHS-Ac) (4.46 g, 26.38 mmol) in HEPES buffer (10 mM HEPES, 150 mM NaCl, 10 mM EDTA, pH 7.2) overnight and purified through dialysis in a 100 mM to 0 mM salt gradient for 1 day followed by dialysis in DI water for 3-4 days before lyophilization. The degree of acrylation was determined to be ~12 % using 1H-NMR (D_2O) by taking the ratio of the multiplet peak at δ = 6.2 corresponding to the cis and trans acrylate hydrogens to the singlet peak of the acetyl methyl protons in HA (δ = 1.88).

7.2.3 Polyplex lyophilization

For CnE, plasmid DNA (250 µg) and L-PEI (228.3 µg, N/P = 7) were mixed in 3.5 mL water in the presence of 35 mg (0.10 mmol) of sucrose (Ultra pure, MP Biomedicals, Santa Ana, CA) and incubated at room temperature for 15 min. Low-melting point

agarose (1.0 mg, UltraPureTM Agarose, Tm = 34.5-37.5 °C, Invitrogen, Grand Islands, NY) in 1.5 mL water was added before lyophilization. Each aliquot was intended for a 100 µL hydrogel. For smaller hydrogel volumes, both sucrose and agarose were scaled down proportionally.

7.2.4 Design template using PMMA microspheres *(slightly different than procedure in Chapters 4 – 6)*

Microsphere templates for porous hydrogels were prepared using dry PMMA microspheres (27-33, 53-63, and 90-106 µm, Cospheric, Santa Barbara, CA). Approximately 20 mg of microspheres (1.19 mg/µL) were mixed with DI water for a final concentration of 20 mg per 100 µL. Then 100 µL of the microsphere solution was pipetted into each well in a glass-bottom silicon well mold (wells = 6 mm x 2 mm, D x H). The microspheres were then allowed to dry and pack (by naturally settling) over 3-4 h at 37 °C. The glass-bottom silicon wells were then placed into an oven and the microspheres were sintered for 22 h at 150 °C.

7.2.5 Porous (and nano-porous) HA hydrogel formation *(slightly different than procedure in Chapters 4 and 6)*

Hydrogels were formed by Michael-type addition of acrylate-functionalized HA (HA-Ac) with bis-cysteine containing MMP peptide crosslinkers at pH 8.0-8.2. Prior to reaction, a hydrogel precursor solution was made by mixing a fraction of the total HA-Ac with a lyophilized aliquot of cell adhesion peptide, RGD, in .3 M TEOA pH 8.2 for 30 min at 37 °C. After incubation, HA-RGD was mixed with the remaining HA-Ac and .3 M TEOA pH 8.2 for a final gel concentration of 3.0 w/v% HA and 100 µM RGD. Finally lyophilized aliquots of the crosslinker (HS-MMP-SH) were diluted in .3 M TEOA pH 8.2

immediately before addition to a mixture of lyophilized (CnE) DNA/PEI polyplexes and the hydrogel precursor solution. For porous hydrogels, 20 µL of gel solution was then added directly on top of a PMMA microsphere template, covered with a glass slide, and perfused into the template by centrifugation at 1500 rpm for 6 min at 4 °C. The slide was then incubated at 37 °C for 30-45 min to induce polymerization. Once complete, the gels were removed from the silicon wells and placed directly into 100 % acetone for 48 h to dissolve the PMMA microsphere template. The acetone solution was replaced 2-3x during this incubation. The gels were then serially hydrated into sterile PBS and left in PBS until ready for use. For nano-porous hydrogels, the gel solution was sandwiched between two Sigmacoted slides using 1 mm thick plastic spacers and incubated at 37 °C for 30-45 min to induce polymerization. Once complete, the gels were placed directly into sterile PBS and left in PBS until ready for use. Prior to surgery all gels were placed in sterile PBS with 1 % P/S overnight.

7.2.6 Subcutaneous implant model *(slightly variable to procedure in Chapter 4)*

All in vivo studies were conducted in compliance with the NIH Guide for Care and Use of Laboratory Animals and UCLA ARC standards. 6 to 8-week old female Balb/c mice each 20-30 grams were used to study cellular infiltration and blood vessel formation in HA hydrogels since this strain and size has been previously used for wound healing and angiogenesis assays [124, 125]. Porous and nano-pore hydrogels were made exactly as described above and cut to 6 mm in diameter using a biopsy punch, for final overall dimensions of 6 mm x 1 mm, D x H. In fabricating the hydrogels, the starting reagents were sterilized through filtering with a 0.22 µm filter. After scaffold fabrication, the hydrogels were washed with sterile PBS and kept in PBS with 1 % P/S. Immediately prior to surgery, mice were anesthetized with 4-5 %

isoflurane through a nose cone inhaler. After anesthesia induction, the isoflurane concentration was lowered to 1.5-2.5 % for the remainder of the surgery. The back of the mouse was subsequently shaved and washed with Betadine and 70 % ethanol. Two incisions appropriate to the size of the implant were made in the skin aside the midline of the animal using scissors. Two subcutaneous pockets were subsequently created by blunt dissection using hemostats. Within the created pockets, the implants were inserted. After insertion of the hydrogels, each incision was subsequently closed with a single wound clip. All animals were observed daily for signs of inflammation and pain and also administered Carprofen injections for the first 48 h post survival surgery. For the preliminary study with directly encapsulated polyplexes, mice (n = 4) were sacrificed after 3 weeks with isoflurane overdose. For the second (main) study with CnE encapsulated polyplexes, mice (n = 4) were sacrificed after 1, 3, and 6 weeks. Two 1 cm^2 pieces of tissue were collected from each mouse containing the implant and the surrounding tissue and skin, fixed in 2 % PFA overnight at 4 ^oC, dehydrated in 70 % EtOH, and finally paraffin embedded.

7.2.7 Immunofluorescence and immunohistochemistry

Paraffin embedded sections (5 µm) were deparaffinized by incubation in multiple xylene washes followed by serial hydration from 100 % ethanol into 100 % water. For CD31/α-SMA staining, antigen-retrieval was conducted with a 15 min incubation at 37 ^oC in 0.1 mg/mL proteinase K solution. Sections were then washed with PBS and incubated in blocking buffer (1 % goat serum (Invitrogen, Grand Islands, NY) + 0.05 % Tween-20 in PBS) for 1 h at RT before being incubated in primary antibody solution (1:100 dilution in blocking buffer of rat anti-mouse CD31 (BD Pharmingen, San Diego, CA)) overnight at 4 ^oC. Sections were again washed with PBS and incubated in

blocking buffer for 10 min at RT before being incubated for 2 h at RT in secondary antibody solution (1:100 dilution in blocking buffer of goat anti-rat Alexa 568 (Invitrogen, Grand Islands, NY) which also contained α-smooth muscle actin-FITC (1:100 dilution, Sigma-Aldrich, St. Louis, MO) and DAPI nuclear stain (1:400 dilution, Invitrogen). Sections were then washed twice in PBS, mounted and imaged using an inverted Zeiss fluorescence microscope. For GFP staining, neither protease nor heat-mediated antigen-retrieval was conducted as these were found to eliminate any GFP signal. All other procedures were conducted exactly as described above with a 1:50 dilution of the primary GFP antibody (Invitrogen, Grand Islands, PA) and 1:100 and 1:400 dilutions of the goat anti-rabbit Alexa 488 secondary antibody (Invitrogen, Grand Islands, PA) and DAPI, respectively. All hematoxylin and eosin staining of sections was conducted by the Translational Pathology Core Laboratory (TPCL) at UCLA.

7.2.8 Vessel quantification, characterization, and statistical analysis

Three separate sections at least 100 – 150 μm apart were analyzed for each sample. Ten randomly chosen areas were imaged in each section. Vessels were counted manually in each section, totaled from all 30 sections, and finally normalized to the total imaged area. The bar graph in Figure 7.5A represent the average vessels/mm^2 from 4 different animals. For samples that contained an average of at 15 vessels/mm^2 (i.e. at least 1 vessel in 50 % of captured images, designated by dotted red line in Figure 7.5A), the diameter of each vessel was manually measured using Zen imaging and analysis software (Zeiss). Percentages were determined using the entire vessel set.

All statistical analysis was performed using Prism (GraphPad, San Diego, CA). Experiments were statistically analyzed using the Tukey test to compare all pairs of

columns using a 95 % confidence interval. All errors bars represent the standard error of the mean (SEM).

7.3 Results and Discussion

7.3.1 Experimental design and rationale

In an attempt to rationally design a hydrogel scaffold to promote angiogenesis in vivo, we utilized the same technique to incorporate encapsulated polyplexes described in Chapter 6 to incorporate pVEGF and pGFPluc polyplexes at concentrations which have previously shown to be effective in vivo [71, 100]. These polyplexes were incorporated into 100 and 60 µm porous and nano-pore hydrogels and implanted subcutaneously into the backs of Balb/c mice. Each mouse had implanted a pVEGF containing gel and its respective pGFPluc loaded control. Unlike the in vitro studies, 30 µm porous hydrogels were not used in vivo due to technical difficulties in reproducible production.

Hydrogels were excised and analyzed at one, three, and six weeks. These time points were strategically chosen in order to observe initial differences in cellular infiltration and possible immediate immune response (week 1), initial appearances of small capillaries and other small vessels (week 3), and sustained presence of new vasculature (week 6). Hematoxylin and eosin (H&E) staining of hydrogel cross-sections indicated increasing cellular infiltration with time and porosity **(Figure 7.1)**, although no distinguishable differences could be observed between 100 and 60 µm porous hydrogels at any time. Importantly, there were no visible differences in infiltration in hydrogels loaded with pVEGF or pGFPluc loaded polyplexes. Small vessels perfused with erythrocytes (i.e. red blood cells) could be observed in all porous hydrogels at three and six weeks. No vessels seemed to be present in nano-pore hydrogels by six

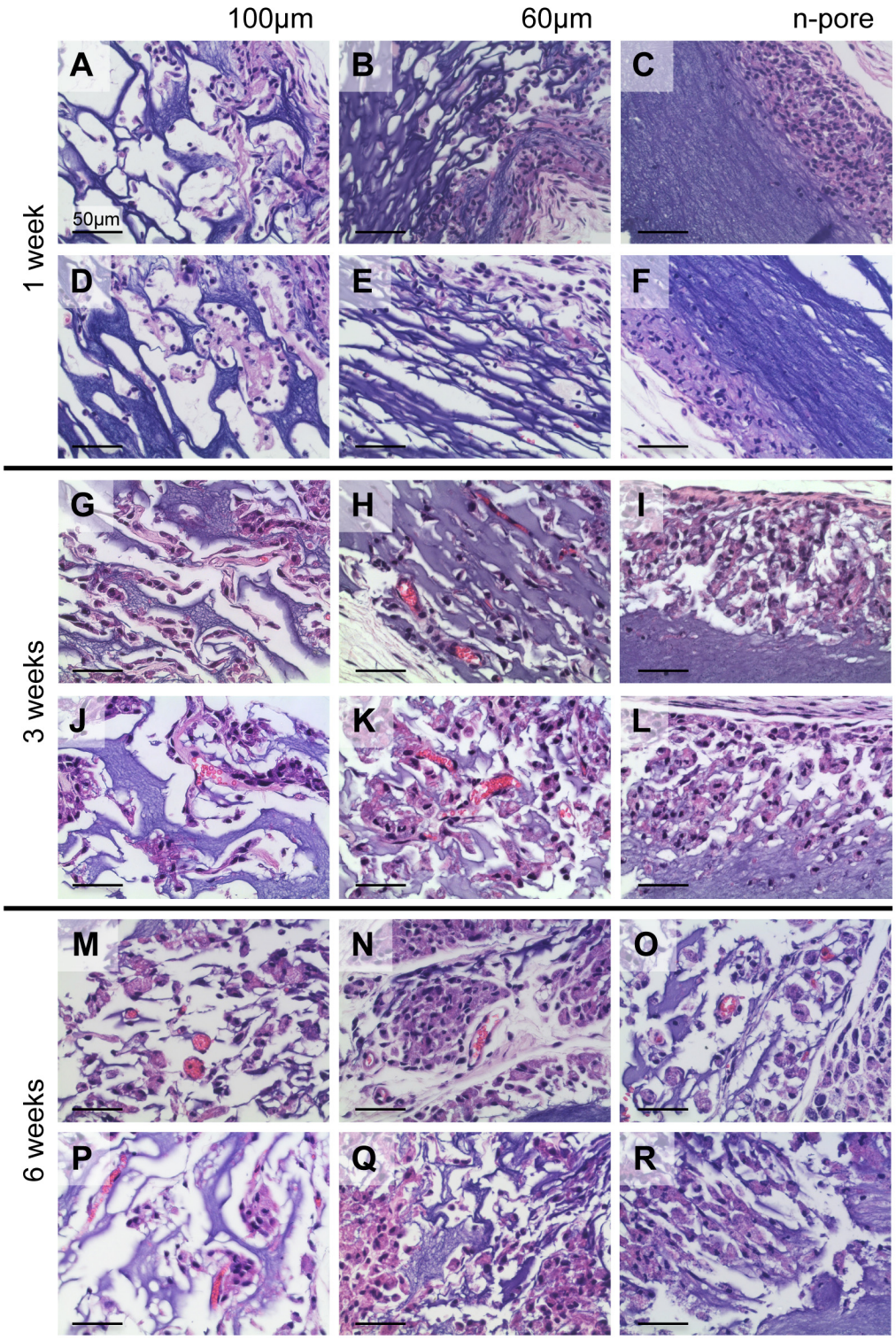

Figure 7.1: H&E stained sections of 2.5 µg/µl pVEGF loaded 3.0% HA 100 (A, G, M) and 60 µm (B, H, N) porous and nano-pore (C, I, O) hydrogels at 1 (A, B, C), 3 (G, H, I), and 6 (M, N, O) weeks after subcutaneous implantation. Control pGFPluc loaded 100 (D, J, P) and 60 µm (E, K, Q) porous and nano-pore (F, L, R) hydrogels at 1 (D, E, F), 3 (J, K, L), and 6 (P, Q, R) weeks exhibit relatively similar levels of cellular infiltration. Blood vessels are apparent in all 100 and 60 µm porous hydrogels at 3 and 6 weeks. All images are 40x magnifications.

weeks even though hydrogel degradation, and subsequent polyplex release, did continue to increase over time.

7.3.2 in vivo transfection

Since no visible differences could be seen between hydrogels loaded with pVEGF or pGFPluc polyplexes, it became crucial to determine if the released polyplexes were in fact able to transfect infiltrating cells in vivo and, if so, to what extent these cells were being transfected. Immunofluorescence staining for GFP in pGFPluc loaded control hydrogels indicated that several transfected cells were present in each hydrogel over the course of the study **(Figure 7.2)**, although the number of transfected

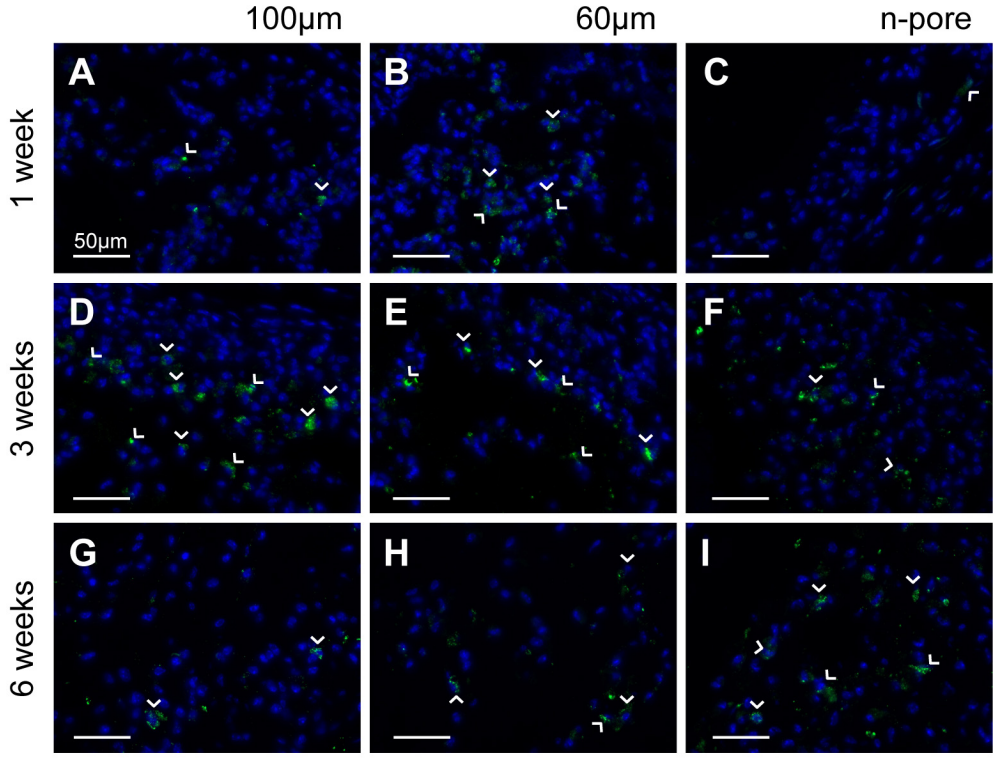

Figure 7.2: Immunofluorescence staining of GFP in pGFPluc loaded control 100 (A, D, G) and 60 µm (B, E, H) porous and nano-pore (C, F, I) hydrogels at 1 (A, B, C), 3 (D, E, F), and 6 (G, H, I) weeks indicates several transfected cells are present in each hydrogel over the 6 week period. Transfected cells in nano-pore hydrogels, however, are only located around the hydrogel periphery where there is infiltration and gel degradation, while transfected cells in 100 and 60 µm porous gels can be found throughout. GFP positive cells = green, cell nuclei = blue. All images are 40x magnifications.

cells in both 100 and 60 µm porous hydrogels seemed to peak around three weeks **(Figure 7.2D, E)**. This may be reflective of the degree of hydrogel degradation between one and three weeks and three and six weeks. If after three weeks cells which had already infiltrated the scaffold become quiescent as a result of minimal immune response to the natural hydrogel material and slowly released polyplexes (i.e. low pDNA/PEI concentration at any given time), degradation of the surrounding matrix and release and transfection of entrapped polyplexes could potentially slow down. Alternatively, the number of transfected cells in nano-pore hydrogels continued to increase with time as a result of continuous gel degradation allowing for exposure to fresh polyplexes **(Figure 7.2C, F, I)**. This was similar to the continuous transfection observed for cell clots encapsulated into hydrogels loaded with polyplexes in vitro [95]. Transfected cells in nano-pore hydrogels, thus, were only located around the hydrogel periphery where there was continuous infiltration and gel degradation, while transfected cells in 100 and 60 µm porous gels could be found throughout **(Figure 7.2A, B, D, E, G, H)**.

7.3.3 Angiogenic response to pVEGF transfection

To determine if the degree of transfection observed led to an enhancement in angiogenesis in pVEGF loaded hydrogels, all samples were analyzed by immunofluorescence for PECAM positive endothelial cells. The differences in angiogenesis between porous and nano-pore hydrogels, similar to what was observed in the preliminary in vivo study described in Chapter 4, were already clear from both H&E stained sections and visible vessels which could directly be observed by visual inspection upon excision **(Figure 7.3)**. Upon staining for PECAM positive endothelial cells and smooth muscle cells, small capillaries and other small vessels were found to

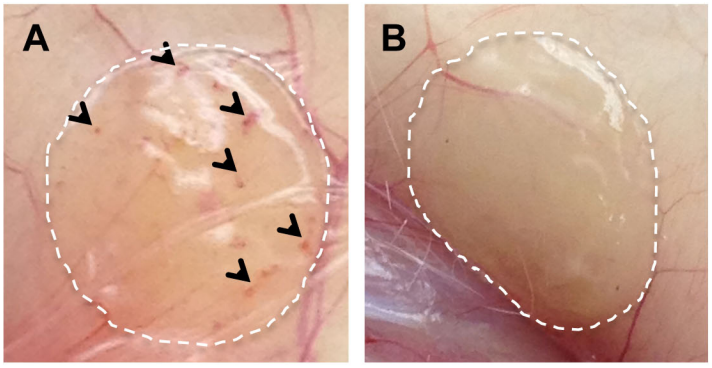

Figure 7.3: Digital images of pVEGF loaded 60 µm porous (A) and nano-pore (B) hydrogels at 6 weeks demonstrate visible differences in angiogenesis.

be present in only a few pVEGF **(Figure 7.4A, G)** and pGFPluc **(Figure 7.4D, J)** loaded 100 µm porous hydrogels at three and six weeks, respectively. For 60 µm porous hydrogels, all samples appeared to have vessels present. However, with these samples it appeared that the number of vessels per image area was higher in both the pVEGF **(Figure 7.4B, H)** and pGFPluc **(Figure 7.4E, K)** loaded hydrogels at three weeks in comparison to those at six weeks, respectively. As expected, no vessels were observed in either pVEGF **(Figure 7.4C)** or pGFPluc **(Figure 7.4F)** loaded nano-pore hydrogels at three weeks. However, detailed staining revealed some small vessels in the degraded gel area surrounding the bulk hydrogel in about half of pVEGF **(Figure 7.4I)** and pGFPluc **(Figure 7.4L)** loaded nano-pore hydrogels at 6 weeks. For all conditions, hydrogels from week one were not further analyzed for angiogenesis since no vessels could be observed from H&E stained sections.

To validate these observed differences, vessels in three separate sections of each sample (n = 3-4, note: in two separate mice, one of two gels could not be identified and excised) were quantified and represented as averages ± SEM in **Figure 7.5A**. Those hydrogels that contained only a few, but still less than 15 vessels/mm^2, fell below the dotted red line. A summary of all the samples positive for PECAM

positive blood vessels is found in **Table 7.1**. The results of the vessel quantification revealed several things that were not directly apparent from the immunofluorescence images. As expected, all nano-pore hydrogels had significantly fewer vessels present than their corresponding 60 µm porous hydrogels at three weeks. However, only in the absence of VEGF delivery (i.e. in pGFPluc loaded hydrogels) was there a significant

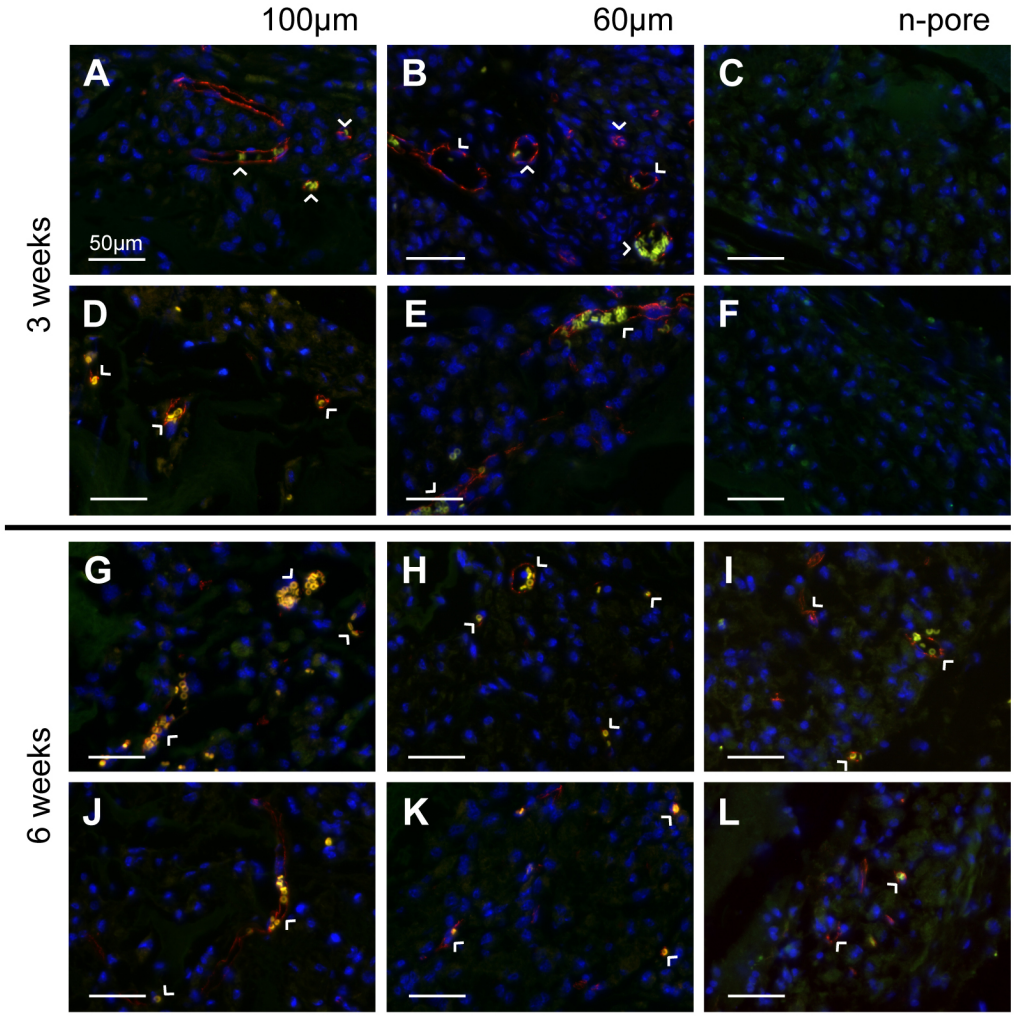

Figure 7.4: Staining for endothelial markers at 3 (A-F) weeks indicated significant positive staining for 100 and 60 µm porous hydrogel implants loaded with pVEGF (A, B) and pGFPluc (D, E), respectively, and not for the n-pore implants loaded either with pVEGF (C) or pGFPluc (F). By 6 weeks (G-L), positive staining for endothelial markers was present in most samples, including 100 and 60 µm porous and several nano-pore hydrogels loaded both with pVEGF (G-I) and pGFPluc (J-L), respectively. Red = PECAM positive staining = endothelial cells, yellow = erythrocytes, blue = cell nuclei. All images are 40x magnifications.

difference between the 60 and 100 µm porous hydrogels, with the 60 µm gels having significantly more vessels at three weeks. It was unclear, however, whether the reason there was no significant difference between the 100 and 60 µm pVEGF loaded hydrogels was, in fact, due to VEGF expression or if there was just too much variability between the 100 µm samples for statistical differences to be apparent. One hypothesis is that the 60 µm porous gels have more vessels present per cross-sectional area than 100 µm porous gels because the smaller, interconnected pores create more rigid and

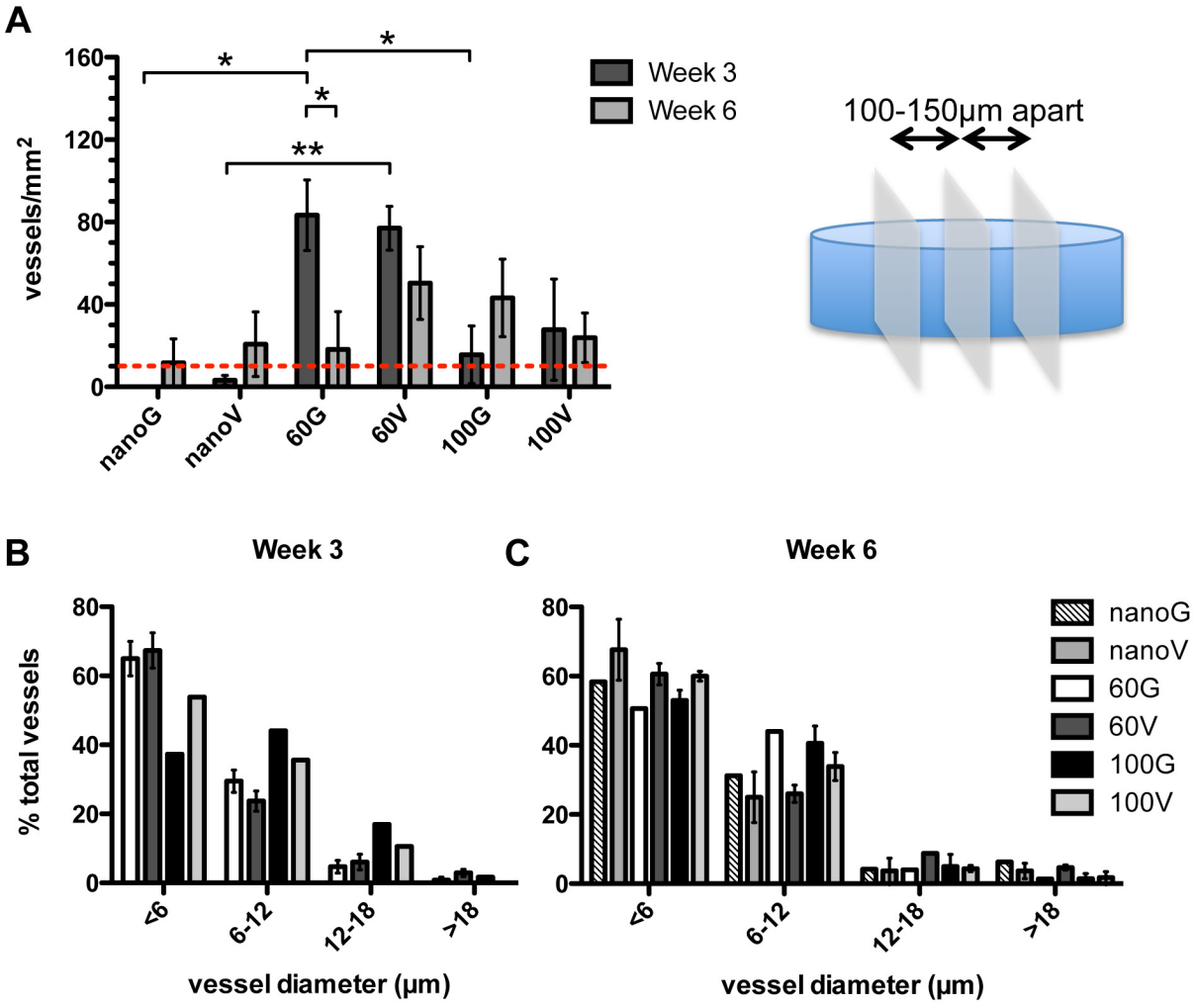

Figure 7.5: Vessel quantification and characterization. (A) Vessels in 30 images over 3 sections separated by 100 – 150 µm were quantified and normalized to the total image area. The bar graph represents the average of 4 separate samples. For those samples that contained vessels (above dotted red line), vessel diameters were measured. At 3 (B) and 6 (C) weeks approximately 50% of vessels in all samples were less than 6 µm in diameter. G = pGFPluc, V = pVEGF loaded hydrogels.

clear channels for vessels to extend through. The pores in the 100 µm porous gels, especially when using a soft hydrogel material containing only 3 % HA, are much more weak and deformable. This might also explain why fewer vessels seemed to be present in the 100 µm 3 % HA porous hydrogels described here in comparison to the 100 µm 4 % HA porous hydrogels described in the initial in vivo experiment in Chapter 4. Potentially a more rigid structure can help guide angiogenesis in its initial stages. On the other hand, by 6 weeks there were no statistical differences between any samples. It is important to note that vessels were only present in regions of the gels that were infiltrated. Thus, in nano-pore hydrogel samples, all the vessels that were present were located around the gel edge in the degraded regions and not in the bulk gel. The distribution of vessels was similar to the distribution of transfected cells. Finally, it was revealed that the 60 µm porous hydrogels that had the highest average numbers of vessels per area at three weeks were the only ones to have a significant reduction in vessels by six weeks (i.e. vessel regression). This vessel regression was not observed, however, for pVEGF loaded 60 µm porous gels which seemed to be a consequence of VEGF expression. Most importantly, at no time was there any significant increase in the

Hydrogel type	Samples positive for vessels	
	Week 3	Week 6
nanoG	0/4	1/4
nanoV	0/3	2/4
60G	4/4	1/4
60V	4/4	3/4
100G	1/4	2/3
100V	1/4	2/4

Table 7.1: Summary of hydrogel samples at 3 and 6 weeks that were positive for blood vessels. Positive samples contained an average of at 15 vessels/mm^2, which corresponded to at least 1 vessel in 50% of captured images.

number of vessels per area between pVEGF and corresponding pGFPluc loaded hydrogels. Thus, any VEGF that was being expressed was not at a high enough level to induce an angiogenic response, but may have been enough to sustain vessels that had already formed as a result of the open pore structure. Future studies with a range of pVEGF concentrations above and below 2.5 µg/µL and a larger number of animals per condition (n=6) are required to verify these findings.

7.3.4 Vessel characterization

If VEGF expression had been too low to affect the number of vessels infiltrating the scaffold, there was still a possibility that VEGF expression could have affected vessel maturity and size. Pericyte or smooth muscle cell lining is one indicator of vessel maturity [3, 4, 108]. In **Figure 7.4** all sections were also stained directly for smooth muscle cells using an antibody against α-smooth muscle actin. Regardless of VEGF expression, no smooth muscle actin staining was observed on vessels within any hydrogel cross-sections. To characterize vessel size distribution, the diameters of all vessels in samples that were positive for blood vessels were manually measured. Vessels from samples that fell below this threshold were not included in the vessel size characterization analysis to prevent biasing by a few large vessels. It was clear that in all samples about 50-60 % of all vessels were <6 µm, or the width of a single red blood cell, in diameter both at three **(Figure 7.5B)** and six **(Figure 7.5C)** weeks. Unfortunately, there were no striking differences in vessel size between pVEGF and corresponding pGFPluc loaded hydrogels. Also since the number of positive samples in certain gel conditions was low (i.e. only 1 or 2), further statistical analysis could not be performed.

7.4 Conclusions

Porous and nano-pore HA hydrogels loaded with pro-angiogenic (pVEGF) or reporter (pGFPluc) plasmids were tested for their ability to induce an enhanced angiogenic response by transfecting infiltrating cells in vivo. Although GFP-expressing transfected cells were present inside all hydrogel samples over the six-week study, transfection levels peaked around week three for 100 and 60 μm porous hydrogels while it continued to increase along with continued gel degradation in nano-pore hydrogels. Transfection levels of pVEGF, however, did not seem to be high enough to enhance angiogenesis by increasing vessel number, maturity, or size. Only in 60 μm porous hydrogels did the VEGF expression play a role in preventing vessel regression and helping to sustain the number of vessels present from three to six weeks. Regardless, pore size seemed to be the dominant factor in determining the angiogenic response. Despite what might be expected, that vessel numbers increase with increasing pore size [12], here 60 μm porous hydrogels had more vessels present per area than 100 μm porous hydrogels at the initial onset of angiogenesis at three weeks. Increased pore rigidity may have been a key factor. Combined these results, show promise for the use of polyplex loaded porous hydrogels to transfect infiltrating cells in vivo. It will be crucial in future studies to find a way to deliver either more DNA or deliver the polyplexes more rapidly for increased transfection and angiogenic response.

CHAPTER 8

APPLICATION OF DNA DELIVERY FROM POROUS HYALURONIC ACID HYDROGELS TO MOUSE WOUND HEALING

8.1 Introduction

In Chapter 7, the proposed hydrogel system was tested in vivo in a mouse subcutaneous implant model. Although this model holds several advantages, which include a simple surgical procedure with quick recovery and minimal surgical complications for mice, in addition to easy sample recovery, it is not directly representative of any relevant human disease or injury. Hydrogels and their incorporated DNA are still present even after six weeks, indicating relatively low protease levels. Alternatively, in human tissue injuries such as skin wounds proteases are up-regulated in the local microenvironment. Upon injury, MMP expression profiles during adult wound healing show that MMP-9, -11, and -13 are up-regulated early during the inflammatory phase and MMP-2, -7, and -14 are up-regulated later during the proliferation and remodeling phases [113, 140-142]. In extreme cases, protease over-expression and tissue remodeling overpower the healing process, leaving the body with chronic wounds [143-146]. Angiogenesis is suppressed while the inflammatory phase persists and new, functional tissue is unable to form. In these instances a bioresponsive hydrogel that can provide mechanical, biological, and chemical cues to

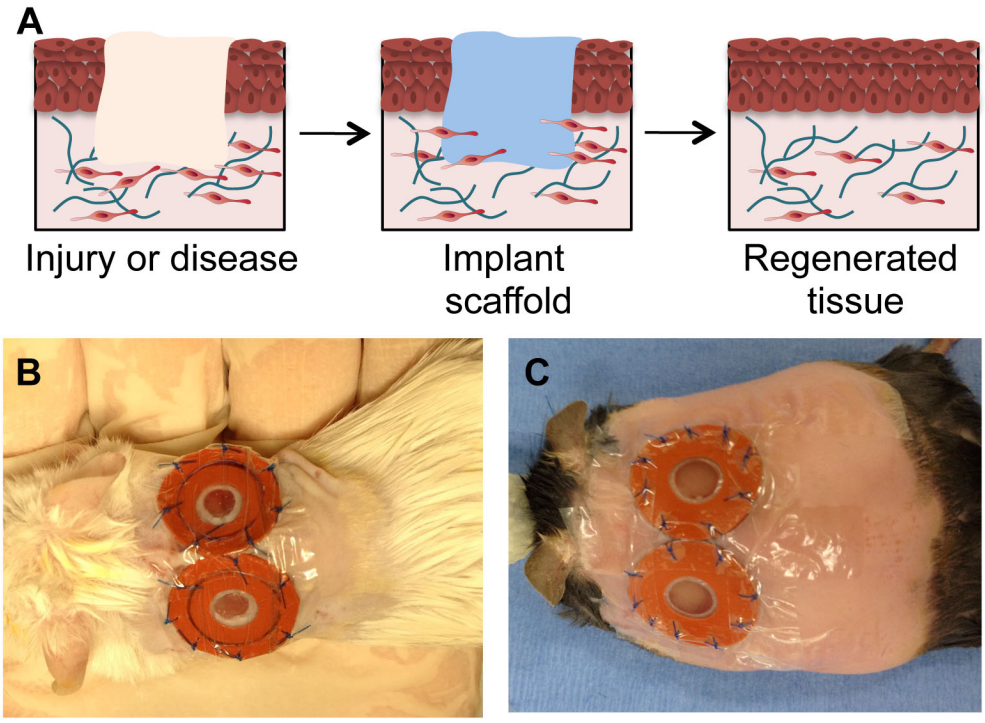

Figure 8.1: (A) Schematic illustrating ideal regeneration of tissue after hydrogel implantation into a skin wound. Two side-by-side full thickness splinted wounds can be monitored in either normal (balb/c, B) or diabetic (db/db, C) mice.

the injured tissue has the potential to aid in its regeneration in ways that are not currently possible.

Here we evaluated the effects of therapeutic DNA delivery from porous and nano-pore HA hydrogels to full-thickness dermal wounds in mice **(Figure 8.1A)**. Similar to previously published murine wound healing models, we used a modified splinted wound healing model in which the splint promotes wound closure by re-epithelialization and granulation tissue formation (i.e. the major mode of healing in humans [147]) instead of wound contraction (i.e. the major mode of healing in mice [148]). Unlike in the experiments conducted in Chapters 4 and 7, here a diabetic mouse strain was used for two reasons: (1) treatments for diabetic wounds present a pressing medical need and (2) since wound closure in normal mice is relatively faster than in diabetic mice the effects of pVEGF delivery on wound closure (although not necessarily

on granulation tissue formation and final tissue morphology) may have been more difficult to differentiate in normal mice. (Note: It is also technically more difficult to conduct the wound healing model on normal mice because they are much smaller and their backs are arched **(Figure 8.1B, C)**, making the surgery difficult. Also, normal mice are much more agile than diabetic mice and generally are able to scratch and bite off their splints!) Homozygous db/db mice model Type II diabetes mellitus and have documented impairments in wound healing due to prolonged inflammatory responses, dysfunctional matrix deposition, and altered blood flow and angiogenesis [149]. The work described here aims to deliver pro-angiogenic pVEGF polyplexes to infiltrating cells in full-thickness skin wounds to promote angiogenesis, granulation tissue formation and wound closure. Again, plasmid DNA encoding for GFP-luciferase is used as a negative control plasmid for angiogenesis assessment and to monitor transfection.

8.2 Materials and Methods

All materials and methods used for hydrogel preparation in Chapter 8 are identical to those listed in Chapter 7. Only differences are with the surgical and post-surgical techniques described below.

8.2.1 Splinted wound healing model

All in vivo studies were conducted in compliance with the NIH Guide for Care and Use of Laboratory Animals and UCLA ARC standards. 10 to 12-week old female db/db mice each 30-40 grams were used to study cellular infiltration and blood vessel formation in HA hydrogels since this strain and size has been previously used for wound healing and angiogenesis assays [138, 139, 148]. Porous or nano-pore hydrogels were made exactly as described in Chapter 7 and cut to 6 mm in diameter using a

biopsy punch, for final overall dimensions of 6 mm x 1 mm, D x H. In fabricating the hydrogels, the starting reagents were sterilized through filtering with a 0.22 µm filter. After scaffold fabrication, the hydrogels were washed with sterile PBS and kept in PBS with 1 % P/S. Immediately prior to surgery, mice were anesthetized with 4-5 % isoflurane through a nose cone inhaler. After anesthesia induction, the isoflurane concentration was lowered to 1.5-2.5 % for the remainder of the surgery. The back of the mouse was subsequently shaved, all remaining hair was removed with Nair (1 min), and finally sterilized with Betadine and 70 % ethanol. Two full-thickness wounds were then be generated using a 6 mm biopsy punch and the hydrogels were placed directly into the wounds. Sterilized 8 mm (D) silicon rings (0.5 mm thick) sandwiched between two sterile pieces of Tegaderm (i.e. splints with non-stick, clear windows) were fixed to the outside of the wound using a tissue adhesive, Mastisol. The splints were then lightly pressed down to come into contact with the hydrogel. Eight (5-0) interrupted sutures were also utilized to hold the splint in place. Finally, additional adhesive was placed around the outer edges of the splints and used to secure strips of Tegaderm to cover the splint edges and sutures, preventing the mice from removing the splints during the study. All animals were observed daily for signs of inflammation and pain and also administered Buprenorphine injections every 12 h for the first 48 h post survival surgery. At the end of the study (14 days), animals were sacrificed with isoflurane overdose. Two 8 mm diameter pieces of tissue were collected from each mouse containing the implant and the surrounding tissue and skin using a biopsy punch, fixed in 2 % PFA overnight at 4 ^{o}C, dehydrated in 70 % EtOH, and finally paraffin embedded.

8.2.2 Live imaging and wound closure analysis

Every two days over the course of the study, each mouse was anesthetized (as described above) and both wounds were imaged using a Zeiss inverted stereomicroscope. Wound area was manually measured using ImageJ software. The fixed splint area was used to calibrate measurements in each image.

8.2.3 Immunofluorescence and immunohistochemistry

Paraffin embedded sections (5 μm) were deparaffinized by incubation in multiple xylene washes followed by serial hydration from 100 % ethanol into 100 % water. For CD31/α-SMA staining, antigen-retrieval was conducted with a 15 min incubation at 37 °C in 0.1 mg/mL proteinase K solution. Sections were then washed with PBS and incubated in blocking buffer (1 % goat serum (Invitrogen, Grand Islands, NY) + 0.05 % Tween-20 in PBS) for 1 h at RT before being incubated in primary antibody solution (1:100 dilution in blocking buffer of rat anti-mouse CD31 (BD Pharmingen, San Diego, CA)) overnight at 4 °C. Sections were again washed with PBS and incubated in blocking buffer for 10 min at RT before being incubated for 2 h at RT in secondary antibody solution (1:100 dilution in blocking buffer of goat anti-rat Alexa 568 (Invitrogen, Grand Islands, NY) which also contained α-smooth muscle actin-FITC (1:100 dilution, Sigma-Aldrich, St. Louis, MO) and DAPI nuclear stain (1:400 dilution, Invitrogen). Sections were then washed twice in PBS, mounted and imaged using an inverted Zeiss fluorescence microscope. For GFP staining, neither protease nor heat-mediated antigen-retrieval was conducted as these were found to eliminate any GFP signal. All other procedures were conducted exactly as described above with a 1:50 dilution of the primary GFP antibody (Invitrogen, Grand Islands, PA) and 1:100 and 1:400 dilutions of the goat anti-rabbit Alexa 488 secondary antibody (Invitrogen, Grand

Islands, PA) and DAPI, respectively. All hematoxylin and eosin staining of sections was conducted by the Translational Pathology Core Laboratory (TPCL) at UCLA.

8.2.4 Granulation vessel quantification, characterization, and statistical analysis

Two separate sections at least 50 – 100 μm apart were analyzed for each sample. Five to ten randomly chosen areas within the newly formed granulation tissue were imaged in each section. Vessels were counted manually in each section, totaled from all sections, and finally normalized to the total imaged area. The bar graph in Figure 8.5G represent the average vessels/mm^2 from 3 – 5 different animals. For all samples the diameter of each vessel was manually measured using Zen imaging and analysis software (Zeiss). Percentages were determined using the entire vessel set.

All statistical analysis was performed using Prism (GraphPad, San Diego, CA). Experiments were statistically analyzed using the Tukey test to compare all pairs of columns using a 95 % confidence interval. All errors bars represent the standard error of the mean (SEM).

8.3 Results and Discussion

8.3.1 Experimental design and rationale

DNA delivery from porous and nano-pore HA hydrogels was assessed in a relevant mouse wound healing model. In the subcutaneous implant model described in Chapter 7 the degree of gel degradation and DNA release was too slow to produce any pronounced angiogenic response. In a diabetic wound (although in this model the wound is not representative of a chronic diabetic wound) the protease expression levels are elevated with respect to normal wounds and even more so than in a minimally invasive subcutaneous pocket. Although the length of the study (14 days)

was significantly shorter than the six-week subcutaneous implant study, this timeframe has previously been shown to allow for 60-70 % wound closure for untreated wounds [148] and 100 % closure for VEGF treated wounds [138] in similar splinted full-thickness wound studies. (Note: The splinted wound healing model studies in UCLA protocol 2010-011-03 are only approved to last 14 days due to the presence of the splint. In general, anything added to the mice needs to be removed within 7-14 days after surgery unless scientifically justified. If more time is proven to

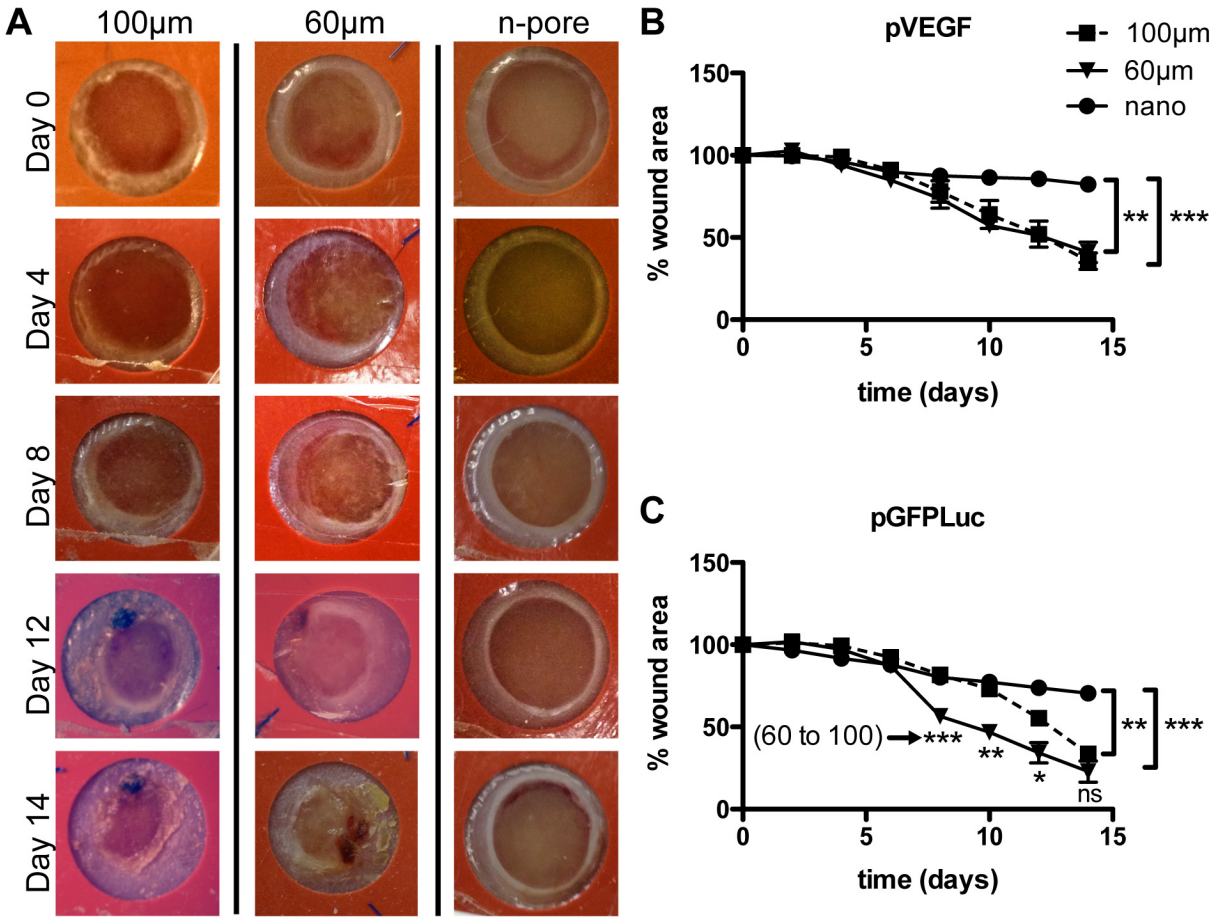

Figure 8.2: (A) Representative images of live wound imaging over the course of the study. Wound area was manually measured and reported as a percentage with respect to the wound area at t = 0. Wound closure measurements of wounds with pVEGF (B) or pGFPluc (C) loaded hydrogels showed significant differences between porous and nano-pore hydrogels.

be required then justification can be provided to the ARC to extend the study possibly to 21 days or until wounds are completely closed.) Rapid cellular response and elevated protease levels were anticipated to fully degrade the implanted hydrogels upon wound closure.

8.3.2 Wound closure analysis

Wound closure was monitored every two days by digital images. **Figure 8.2A** shows representative live wound images of pVEGF loaded hydrogels over the course of the study. Upon visual inspection it was clear that 100 and 60 µm porous hydrogels allowed for rapid wound closure, while wounds filled with nano-pore hydrogels remained almost unchanged even after 14 days. Most wounds with nano-pore hydrogels also showed signs of tissue maceration (i.e. whitening) around the wound edge. This was later determined to be a result of excessive moisture retention, causing a buildup of leukocytes, albumin, macrophages, and cell debris around the inner edge of the wound. Tissue maceration can potentially prolong wound healing and may, at least in part, explain the poor wound closure observed for both pVEGF and pGFPluc loaded hydrogels. For a quantitative representation of wound closure, wound area was manually measured from digital images and reported as a percentage with respect to the initial wound area. Wound closure measurements of wounds with pVEGF **(Figure 8.2B)** or pGFPluc **(Figure 8.2C)** loaded hydrogels showed all wounds remained relatively unchanged over the first six days. However by day eight, most porous hydrogel filled wounds started to exhibit evidence of closure and, by day 14, statistically significant differences between porous and nano-pore hydrogels were apparent. There was no statistical significance in wound closure between 100 and 60 µm pVEGF-loaded hydrogels at any time. Unexpectedly, 60 µm pGFPluc loaded

hydrogel wounds demonstrated a large degree of wound closure between day six and day eight. This resulted in significant differences in wound closure between the corresponding 100 µm porous hydrogel wounds. Yet this gap slowly started to close and by day 14 the difference in closure was not significant between the two conditions, mirroring the trend observed in the pVEGF loaded hydrogel wounds. The reason for this sudden burst in closure remains unclear and a larger number of animals in a follow-up study may need to be tested to confirm these results. Since there is no difference between different pore sizes it may be that the difference observed between porous and nano-pore hydrogels is a direct response to total porosity (which is the same for 100 and 60 µm porous hydrogels; theoretical porosity for hexagonal close-packed bead template = 76 %, actual porosity = 45 – 65 %) and not pore size.

8.3.3 Histological analysis of wounds, gels, and granulation tissue

Further analysis was conducted to study wound closure between different pore size hydrogels loaded with either pVEGF or pGFPluc polyplexes. H&E staining of wound sections were used to observe morphological differences in the wound tissue **(Figure 8.3)**. At day 14, all mice were sacrificed and wounds (with any remaining hydrogel inside) were retrieved, fixed, bisected, and finally paraffin embedded. Full wound cross-sections demonstrated very clear differences between porous **(Figure 8.3A, C, E, G)** and nano-pore **(Figure 8.3I, K)** hydrogels. Despite the harsh wound environment, host cells were unable to effectively infiltrate the nano-pore HA-MMP degradable hydrogels **(Figure 8.3J, L)**. Relative to the porous hydrogel wounds, nano-pore hydrogel wounds had minimal granulation tissue formation, especially below the hydrogel surface. Granulation tissue is newly formed connective tissue composed of fibroblasts and capillaries, and its presence in wound beds over time is indicative of wound

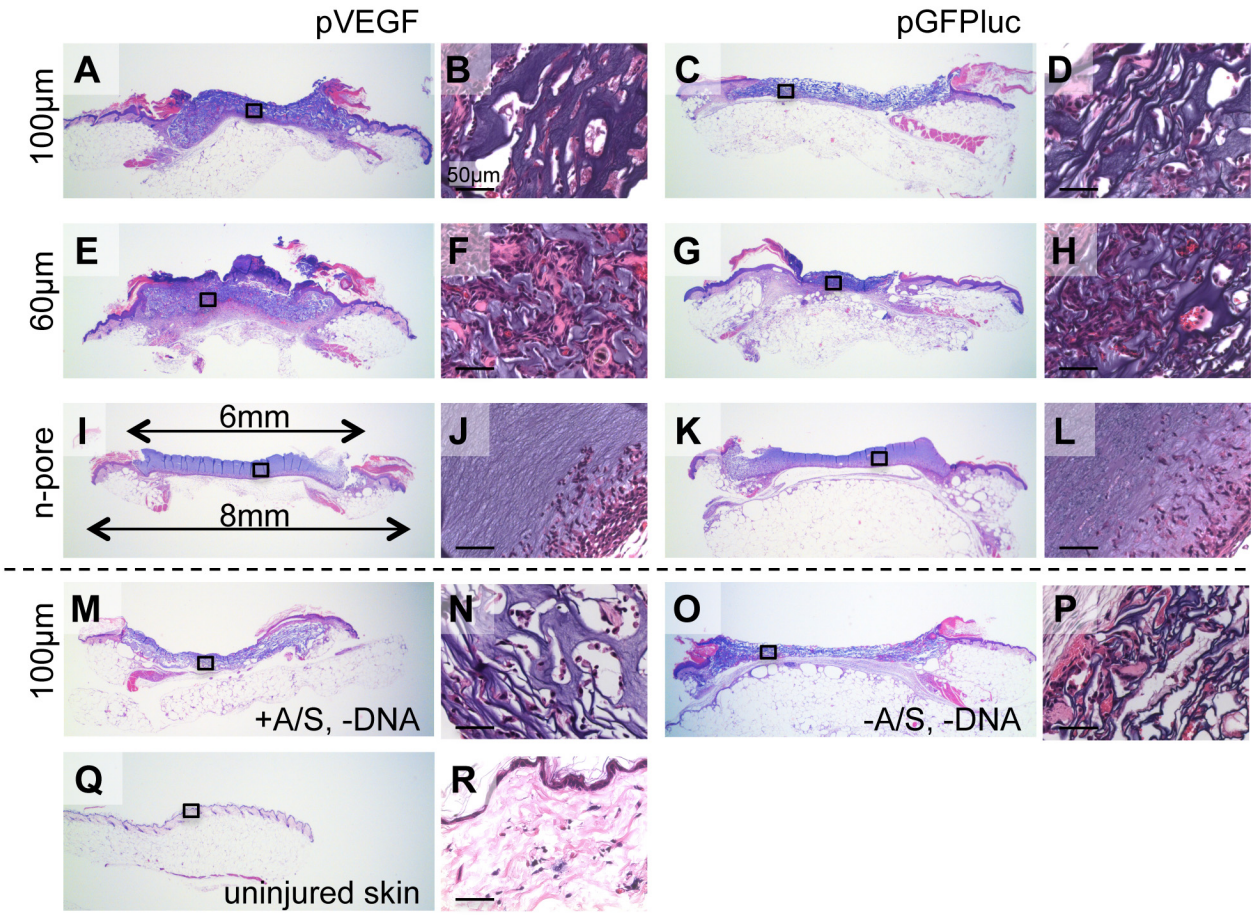

Figure 8.3: Representative H&E stained full wound cross-sections (1.6x magnification) with corresponding 40x magnification images of the gel area designated by black boxes. 100 (A-D) and 60 µm (E-H) porous and nano-pore (I-L) hydrogels loaded with pVEGF (A, B, E, F, I, J) or pGFPluc (C, D, G, H, K, L). 100 µm porous control hydrogels without DNA but with agarose/sucrose (M, N), without DNA or agarose/sucrose (O, P), and uninjured skin (Q, R) are shown for comparison.

closure and healing. Many 100 **(Figure 8.3B, D)** and 60 µm **(Figure 8.3F, H)** porous hydrogels were highly infiltrated, partially or almost fully degraded, and surrounded by granulation tissue. Numerous red blood cells were present throughout many pores in both pore size hydrogels, however, they mostly appeared as scattered cells most likely from bleeding and not aligned as if in vessels. Although wound closure was visibly observed, the degree of hydrogel degradation made it difficult to determine the start of the wound edges and subsequent degree of re-epithelialization in most porous hydrogel filled wounds. There was also no observable re-epithelialization in the nano-

pore hydrogel samples. Importantly, the presence of pVEGF polyplexes had no visible effect on the degree of cellular infiltration and granulation tissue formation.

Negative control 100 µm porous hydrogels that had no polyplexes **(Figure 8.3M, N)** or no polyplexes and no agarose/sucrose **(Figure 8.3O, P)** were also implanted (n = 2) to ensure that the presence of polyplexes and/or agarose/sucrose were not influencing surrounding cells and inducing an immune response. No obvious differences were observed through H&E stained sections. (Note: Antibodies to stain against specific immune cell markers (i.e. general leukocyte marker = CD45, macrophages = F4/80, neutrophils = Ly6G/Gr-1, dendritic cells = MHCII, T cells = CD3, B cells = CD45R) were utilized, however, the staining was unsuccessful. For future studies, either half or the entire wound should be cryo-preserved for staining to be possible. Many antigens are disrupted from fixation and paraffin embedding and cannot be sufficiently retrieved using common (i.e. heat or protease-mediated) antigen-retrieval techniques. On the other hand, tissue and specifically the hydrogel structure is better maintained through fixation and paraffin embedding.) A biopsy of an uninjured portion of skin was taken for reference **(Figure 8.3Q, R)**.

Further inspection of the granulation tissue was conducted to understand the direct impact of hydrogel porosity and DNA delivery on the new tissue being formed. H&E staining of granulation tissue surrounding pVEGF and pGFPluc loaded 100 **(Figure 8.4A, D)** and 60 µm **(Figure 8.4B, E)** porous and nano-pore **(Figure 8.4C, F)** hydrogels, respectively, again did not show any obvious morphological differences between pVEGF and corresponding pGFPluc loaded hydrogels. Vessels were present throughout the granulation tissue in all samples. In general it also seemed that granulation tissue had only formed where the hydrogels had degraded. Thus, immunofluorescence staining of GFP in pGFPluc loaded hydrogel samples was conducted to determine if

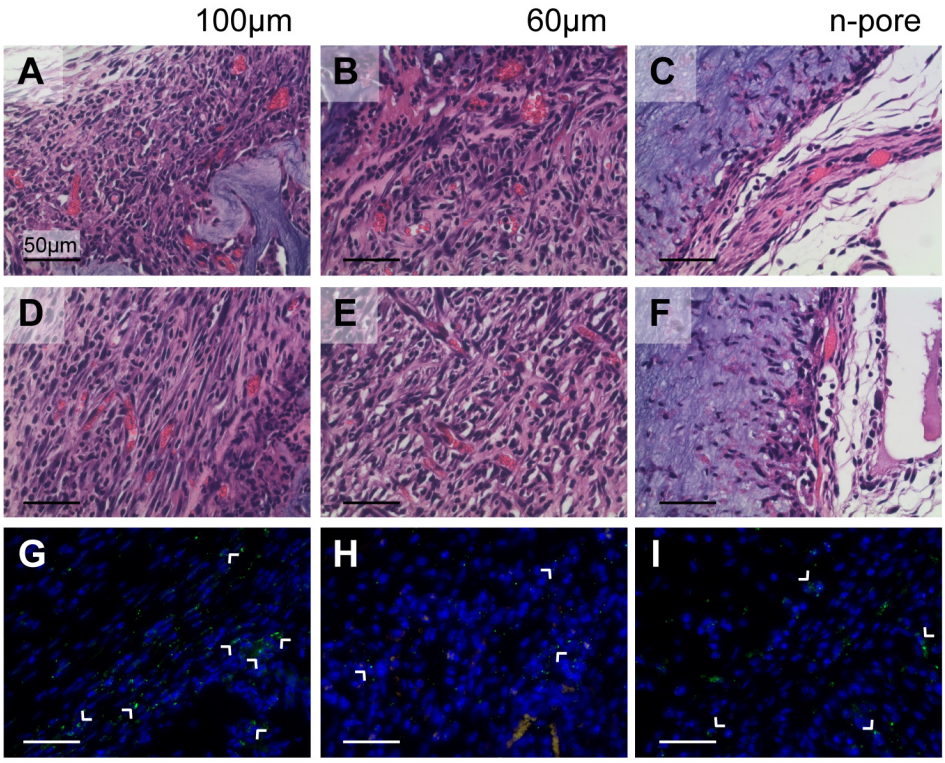

Figure 8.4: H&E stained sections of newly formed granulation tissue surrounding pVEGF loaded 100 (A) and 60 µm (B) porous and nano-pore (C) hydrogels 2 weeks after wounds were formed. pGFPluc loaded 100 (D) and 60 µm (E) porous and nano-pore (F) hydrogels seem to have relatively similar levels of granulation tissue formation and vessel infiltration when compared to pVEGF loaded gels. Immunofluorescence staining of GFP in pGFPluc loaded control 100 (G) and 60 µm (H) porous and nano-pore (I) hydrogels indicates several transfected cells are present throughout the granulation tissue in each sample. GFP positive cells = green, cell nuclei = blue. All images are 40x magnifications.

released polyplexes from the degraded hydrogel portions were themselves not degraded and had transfected cells in the newly formed tissue. Numerous transfected cells were present in the granulation tissue surrounding all 100 **(Figure 8.4G)** and 60 µm **(Figure 8.4H)** porous and nano-pore **(Figure 8.4I)** hydrogels. Although the positive GFP staining per cell was less pronounced than what was observed in the subcutaneous implant samples, more cells were transfected overall. Transfection of cells within the remaining hydrogel pores and even in the nano-pore hydrogels surprisingly could not be detected. It was unclear, however, whether this was due to increased background from the high cell density.

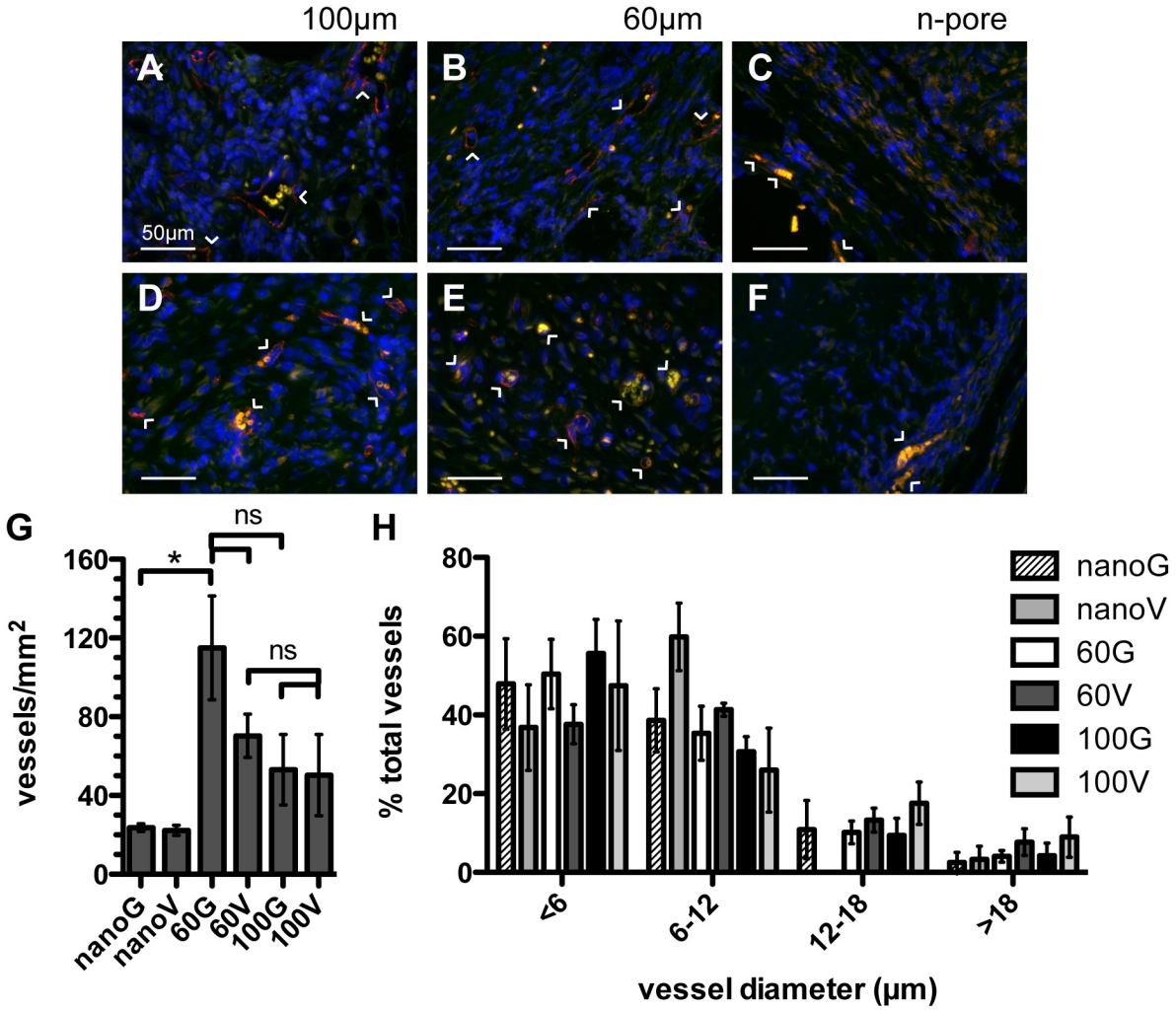

Figure 8.5: Staining for endothelial markers within the granulation tissue indicated significant positive staining for 100 and 60 µm porous hydrogel implants loaded with pVEGF (A, B) and pGFPluc (D, E), respectively. For nano-pore implants loaded either with pVEGF (C) or pGFPluc (F) few vessels could be observed. Red = PECAM positive staining = endothelial cells, yellow = erythrocytes, blue = cell nuclei. All images are 40x magnifications. (G) Vessels in 10-20 images across the granulation tissue area in 2 sections separated by 50 – 100 µm were quantified and normalized to the total image area. The bar graph represents the average of 3-5 separate samples. For all samples vessel diameters were measured (H). Approximately 40-50% of vessels in all samples were less than 6 µm in diameter. G = pGFPluc, V = pVEGF loaded hydrogels.

8.3.4 Angiogenesis within granulation tissue

Since the majority of transfected cells in all wound samples were found in the granulation tissue, qualitative and quantitative assessment of angiogenesis as a function of pore size and pVEGF delivery was conducted on the granulation tissue. As

expected from H&E images **(Figure 8.4A-F)**, multiple vessels were present in each image area of the PECAM/α-SMA stained granulation tissue surrounding 100 **(Figure 8.5A, D)** and 60 μm **(Figure 8.5B, E)** porous hydrogels loaded with pVEGF and pGFPluc polyplexes, respectively. Vessels density appeared higher at two weeks than what was observed inside gels in the subcutaneous implant model at the angiogenic peak at three weeks. Vessels were also present, but at a lower density, surrounding pVEGF **(Figure 8.5C)** and pGFPluc **(Figure 8.5F)** loaded nano-pore hydrogels. Markedly, for both porous and nano-pore hydrogels the number of vessels at the wound/hydrogel edges was higher than below the hydrogel surface. Qualitative differences in vasculature could not be attributed to the absence or presence of enhanced VEGF expression in the granulation tissue surrounding all hydrogel samples. Quantitative characterization of vessels in the granulation tissue confirmed this **(Figure 8.5G)**. Although differences in the total granulation area were apparent from full wound cross-section sections, the number of vessels when normalized to the area was not different between any of the hydrogel conditions except for one. There was only a significant difference in the number of vessels/mm^2 between pGFPluc loaded 60 μm porous and nano-pore hydrogels. Interestingly these 60 μm porous were the ones that exhibited the fastest wound closure **(Figure 8.2C)**. Although it was somewhat unclear why this happened, there is a possibility that increased vessel density correlates to increased wound closure. In a follow-up study, vessel density closer to the time differences between samples initially become apparent (i.e. between 8-10 days) should be assessed.

Vessel maturity and size were assessed, as was done for the subcutaneous implant model described in Chapter 7.3.4, to determine if VEGF expression could have influenced these factors. All sections were also stained directly for smooth muscle

cells using an antibody against α-smooth muscle actin **(Figure 8.5A-F)**. Regardless of VEGF expression no positive smooth muscle actin staining was observed on vessels within any hydrogel cross-sections. To characterize vessel size distribution, the diameters of all vessels in images spanning across the total granulation tissue area in two separate sections were manually measured. In all samples about 40-50 % of all vessels were <6 μm, or the width of a single red blood cell, in diameter **(Figure 8.5H)**. Relative to the vessels formed in the subcutaneous implant model, more vessels were 6-12 μm in diameter with approximately 30-40 % of all vessels falling into this size group. For all three types of hydrogels, the pVEGF loaded hydrogels had on average ~10 % less small capillaries (<6 μm) and subsequently an increased number of larger vessels than their corresponding pGFPluc loaded hydrogels. Due to degree of variability in all samples, however, observed differences were not statistically significant and no clear conclusions could be made regarding the vessel size enhancement provided by VEGF expression.

8.4 Conclusions

Using a human relevant splinted mouse wound healing model, porous and nano-pore HA hydrogels loaded with pro-angiogenic (pVEGF) or reporter (pGFPluc) plasmids were tested for their ability to promote wound closure and induce an enhanced angiogenic response by transfecting infiltrating cells. 100 and 60 μm porous hydrogels allowed for significantly faster wound closure than nano-pore hydrogels which did not degrade and provided a mechanical barrier to closure. Regardless, total porosity and not specific wound size seemed to be the dominant factor in determining the wound closure rates. GFP-expressing transfected cells were present throughout the granulation tissue surrounding all hydrogel samples over the two-week study.

Transfection levels of pVEGF, however, did not seem to be high enough to enhance angiogenesis by statistically increasing vessel number, maturity, or size. These results, show promise for the use of polyplex loaded porous hydrogels to transfect infiltrating cells in vivo. As was the case in the subcutaneous implant model, future wound healing studies will need to incorporate hydrogels with the ability to deliver either more DNA or deliver the polyplexes more rapidly for increased transfection and angiogenic response. Likewise, the hydrogel degradation rate will need to be increased to allow for degradation and wound closure to occur at equal rates.

CHAPTER 9

CONCLUSIONS AND FUTURE DIRECTIONS

9.1 Introduction

The goal of the research presented in this dissertation was to design a porous hyaluronic acid hydrogel for controlled non-viral gene delivery to promote angiogenesis in vivo for the eventual application of full-thickness skin wound repair. Although several strategies have previously been reported to promote angiogenesis within implanted scaffolds, these strategies have not come together to form a rationally designed hydrogel that promotes angiogenesis over the therapeutic timeframe required for new tissue formation. The following section re-visits the proposed specific aims and hypotheses, followed by the major conclusions and possible future experimental directions.

9.2 Specific aim 1 (Chapter 4)

This aim investigated porous HA hydrogels for enhancement of scaffold vascularization in a mouse subcutaneous implant model. Although we hypothesized that the pre-formed pores would allow for faster angiogenesis into the hydrogel scaffold (based on the limited information available about micron-sized pores at the time of these experiments), we had two major concerns: (1) nano-pore HA hydrogels could potentially degrade fast enough to induce a strong angiogenic response as a result of degraded HA fragments and (2) that the potential benefits from introducing

pores might not outweigh the extended porous gel processing time. The subcutaneous implant model was also optimized in this aim for the Segura laboratory.

Hypothesis 1: The presence of interconnected, micron-sized pores will allow for rapid vascular infiltration in comparison to more traditional nano-pore HA hydrogels which require sufficient degradation for cells to infiltrate.

Although the processing time to create porous hydrogels compared to the more commonly used nano-pore HA hydrogels is significantly longer (3.5 days compared to ~1 h), these results highlighted the potential for the use of porous hydrogels in vivo. By three weeks vessels were present throughout several pores in every 100 μm porous HA hydrogel, while corresponding 4 % nano-pore gels still had minimal surface degradation at this time. It is important to note, however, that we also assumed the HA was playing a role in promoting angiogenesis upon degradation. To verify this, future studies should include biologically inert scaffolds (i.e. PEG-MMP) as controls in order to decouple the effects seen due to the pores and those due to the degradation fragments of HA in the local microenvironment. However, it was clear that the interconnected pores were able to provide channels for vessels to grow into. We anticipated that with the addition of pro-angiogenic growth factors through the delivery of non-viral vectors encoding for the factors, blood vessel formation within porous hydrogels could further enhance vessel number, maturity, and rate of formation. These preliminary in vivo studies dictated the future direction of this research.

9.3 Specific aim 2 (Chapter 5)

This aim developed a strategy to deliver tethered nanoparticles, similar in size to DNA polyplexes, in vitro to mouse mesenchymal stem cells from both two-dimensional surfaces and three-dimensional porous PEG hydrogels. The tethers utilized in this aim were matrix metalloproteinase (MMP) degradable peptide tethers previously reported to have varying sensitivities to MMP-1 and MMP-2.

Hypothesis 2: The sequence (and specificity to MMP-2) of the peptide tethers will determine the release and internalization of the nanoparticles by MMP-2 expressing cells. Alternatively, if cells do not express the appropriate protease they will not be able to cleave the peptide tethers and internalize the nanoparticles.

Hypothesis 3: Increasing tethering to the biomaterial surface by increasing the number of tethers on the nanoparticle surface will slow down the release and internalization of the nanoparticles.

Here we demonstrated that the cell-demanded release of tethered nanoparticles could be controlled by the tether's (i.e. peptide) sensitivity to proteases, the number of tethers between the nanoparticle and the surface, and protease concentration. Cellular internalization was likewise a function of the peptide sensitivity to proteases and the number of tethers on the nanoparticle. However, release and internalization were shown to vary significantly in the presence or absence of cells, which could have been expected due to the high local MMP concentration surrounding MMP-expressing mMSCs. We observed that the protease (namely MMP) expression profile of the seeded cells was the main factor in determining the release and internalization kinetics of MMP-sensitive peptide-modified particles. Similar trends were observed in three-dimensional 100 μm porous PEG hydrogels when nanoparticles were immobilized to the pore

surfaces. With increasing pore size, pore surfaces are essentially curved two-dimensional surfaces, providing justification for the similarities observed. Although the results from these experiments strongly confirmed both Hypotheses 2 and 3, the translation of this system is difficult for unstable DNA polyplexes. Future studies may aim to modify other non-viral DNA nanoparticles or potentially stable micelles that can carry large DNA (or siRNA) loads.

9.4 Specific aim 3 (Chapter 6)

This aim tested the strategy to deliver encapsulated non-viral DNA nanoparticles in vitro to mMSCs from porous HA hydrogels. Since the ultimate goal was to be able to use these hydrogels in vivo, we directly utilized a previously described technique to load high concentrations of DNA/PEI polyplexes into the hydrogels that would later be suitable for in vivo applications. Based on our preliminary experiments and what other groups had published at the time, we also anticipated that gene transfer would be a function of hydrogel pore size. However, in order to minimize the number of animals that would need to be used to test each of these parameters, in vitro gene transfer was studied as a potential screen for the optimal gene transfer conditions to later use in vivo.

Hypothesis 4: Cells will be transfected with non-viral DNA as the DNA nanoparticles are released from the hydrogel upon hydrogel degradation by cell-secreted MMPs.

Porous HA-MMP hydrogels were used to encapsulate DNA/PEI polyplexes and transfect seeded stem cells as they slowly degraded the matrix. Porous hydrogels

allowed for effective cell seeding in vitro post scaffold fabrication, and when coupled with high loading efficiency of DNA polyplexes, allowed for long-term sustained transfection and transgene expression of incorporated mMSCs in various pore size μ-pore hydrogels. For all investigated pore sizes transgene expression was sustained for up to ten days, confirming that the hydrogel processing (i.e. 48 h in acetone to dissolve away PMMA beads) was not affecting the polyplexes ability to transfect cells. Cell viability was also shown to remain high over time in all pore size hydrogels, even in the presence of high concentrations of DNA polyplexes. Based on these results we believed that the proposed hydrogel system could be used for the controlled release of DNA polyplexes for in vivo tissue engineering and blood vessel formation.

9.5 Specific aim 4 (Chapter 7)

This aim used the encapsulated non-viral DNA nanoparticle strategy to enhance angiogenesis in a mouse subcutaneous implant model over a six-week period. Although differences in transfection of mMSCs in vitro with respect to pore size was not observed, we hypothesized that pore size would play a greater role in vivo by dictating the rate of cellular infiltration and subsequent gel degradation and polyplex release. Techniques for the assessment of transfection and angiogenesis were also developed and optimized in this aim for the Segura laboratory.

Hypothesis 5: Host cells infiltrating the hydrogels will be transfected with non-viral DNA as the DNA nanoparticles are released from the hydrogel upon hydrogel degradation by cell-secreted MMPs.

Hypothesis 6: The incorporation of therapeutic (i.e. pro-angiogenic) VEGF plasmid containing DNA nanoparticles will additionally enhance angiogenesis within

porous hydrogels. As infiltrating cells are transfected and VEGF is expressed within the pores of the hydrogels, blood vessels and, specifically, endothelial cells will be directed to migrate into the hydrogel pores.

Hypothesis 7: Pore size will play a role in cellular infiltration and subsequent transfection and angiogenesis in vivo.

Porous and nano-pore HA hydrogels loaded with pro-angiogenic (pVEGF) or reporter (pGFPluc) plasmids were tested for their ability to induce an enhanced angiogenic response by transfecting infiltrating host cells in vivo. Although GFP-expressing transfected cells were present inside all hydrogel samples over six weeks, transfection levels peaked around week three for 100 and 60 μm porous hydrogels while it continued to increase along with continued gel degradation in nano-pore hydrogels. And although we were not able to successfully stain for immune cells, we further hypothesized that any minimal immune response may have subsided after the first few weeks and that cells residing within the pores eventually became quiescent and stopped degrading the remaining scaffold. Without degradation, based on our in vitro findings, we did not expect polyplexes to be released. Thus, although there were positively transfected cells present, the transfection levels of pVEGF did not seem to be high enough to enhance angiogenesis by increasing vessel number, maturity, or size. Only in 60 μm porous hydrogels did the VEGF expression play a role in preventing vessel regression and helping to sustain the number of vessels present from three to six weeks. Regardless, pore size seemed to be the dominant factor in determining the angiogenic response. Despite what might be expected, that vessel numbers increase with increasing pore size [12], here 60 μm porous hydrogels had more vessels present per area than 100 μm porous hydrogels at the initial onset of angiogenesis at three

weeks. Increased pore rigidity may have been a key factor. Combined these results, show promise for the use of polyplex loaded porous HA hydrogels to transfect infiltrating cells in vivo. It will be crucial in future studies to find a way to deliver either more DNA or deliver the polyplexes more rapidly for increased transfection and angiogenic response. One possible way may be to introduce even more pores to the bulk hydrogel material by mixing ≤10 μm PMMA beads with the hydrogel precursor prior to gelling. Incorporation of the cytokine tumor necrosis factor-alpha (TNF-α) can also be used as a means to up-regulate MMP expression of infiltrating cells to increase the rate of hydrogel degradation. Additionally, it may be worthwhile to investigate hydrogel stiffness and its correlation to angiogenesis (even in the absence of DNA polyplexes) to verify the differences seen between the 100 μm porous hydrogels in Chapter 4 (4 % HA) and Chapter 7 (3 % HA). Stiffness can also be varied by changing the crosslinker concentration (r-ratio, SH/Ac).

9.6 Specific aim 5 (Chapter 8)

This aim used the encapsulated non-viral DNA nanoparticle strategy to enhance angiogenesis and wound closure in a splinted mouse wound healing model over a 14-day period. The splinted wound healing model was also developed in this aim for the Segura lab from previously reported techniques and hydrogel characterization techniques were determined.

Hypothesis 8: The HA hydrogel will aid in wound healing by providing mechanical support to the surrounding tissue, a bridge for re-epithelialization, and, combined with the splint, a barrier for tissue contraction.

Hypothesis 9: Host cells infiltrating the hydrogels will be transfected with non-viral DNA as the DNA nanoparticles are released from the hydrogel upon hydrogel degradation by cell-secreted MMPs.

Hypothesis 10: The incorporation of therapeutic (i.e. pro-angiogenic) VEGF plasmid containing DNA nanoparticles will additionally enhance angiogenesis within porous hydrogels. This will result in faster wound closure and more mature tissue regeneration.

Hypothesis 11: Pore size will play a role in cellular infiltration, re-epithelialization, and wound closure in vivo. Subsequently, transfection and angiogenesis will be affected.

Although this model proved to be very challenging, we were finally able to test porous and nano-pore HA hydrogels loaded with pro-angiogenic (pVEGF) or reporter (pGFPluc) plasmids for their ability to promote wound closure and induce an enhanced angiogenic response by transfecting infiltrating host cells. 100 and 60 μm porous hydrogels allowed for significantly faster wound closure than nano-pore hydrogels, which did not degrade and instead provided a mechanical barrier to closure. Regardless, total porosity (45 – 65 %) and not specific wound size seemed to be the dominant factor in determining the wound closure rates. GFP-expressing transfected cells were present throughout the granulation tissue surrounding all hydrogel samples at the end of the two-week study. Transfection levels of pVEGF, however, did not seem to be high enough to enhance angiogenesis by statistically increasing vessel number, maturity, or size. These results show promise for the use of polyplex loaded porous hydrogels to transfect infiltrating cells in vivo. As was the case in the subcutaneous implant model, future wound healing studies will need to incorporate hydrogels with

the ability to deliver either more DNA or deliver the polyplexes more rapidly for increased transfection and angiogenic response. Likewise, the hydrogel degradation rate will need to be increased to allow for degradation and wound closure to occur at equal rates. To enhance vessel maturity, pVEGF may be replaced with pHIF-1α to simultaneously up-regulate VEGF and PDGF levels upon transfection. As a final experimental suggestion, for wound healing studies which take place over a short two-week period, surface coated or tethered growth factors (i.e. VEGF) in addition to encapsulated non-viral DNA polyplexes will most likely increase the rate at which wound closure and angiogenesis occur, while also providing long-term VEGF expression through sustained transfection.

For this model to progress, several technical issues also need to be addressed, including avoiding tissue maceration (i.e. whitening) and better tissue preservation. To avoid tissue maceration one suggestion is to allow the wound to "breathe" during dressing changes at the time of live imaging. During imaging the mice are under anesthesia, ensuring that the mice are not moving and that the wounds can be kept as sterile as possible while directly exposed to air. Also in some samples, it appeared as if the re-epithelialization was forced to occur between the gel and the wound. Reducing hydrogel thickness (even from 1.0 mm to 0.7 – 0.8 mm) may help to alleviate this issue. Lastly, it remains to be determined whether or not immune cell staining is possible with PFA-fixed, paraffin-embedded tissue sections or if cryo-preservation of tissue will be required for this purpose. In any case, one half of the tissue should always be fixed and paraffin-embedded for H&E staining since this has already been determined to be the better technique for structural preservation of the hydrogel and surrounding tissue. Lastly, a larger number of mice should be used for each condition (n=6) to compensate for the high degree of variability observed in these studies. Once these issues are

addressed, experiments can be conducted easily and focused on hydrogel design and biological responses rather than the technical procedures.

CHAPTER 10

REFERENCES

[1] Berthiaume F, Maguire TJ, Yarmush ML. Tissue Engineering and Regenerative Medicine: History, Progress, and Challenges. In: Prausnitz JM, editor. Annual Review of Chemical and Biomolecular Engineering, Vol 2. Palo Alto: Annual Reviews; 2011. p. 403-30.

[2] Novosel EC, Kleinhans C, Kluger PJ. Vascularization is the key challenge in tissue engineering. Advanced Drug Delivery Reviews 2011;63:300-11.

[3] Bramfeldt H, Sabra G, Centis V, Vermette P. Scaffold Vascularization: A Challenge for Three-Dimensional Tissue Engineering. Current Medicinal Chemistry 2010;17:3944-67.

[4] Carmeliet P, Jain RK. Molecular mechanisms and clinical applications of angiogenesis. Nature 2011;473:298-307.

[5] Laschke MW, Menger MD. Vascularization in Tissue Engineering: Angiogenesis versus Inosculation. European Surgical Research 2012;48:85-92.

[6] Orr AW, Elzie CA, Kucik DF, Murphy-Ullrich JE. Thrombospondin signaling through the calreticulin/LDL receptor-related protein co-complex stimulates random and directed cell migration. Journal of Cell Science 2003;116:2917-27.

[7] Zarem H. The microcirculatory events within full-thickness skin allografts (homografts) in mice. Surgery 1969;66:392.

[8] Mikos AG, Sarakinos G, Lyman MD, Ingber DE, Vacanti JP, Langer R. Prevascularization of porous biodegradable polymers. Biotechnology and Bioengineering 1993;42:716-23.

[9] Chen X, Aledia AS, Ghajar CM, Griffith CK, Putnam AJ, Hughes CCW, et al. Prevascularization of a fibrin-based tissue construct accelerates the formation of functional anastomosis with host vasculature. Tissue Engineering Part A 2008;15:1363-71.

[10] Papavasiliou G, Cheng M-H, Brey EM. Strategies for Vascularization of Polymer Scaffolds. Journal of Investigative Medicine 2010;58:838-44.

[11] Chiu Y, Larson J, Isom AJ, Brey E. Generation of Porous Poly(Ethylene Glycol) Hydrogels by Salt Leaching Tissue Engineering: Part C 2010;16:905-12.

[12] Chiu Y-C, Cheng M-H, Engel H, Kao S-W, Larson JC, Gupta S, et al. The role of pore size on vascularization and tissue remodeling in PEG hydrogels. Biomaterials 2011;32:6045-51.

[13] Huang X, Zhang Y, Donahue H, Lowe T. Porous thermoresponsive-co-biodegradable hydrogels as tissue-engineering scaffolds for 3-dimensional in vitro culture of chondrocytes. Tissue Engineering 2007;13:2645-52.

[14] Huang YC, Riddle K, Rice KG, Mooney DJ. Long-term in vivo gene expression via delivery of PEI-DNA condensates from porous polymer scaffolds. Human Gene Therapy 2005;16:609-17.

[15] Jang JH, Rives CB, Shea LD. Plasmid delivery in vivo from porous tissue-engineering scaffolds: transgene expression and cellular transfection. Molecular Therapy 2005;12:475-83.

[16] Nam YS, Yoon JJ, Park TG. A novel fabrication method of macroporous biodegradable polymer scaffolds using gas foaming salt as a porogen additive. Journal of Biomedical Materials Research 2000;53:1-7.

[17] Iyer P, Walker KJ, Madihally SV. Increased matrix synthesis by fibroblasts with decreased proliferation on synthetic chitosan–gelatin porous structures. Biotechnology and Bioengineering 2011;109:1314-25.

[18] Kang H-W, Tabata Y, Ikada Y. Fabrication of porous gelatin scaffolds for tissue engineering. Biomaterials 1999;20:1339-44.

[19] Kang JY, Chung CW, Sung J-H, Park B-S, Choi J-Y, Lee SJ, et al. Novel porous matrix of hyaluronic acid for the three-dimensional culture of chondrocytes. International Journal of Pharmaceutics 2009;369:114-20.

[20] Van Vlierberghe S, Cnudde V, Masschaele B, Dubruel P, De Paepe I, Jacobs PJS, et al. Porous gelatin cryogels as cell delivery tool in tissue engineering. Journal of Controlled Release 2006;116:e95-e8.

[21] Galperin A, Long TJ, Ratner BD. Degradable, Thermo-Sensitive Poly(N-isopropyl acrylamide)-Based Scaffolds with Controlled Porosity for Tissue Engineering Applications. Biomacromolecules 2010;11:2583-92.

[22] Madden LR, Mortisen DJ, Sussman EM, Dupras SK, Fugate JA, Cuy JL, et al. Proangiogenic scaffolds as functional templates for cardiac tissue engineering. Proceedings of the National Academy of Sciences 2010;107:15211-6.

[23] Saul JM, Linnes MP, Ratner BD, Giachelli CM, Pun SH. Delivery of non-viral gene carriers from sphere-templated fibrin scaffolds for sustained transgene expression. Biomaterials 2007;28:4705-16.

[24] Stachowiak AN, Bershteyn A, Tzatzaloz E, Irvine DJ. Bioactive Hydrogels with an Ordered Cellular Structure Combine Interconnected Macroporosity and Robust Mechanical Properties. Advanced Materials 2005;17:399-403.

[25] Peyton SR, Kalcioglu ZI, Cohen JC, Runkle AP, Van Vliet KJ, Lauffenburger DA, et al. Marrow-Derived stem cell motility in 3D synthetic scaffold is governed by geometry along with adhesivity and stiffness. Biotechnology and Bioengineering 2011;108:1181-93.

[26] Stachowiak AN, Irvine DJ. Inverse opal hydrogel-collagen composite scaffolds as a supportive microenvironment for immune cell migration. Journal of Biomedical Materials Research A 2008;85:815-28.

[27] Andreadis ST, Geer DJ. Biomimetic approaches to protein and gene delivery for tissue regeneration. Trends in Biotechnology 2006;24:331-7.

[28] Fischbach C, Mooney DJ. Polymers for pro- and anti-angiogenic therapy. Biomaterials 2007;28:2069-76.

[29] Friedlaender GE, Perry CR, Cole JD, Cook SD, Cierny G, Muschler GF, et al. Osteogenic Protein-1 (Bone Morphogenetic Protein-7) in the Treatment of Tibial Nonunions A Prospective, Randomized Clinical Trial Comparing rhOP-1 with Fresh Bone Autograft*. The Journal of Bone & Joint Surgery 2001;83:151-S8.

[30] Rücker M, Laschke MW, Junker D, Carvalho C, Schramm A, Mülhaupt R, et al. Angiogenic and inflammatory response to biodegradable scaffolds in dorsal skinfold chambers of mice. Biomaterials 2006;27:5027-38.

[31] Fraser JR, Laurent TC, Laurent UB. Hyaluronan: its nature, distribution, functions and turnover. Journal of Internal Medicine 1997;242:27-33.

[32] Gaffney J, Matou-Nasri S, Grau-Olivares M, Slevin M. Therapeutic applications of hyaluronan. Molecular BioSystems 2010;6:437-43.

[33] Leach JB, Bivens KA, Patrick CW, Schmidt CE. Photocrosslinked hyaluronic acid hydrogels: Natural, biodegradable tissue engineering scaffolds. Biotechnology and Bioengineering 2003;82:578-89.

[34] Park YD, Tirelli N, Hubbell JA. Photopolymerized hyaluronic acid-based hydrogels and interpenetrating networks. Biomaterials 2003;24:893-900.

[35] Shu XZ, Liu YC, Palumbo FS, Lu Y, Prestwich GD. In situ crosslinkable hyaluronan hydrogels for tissue engineering. Biomaterials 2004;25:1339-48.

[36] Yeo Y, Highley CB, Bellas E, Ito T, Marini R, Langer R, et al. In situ cross-linkable hyaluronic acid hydrogels prevent post-operative abdominal adhesions in a rabbit model. Biomaterials 2006;27:4698-705.

[37] Eldridge L, Moldobaeva A, Wagner EM. Increased hyaluronan fragmentation during pulmonary ischemia. American Journal of Physiology - Lung Cellular and Molecular Physiology 2011;301:L782-L8.

[38] Gao F, Liu Y, He Y, Yang C, Wang Y, Shi X, et al. Hyaluronan oligosaccharides promote excisional wound healing through enhanced angiogenesis. Matrix Biology 2010;29:107-16.

[39] Voelcker V, Gebhardt C, Averbeck M, Saalbach A, Wolf V, Weih F, et al. Hyaluronan fragments induce cytokine and metalloprotease upregulation in human melanoma cells in part by signalling via TLR4. Experimental Dermatology 2008;17:100-7.

[40] Aruffo A, Stamenkovic I, Melnick M, Underhill CB, Seed B. CD44 is the principal cell surface receptor for hyaluronate. Cell 1990;61:1303-13.

[41] Sherman L, Sleeman J, Herrlich P, Ponta H. Hyaluronate Receptors - Key Players in Growth, Differentiation, Migration and Tumor Progression. Current Opinion in Cell Biology 1994;6:726-33.

[42] Burdick JA, Prestwich GD. Hyaluronic Acid Hydrogels for Biomedical Applications. Advanced Materials 2011;23:H41-H56.

[43] Bulpitt P, Aeschlimann D. New strategy for chemical modification of hyaluronic acid: preparation of functionalized derivatives and their use in the formation of novel biocompatible hydrogels. Journal of Biomedical Materials Research 1999;47:152-69.

[44] Oh EJ, Park K, Kim KS, Kim J, Yang JA, Kong JH, et al. Target specific and long-acting delivery of protein, peptide, and nucleotide therapeutics using hyaluronic acid derivatives. Journal of Controlled Release 2010;141:2-12.

[45] Chung C, Burdick JA. Influence of Three-Dimensional Hyaluronic Acid Microenvironments on Mesenchymal Stem Cell Chondrogenesis. Tissue Engineering Part A 2009;15:243-54.

[46] Gerecht S, Burdick JA, Ferreira LS, Townsend SA, Langer R, Vunjak-Novakovic G. Hyaluronic acid hydrogel for controlled self-renewal and differentiation of human embryonic stem cells. Proceedings of the National Academy of Sciences 2007;104:11298-303.

[47] Kim J, Park Y, Tae G, Lee KB, Hwang CM, Hwang SJ, et al. Characterization of low-molecular-weight hyaluronic acid-based hydrogel and differential stem cell responses in the hydrogel microenvironments. Journal of Biomedical Materials Research Part A 2009;88A:967-75.

[48] Pan LJ, Ren YJ, Cui FZ, Xu QY. Viability and Differentiation of Neural Precursors on Hyaluronic Acid Hydrogel Scaffold. Journal of Neuroscience Research 2009;87:3207-20.

[49] Lei Y, Gojgini S, Lam J, Segura T. The spreading, migration and proliferation of mouse mesenchymal stem cells cultured inside hyaluronic acid hydrogels. Biomaterials 2011;32:39-47.

[50] Kim J, Park Y, Tae G, Lee KB, Hwang SJ, Kim IS, et al. Synthesis and characterization of matrix metalloprotease sensitive-low molecular weight hyaluronic acid based hydrogels. Journal of Materials Science-Materials in Medicine 2008;19:3311-8.

[51] Bowen-Pope DF, Malpass TW, Foster DM, Ross R. Platelet-derived growth factor in vivo: levels, activity, and rate of clearance. Blood 1984;64:458-69.

[52] Edelman ER, Nugent MA, Karnovsky MJ. Perivascular and intravenous administration of basic fibroblast growth factor: vascular and solid organ deposition. Proceedings of the National Academy of Sciences 1993;90:1513-7.

[53] Eppler SM, Combs DL, Henry TD, Lopez JJ, Ellis SG, Yi JH, et al. A target-mediated model to describe the pharmacokinetics and hemodynamic effects of recombinant human vascular endothelial growth factor in humans. Clinical Pharmacology and Therapeutics 2002;72:20-32.

[54] Biondi M, Ungaro F, Quaglia F, Netti PA. Controlled drug delivery in tissue engineering. Advanced Drug Delivery Reviews 2008;60:229-42.

[55] Panyam J, Labhasetwar V. Biodegradable nanoparticles for drug and gene delivery to cells and tissue. Advanced Drug Delivery Reviews 2003;55:329-47.

[56] Moon JJ, Saik JE, Poché RA, Leslie-Barbick JE, Lee S-H, Smith AA, et al. Biomimetic hydrogels with pro-angiogenic properties. Biomaterials 2010;31:3840-7.

[57] Phelps EA, Landazuri N, Thule PM, Taylor WR, Garcia AJ. Bioartificial matrices for therapeutic vascularization. Proceedings of the National Academy of Sciences 2010;107:3323-8.

[58] Silva EA, Mooney DJ. Spatiotemporal control of vascular endothelial growth factor delivery from injectable hydrogels enhances angiogenesis. Journal of Thrombosis and Haemostasis 2007;5:590-8.

[59] Richardson TP, Peters MC, Ennett AB, Mooney DJ. Polymeric system for dual growth factor delivery. Nature Biotechnology 2001;19:1029-34.

[60] Peattie RA, Nayate AP, Firpo MA, Shelby J, Fisher RJ, Prestwich GD. Stimulation of in vivo angiogenesis by cytokine-loaded hyaluronic acid hydrogel implants. Biomaterials 2004;25:2789-98.

[61] Elia R, Fuegy PW, VanDelden A, Firpo MA, Prestwich GD, Peattie RA. Stimulation of in vivo angiogenesis by in situ crosslinked, dual growth factor-loaded, glycosaminoglycan hydrogels. Biomaterials 2010;31:4630-8.

[62] Jang J-H, Schaffer DV, Shea LD. Engineering Biomaterial Systems to Enhance Viral Vector Gene Delivery. Molecular Therapy 2011;19:1407-15.

[63] De Laporte L, Shea LD. Matrices and scaffolds for DNA delivery in tissue engineering. Advanced Drug Delivery Reviews 2007;59:292-307.

[64] Jafari M, Soltani M, Naahidi S, N. Karunaratne D, Chen P. Nonviral Approach for Targeted Nucleic Acid Delivery. Current Medicinal Chemistry 2012;19:197-208.

[65] Jang J-H, Houchin TL, Shea LD. Gene delivery from polymer scaffolds for tissue engineering. Expert Review of Medical Devices 2004;1:127-38.

[66] Pathak A, Patnaik S, Gupta KC. Recent trends in non-viral vector-mediated gene delivery. Biotechnology Journal 2009;4:1559-72.

[67] Morille M, Passirani C, Vonarbourg A, Clavreul A, Benoit J-P. Progress in developing cationic vectors for non-viral systemic gene therapy against cancer. Biomaterials 2008;29:3477-96.

[68] Bonadio J, Smiley E, Patil P, Goldstein S. Localized, direct plasmid gene delivery in vivo: prolonged therapy results in reproducible tissue regeneration. Nature Medicine 1999;5:753-9.

[69] Chun KW, Lee JB, Kim SH, Park TG. Controlled release of plasmid DNA from photo-cross-linked pluronic hydrogels. Biomaterials 2005;26:3319-26.

[70] Kasper FK, Jerkins E, Tanahashi K, Barry MA, Tabata Y, Mikos AG. Characterization of DNA release from composites of oligo(poly(ethylene glycol) fumarate) and cationized gelatin microspheres in vitro. Journal of Biomedical Materials Research Part A 2006;78A:823-35.

[71] Kong HJ, Kim ES, Huang YC, Mooney DJ. Design of biodegradable hydrogel for the local and sustained delivery of angiogenic plasmid DNA. Pharmaceutical Research 2008;25:1230-8.

[72] Quick DJ, Anseth KS. DNA delivery from photocrosslinked PEG hydrogels: encapsulation efficiency, release profiles, and DNA quality. Journal of Controlled Release 2004;96:341-51.

[73] Yan S, Fu Q, Zhou Y, Wang J, Liu Y, Duan X, et al. High levels of gene expression in the hepatocytes of adult mice, neonatal mice and tree shrews via retro-orbital sinus hydrodynamic injections of naked plasmid DNA. Journal of Controlled Release 2012.

[74] Schaffert D, Wagner E. Gene therapy progress and prospects: synthetic polymer-based systems. Gene Therapy 2008;15:1131-8.

[75] Trentin D, Hall H, Wechsler S, Hubbell JA. Peptide-matrix-mediated gene transfer of an oxygen-insensitive hypoxia-inducible factor-1 alpha variant for local induction of angiogenesis. Proceedings of the National Academy of Sciences of the United States of America 2006;103:2506-11.

[76] Trentin D, Hubbell J, Hall H. Non-viral gene delivery for local and controlled DNA release. Journal of Controlled Release 2005;102:263-75.

[77] Lungwitz U, Breunig M, Blunk T, Gopferich A. Polyethylenimine-based non-viral gene delivery systems. European Journal of Pharmaceutics and Biopharmaceutics 2005;60:247-66.

[78] Godbey W, Wu KK, Mikos AG. Tracking the intracellular path of poly (ethylenimine)/DNA complexes for gene delivery. Proceedings of the National Academy of Sciences 1999;96:5177-81.

[79] Godbey WT, Wu KK, Mikos AG. Poly(ethylenimine) and its role in gene delivery. Journal of Controlled Release 1999;60:149-60.

[80] Abdallah B, Hassan A, Benoist C, Goula D, Behr JP, Demeneix BA. A powerful nonviral vector for in vivo gene transfer into the adult mammalian brain: Polyethylenimine. Human Gene Therapy 1996;7:1947-54.

[81] Wang S, Ma N, Gao SJ, Yu H, Leong KW. Transgene expression in the brain stem effected by intramuscular injection of polyethylenimine/DNA complexes. Molecular Therapy 2001;3:658-64.

[82] Gautam A, Densmore CL, Golunski E, Xu B, Waldrep JC. Transgene expression in mouse airway epithelium by aerosol gene therapy with PEI-DNA complexes. Molecular Therapy 2001;3:551-6.

[83] Kichler A, Chillon M, Leborgne C, Danos O, Frisch B. Intranasal gene delivery with a polyethylenimine-PEG conjugate. Journal of Controlled Release 2002;81:379-88.

[84] Rudolph C, Schillinger U, Plank C, Gessner A, Nicklaus P, Muller RH, et al. Nonviral gene delivery to the lung with copolymer-protected and transferrin-modified polyethylenimine. Biochimica Et Biophysica Acta-General Subjects 2002;1573:75-83.

[85] Wiseman JW, Goddard CA, McLelland D, Colledge WH. A comparison of linear and branched polyethylenimine (PEI) with DCChol/DOPE liposomes for gene delivery to epithelial cells in vitro and in vivo. Gene Therapy 2003;10:1654-62.

[86] Kleemann E, Jekel N, Dailey LA, Roesler S, Fink L, Weissmann N, et al. Enhanced gene expression and reduced toxicity in mice using polyplexes of low-molecular-weight poly(ethylene imine) for pulmonary gene delivery. Journal of Drug Targeting 2009;17:638-51.

[87] Segura T, Schmokel H, Hubbell JA. RNA Interference Targeting Hypoxia Inducible Factor 1[alpha] Reduces Post-Operative Adhesions in Rats. Journal of Surgical Research 2007;141:162-70.

[88] Wong SP, Argyros O, Howe SJ, Harbottle RP. Systemic gene transfer of polyethylenimine (PEI)-plasmid DNA complexes to neonatal mice. Journal of Controlled Release 2011;150:298-306.

[89] Aoki K, Furuhata S, Hatanaka K, Maeda M, Remy JS, Behr JP, et al. Polyethylenimine-mediated gene transfer into pancreatic tumor dissemination in the murine peritoneal cavity. Gene Therapy 2001;8:508-14.

[90] Coll JL, Chollet P, Brambilla E, Desplanques D, Behr JP, Favrot M. In vivo delivery to tumors of DNA complexed with linear polyethylenimine. Human Gene Therapy 1999;10:1659-66.

[91] Iwai M, Harada Y, Tanaka S, Muramatsu A, Mori T, Kashima K, et al. Polyethylenimine-mediated suicide gene transfer induces a therapeutic effect for hepatocellular carcinoma in vivo by using an Epstein-Barr virus-based plasmid vector. Biochemical and Biophysical Research Communications 2002;291:48-54.

[92] Lei P, Padmashali RM, Andreadis ST. Cell-controlled and spatially arrayed gene delivery from fibrin hydrogels. Biomaterials 2009;30:3790-9.

[93] Fukunaka Y, Iwanaga K, Morimoto K, Kakemi M, Tabata Y. Controlled release of plasmid DNA from cationized gelatin hydrogels based on hydrogel degradation. Journal of Controlled Release 2002;80:333-43.

[94] Lei Y, Ng QKT, Segura T. Two and three-dimensional gene transfer from enzymatically degradable hydrogel scaffolds. Microscopy Research and Technique 2010;73:910-7.

[95] Lei Y, Segura T. DNA delivery from matrix metalloproteinase degradable poly(ethylene glycol) hydrogels to mouse cloned mesenchymal stem cells. Biomaterials 2009;30:254-65.

[96] Wieland JA, Houchin-Ray TL, Shea LD. Non-viral vector delivery from PEG-hyaluronic acid hydrogels. Journal of Controlled Release 2007;120:233-41.

[97] Gojgini S, Tokatlian T, Segura T. Utilizing Cell-Matrix Interactions To Modulate Gene Transfer to Stem Cells Inside Hyaluronic Acid Hydrogels. Molecular Pharmaceutics 2011;8:1582-91.

[98] Jang J-H, Shea LD. Intramuscular delivery of DNA releasing microspheres: Microsphere properties and transgene expression. Journal of Controlled Release 2006;112:120-8.

[99] Lei Y, Huang S, Sharif-Kashani P, Chen Y, Kavehpour P, Segura T. Incorporation of active DNA/cationic polymer polyplexes into hydrogel scaffolds. Biomaterials 2010;31:9106-16.

[100] Lei Y, Rahim M, Ng Q, Segura T. Hyaluronic acid and fibrin hydrogels with concentrated DNA/PEI polyplexes for local gene delivery. Journal of Controlled Release 2011;153:255-61.

[101] Pannier AK, Wieland JA, Shea LD. Surface polyethylene glycol enhances substrate-mediated gene delivery by nonspecifically immobilized complexes. Acta Biomaterialia 2008;4:26-39.

[102] Bengali Z, Rea JC, Gibly RF, Shea LD. Efficacy of immobilized polyplexes and lipoplexes for substrate-mediated gene delivery. Biotechnology and bioengineering 2009;102:1679-91.

[103] Jewell CM, Lynn DM. Surface-mediated delivery of DNA: Cationic polymers take charge. Current opinion in colloid & interface science 2008;13:395-402.

[104] Segura T, Shea LD. Surface-Tethered DNA Complexes for Enhanced Gene Delivery. Bioconjug Chem 2002;13:621-9.

[105] Hu WW, Lang MW, Krebsbach PH. Development of adenovirus immobilization strategies for in situ gene therapy. The Journal of Gene Medicine 2008;10:1102-12.

[106] Jang JH, Koerber JT, Gujraty K, Bethi SR, Kane RS, Schaffer DV. Surface immobilization of hexa-histidine-tagged adeno-associated viral vectors for localized gene delivery. Gene Therapy 2010;17:1384-9.

[107] Blocker KM, Kiick KL, Sullivan MO. Surface Immobilization of Plasmid DNA with a Cell-Responsive Tether for Substrate-Mediated Gene Delivery. Langmuir 2011;27:2739-46.

[108] Ehrbar M, Djonov VG, Schnell C, Tschanz SA, Martiny-Baron G, Schenk U, et al. Cell-Demanded Liberation of VEGF121 From Fibrin Implants Induces Local and Controlled Blood Vessel Growth. Circulation Research 2004;94:1124-32.

[109] Geer DJ, Swartz DD, Andreadis ST. Biomimetic Delivery of Keratinocyte Growth Factor upon Cellular Demand for Accelerated Wound Healing *in Vitro* and *in Vivo*. American Journal of Pathology 2005;167:1575-86.

[110] Zisch AH, Lutolf MP, Ehrbar M, Raeber GP, Rizzi SC, Davies N, et al. Cell-demanded release of VEGF from synthetic, biointeractive cell ingrowth matrices for vascularized tissue growth. Faseb Journal 2003;17:2260-2.

[111] Tauro JR, Gemeinhart RA. Matrix Metalloprotease Triggered Delivery of Cancer Chemotherapeutics from Hydrogel Matrixes. Bioconjugate chemistry 2005;16:1133-9.

[112] Tauro JR, Lee B-S, Lateef SS, Gemeinhart RA. Matrix metalloprotease selective peptide substrates cleavage within hydrogel matrices for cancer chemotherapy activation. Peptides 2008;29:1965-73.

[113] Soo C, Shaw WW, Zhang X, Longaker MT, Howard EW, Ting K. Differential expression of matrix metalloproteinases and their tissue-derived inhibitors in cutaneous wound repair. Plastic and Reconstructive Surgery 2000;105:638-47.

[114] Steffensen B, Hakkinen L, Larjava H. Proteolytic events of wound-healing--coordinated interactions among matrix metalloproteinases (MMPs), integrins, and extracellular matrix molecules. Critical Reviews in Oral Biology and Medicine 2001;12:373-98.

[115] Holland TA, Tabata Y, Mikos AG. Dual growth factor delivery from degradable oligo(poly(ethylene glycol) fumarate) hydrogel scaffolds for cartilage tissue engineering. Journal of Controlled Release 2005;101:111-25.

[116] Jaklenec A, Hinckfuss A, Bilgen B, Ciombor DM, Aaron R, Mathiowitz E. Sequential release of bioactive IGF-I and TGF-[beta]1 from PLGA microsphere-based scaffolds. Biomaterials 2008;29:1518-25.

[117] Yilgor P, Tuzlakoglu K, Reis RL, Hasirci N, Hasirci V. Incorporation of a sequential BMP-2/BMP-7 delivery system into chitosan-based scaffolds for bone tissue engineering. Biomaterials 2009;30:3551-9.

[118] Shepard JA, Virani FR, Goodman AG, Gossett TD, Shin S, Shea LD. Hydrogel macroporosity and the prolongation of transgene expression and the enhancement of angiogenesis. Biomaterials 2012;33:7412-21.

[119] Dhaliwal A, Lam J, Maldonado M, Lin C, Segura T. Extracellular matrix modulates non-viral gene transfer to mouse mesenchymal stem cells. Soft Matter 2012;8:1451-9.

[120] Dhaliwal A, Maldonado M, Han Z, Segura T. Differential uptake of DNA-poly(ethylenimine) polyplexes in cells cultured on collagen and fibronectin surfaces. Acta Biomaterialia 2010;6:3436-47.

[121] Kong HJ, Liu J, Riddle K, Matsumoto T, Leach K, Mooney DJ. Non-viral gene delivery regulated by stiffness of cell adhesion substrates. Nature Materials 2005;4:460-4.

[122] Kong HJ, Hsiong S, Mooney DJ. Nanoscale cell adhesion ligand presentation regulates nonviral gene delivery and expression. Nano Letters 2007;7:161-6.

[123] Slaughter BV, Khurshid SS, Fisher OZ, Khademhosseini A, Peppas NA. Hydrogels in regenerative medicine. Advanced Materials 2009;21:3307-29.

[124] Schrementi ME, Ferreira AM, Zender C, DiPietro LA. Site-specific production of TGF- in oral mucosal and cutaneous wounds. Wound Repair and Regeneration 2008;16:80-6.

[125] Szpaderska AM, Zuckerman JD, DiPietro LA. Differential Injury Responses in Oral Mucosal and Cutaneous Wounds. Journal of Dental Research 2003;82:621-6.

[126] Peppas NA, Hilt JZ, Khademhosseini A, Langer R. Hydrogels in Biology and Medicine: From Molecular Principles to Bionanotechnology. Advanced Materials 2006;18:1345-60.

[127] Rejman J, Oberle V, Zuhorn IS, Hoekstra D. Size-dependent internalization of particles via the pathways of clathrin- and caveolae-mediated endocytosis. Biochemical Journal 2004;377:159-69.

[128] Lutolf MP, Lauer-Fields JL, Schmoekel HG, Metters AT, Weber FE, Fields GB, et al. Synthetic matrix metalloproteinase-sensitive hydrogels for the conduction of tissue

regeneration: Engineering cell-invasion characteristics. Proceedings of the National Academy of Sciences 2003;100:5413-8.

[129] Nagase H, Fields GB. Human matrix metalloproteinase specificity studies using collagen sequence-based synthetic peptides. Peptide Science 1998;40:399-416.

[130] Seliktar D, Zisch AH, Lutolf MP, Wrana JL, Hubbell JA. MMP-2 sensitive, VEGF-bearing bioactive hydrogels for promotion of vascular healing. Journal of Biomedical Materials Research A 2004;68:704-16.

[131] Kaiser K, Marek M, Haselgrubler T, Schindler H, Gruber HJ. Basic studies on heterobifunctional biotin-PEG conjugates with a 3-(4-pyridyldithio)propionyl marker on the second terminus. Bioconjugate chemistry 1997;8:545-51.

[132] Lee S-H, Moon JJ, Miller JS, West JL. Poly(ethylene glycol) hydrogels conjugated with a collagenase-sensitive fluorogenic substrate to visualize collagenase activity during three-dimensional cell migration. Biomaterials 2007;28:3163-70.

[133] Chen EI, Kridel SJ, Howard EW, Li W, Godzik A, Smith JW. A unique substrate recognition profile for matrix metalloproteinase-2. The Journal of biological chemistry 2002;277:4485-91.

[134] Bitter T, Muir HM. A modified uronic acid carbazole reaction. Analytical Biochemistry 1962;4:330-4.

[135] Ehrbar M, Zeisberger SM, Raeber GP, Hubbell JA, Schnell C, Zisch AH. The role of actively released fibrin-conjugated VEGF for VEGF receptor 2 gene activation and the enhancement of angiogenesis. Biomaterials 2008;29:1720-9.

[136] Anderson SM, Chen TT, Iruela-Arispe ML, Segura T. The phosphorylation of vascular endothelial growth factor receptor-2 (VEGFR-2) by engineered surfaces with electrostatically or covalently immobilized VEGF. Biomaterials 2009;30:4618-28.

[137] Anderson SM, Siegman SN, Segura T. The effect of vascular endothelial growth factor (VEGF) presentation within fibrin matrices on endothelial cell branching. Biomaterials 2011;32:7432-43.

[138] Galiano RD, Tepper OM, Pelo CR, Bhatt KA, Callaghan M, Bastidas N, et al. Topical vascular endothelial growth factor accelerates diabetic wound healing through increased angiogenesis and by mobilizing and recruiting bone marrow-derived cells. The American Journal of Pathology 2004;164:1935.

[139] Martino MlM, Tortelli F, Mochizuki M, Traub S, Ben-David D, Kuhn GA, et al. Engineering the Growth Factor Microenvironment with Fibronectin Domains to Promote Wound and Bone Tissue Healing. Science Translational Medicine 2011;3:100ra89.

[140] Bullen EC, Longaker MT, Updike DL, Benton R, Ladin D, Hou Z, et al. Tissue Inhibitor of Metalloproteinases-1 Is Decreased and Activated Gelatinases Are Increased in Chronic Wounds. Journal of Investigative Dermatology 1995;104:236-40.

[141] Chen W, Fu X, Ge S, Sun T, Sheng Z. Differential expression of matrix metalloproteinases and tissue-derived inhibitors of metalloproteinase in fetal and adult skins. The International Journal of Biochemistry & Cell Biology 2007;39:997-1005.

[142] Gillard JA, Reed MWR, Buttle D, Cross SS, Brown NJ. Matrix metalloproteinase activity and immunohistochemical profile of matrix metalloproteinase-2 and -9 and tissue inhibitor of metalloproteinase-1 during human dermal wound healing. Wound Repair and Regeneration 2004;12:295-304.

[143] Pirilä E, Korpi JT, Korkiamäki T, Jahkola T, Gutierrez-Fernandez A, Lopez-Otin C, et al. Collagenase-2 (MMP-8) and matrilysin-2 (MMP-26) expression in human wounds of different etiologies. Wound Repair and Regeneration 2007;15:47-57.

[144] Lobmann R, Ambrosch A, Schultz G, Waldmann K, Schiweck S, Lehnert H. Expression of matrix-metalloproteinases and their inhibitors in the wounds of diabetic and non-diabetic patients. Diabetologia 2002;45:1011-6.

[145] Silva JAF, Lorencini M, Peroni LA, Hoz CLRDL, Carvalho HF, Stach-Machado DR. The influence of type I diabetes mellitus on the expression and activity of gelatinases (matrix metalloproteinases-2 and -9) in induced periodontal disease. Journal of Periodontal Research 2008;43:48-54.

[146] Galkowska H, Olszewsk WL, Wojewodzka U, Mijal J, Filipiuk E. Expression of apoptosis- and cell cycle-related proteins in epidermis of venous leg and diabetic foot ulcers. Surgery 2003;134:213-20.

[147] Brown NJ, Smyth EAE, Cross SS, Reed MWR. Angiogenesis induction and regression in human surgical wounds. Wound repair and regeneration 2002;10:245-51.

[148] Galiano RD, Michaels J, Dobryansky M, Levine JP, Gurtner GC. Quantitative and reproducible murine model of excisional wound healing. Wound Repair and Regeneration 2004;12:8.

[149] Schultz GS, Wysocki A. Interactions between extracellular matrix and growth factors in wound healing. Wound Repair and Regeneration 2009;17:153-62.